A COMPARATIVE STUDY OF MAXIMUM LIKELIHOOD AND ADAPTIVE EQUALIZATION FOR HIGH RATE HIGH FREQUENCY DATA COMMUNICATIONS

D.D. Falconer, H.M. Hafez, A.U.H. Sheikh,
E. Eleftheriou, M. Tobis

P
91
.C655
C643
1983

IC

CARLETON UNIVERSITY
SYSTEMS ENGINEERING

[redacted]

This report and the information contained herein is the property of the Government of Canada. It is prepared as partial fulfillment of a contractual agreement between the Department of Communications and the above noted contractor in support of Military Communications Task No. 32B74 sponsored by DND/DMCS/6. Publication of this report does not constitute DOC or DND approval of the report findings or conclusions. Release of this report is subject to approval by the Department of National Defence.

COMMUNICATIONS CANADA
CRC
JUL 26 1983
LIBRARY – BIBLIOTHÈQUE

Department of Systems and Computer Engineering
Carleton University ◦ Ottawa ◦ Canada ◦ K1S 5B6

A COMPARATIVE STUDY OF MAXIMUM LIKELIHOOD AND ADAPTIVE EQUALIZATION FOR HIGH RATE HIGH FREQUENCY DATA COMMUNICATIONS

D.D. Falconer, H.M. Hafez, A.U.H. Sheikh,
E. Eleftheriou, M. Tobis

Industry Canada
Library - Queen

AVR
APR - 2 2013

Industrie Canada
Bibliothèque - Queen

National Defence | Défense nationale

National Defence Headquarters
Ottawa, Canada
K1A 0K2

Quartier général de la Défense nationale
Ottawa, Canada
K1A 0K2

3713-1 (DMCS 6)

9 December 1991

Ms. H. K. Baskin
Communications Research Centre
Administrative and Technical Services
P.O. Box 11490, Stn "H"
Ottawa, Ontario
K2H 8S2

Dear Ms. Baskin:

APPROVAL TO RELEASE DND REPORT

The Department of Communications Contractor Report MC/CR004/83 which was sponsored by DND/DMCS 6 under Military Communications Task No. 32B74, has been reviewed and is approved for release to Canadian Industry.

The DND/DMCS 6 OPI for this report is Lt(N) C. Jansen, DMCS 6-2, 994-8492.

Yours truly,

T. F. Brown

Thomas F. Brown
Captain(N)
Director Maritime Combat Systems

Canada

DOC CONTRACTOR REPORT DOC-CR-CS-(YEAR)-(SERIAL#) MC/CR004/83

DEPARTMENT OF COMMUNICATIONS - OTTAWA - CANADA

RADAR AND COMMUNICATIONS TECHNOLOGY

TITLE: A Comparative Study of Maximum Likelihood and Adaptive Equalization for High Rate, High Frequency Data Communications

AUTHOR(S): D. D. Falconer, H. M. Hafez, A. U. H. Sheikh, E. Eleftheriou, M. Tobis

ISSUED BY CONTRACTOR AS REPORT NO: Final Report

CONTRACTOR: Department of Systems and Computer Engineering, Carleton University

SPONSOR: DND/DMCS/6

DEPARTMENT OF SUPPLY AND SERVICES CONTRACT NO: 03SU.36001-2-1192

DOC. SCIENTIFIC AUTHORITY: D. Clark, Communications Research Centre

CLASSIFICATION: Unclassified.

This report and the information contained herein is the property of the Government of Canada. It is prepared as partial fulfillment of a contractual agreement between the Department of Communications and the above noted contractor in support of Military Communications Task No. 32B74 sponsored by DND/DMCS/6. Publication of this report does not constitute DOC or DND approval of the report findings or conclusions. Release of this report is subject to approval by the Department of National Defence.

DATE: April 29, 1983

COMMUNICATIONS CANADA
CRC
JUL 26 1983
LIBRARY – BIBLIOTHÈQUE

A COMPARATIVE STUDY OF MAXIMUM LIKELIHOOD AND ADAPTIVE EQUALIZATION FOR HIGH RATE HIGH FREQUENCY DATA COMMUNICATIONS

Submitted according to the terms of

DSS Contract No. 03SU.36001-2-1192

(RN: 36001-2-1192)

(FC: 0-884-00000-2703)

Prepared by:

D.D. Falconer (Principal Investigator)
H.M. Hafez
A.U.H. Sheikh
E. Eleftheriou
M. Tobis

Department of Systems and Computer Engineering

Carleton University

Ottawa, Ontario

K1S 5B6

April 1983

Abstract

Data communication at rates near or above 2 kbps on 3 khz-bandwidth HF radio channels is subject to impairment from severe linear dispersion, rapid channel time variation and severe fading. In this investigation recorded 2.4 kbps QPSK signals received from HF channels were processed to extract a time-varying estimate of the channel impulse response, and also to simulate a fast-adapting decision feedback-equalizing receiver. From the estimated channel impulse responses, performance-related parameters were computed for ideal matched filter, maximum-likelihood sequence-estimation (MLSE) and decision feedback equalization (DFE). The results indicated that the simpler DFE receiver suffered only a small theoretical performance degradation relative to the more complex MLSE receiver. Other HF channel impulse response statistics were also obtained to shed light on equalization and filter adaptation techniques. LMS and FRLS (fast recursive least squares) adaptation techniques were investigated for DFE receivers, including new FRLS restart procedures for mitigating numerical instability problems. While the FRLS algorithms offer faster channel-tracking capability in a high-SNR environment, the simpler LMS algorithm may be favoured on a cost-benefit basis for low-SNR HF channels. Techniques of carrier and bit synchronization were also proposed for QPSK signals on fading HF channels.

Acknowledgement

We wish to acknowledge the valuable encouragement and guidance in the project from Mr. David Clark who served as the contract scientific authority on behalf of the Communications Research Centre of the Department of Communications. We are also grateful to Mr. John Cioffi of Stanford University and to Professor John Proakis of Northeastern University for providing preprints of their papers and for sharing their insights on adaptive filtering. Finally, we are grateful to the Communications Research Centre for use of its CP6 computer and to Dr. Peter Driessen of Mobile Data International for advice on computer processing of the tapes.

Table of Contents

List of Figures

List of Notation

Symbol	Equation	Meaning
$r(t)$	(3.1)	Bandpass received waveform
Re	(3.1)	Real part
T	(3.1)	Symbol interval duration
a_n	(3.1)	Complex-valued data symbol
f_o	(3.1)	Carrier frequency
$h_c(t)^*$	(3.1)	Complex baseband channel impulse response
$n_p(t)$	(3.1)	Bandpass complex noise
$y(t)$	(3.2)	Complex baseband demodulated waveform
$h(t)^*$	(3.2)	Complex baseband system impulse response
$v(t)$	(3.2)	Complex baseband noise
J_n	(4.1)	Likelihood sum
N	(4.1)	Duration of channel impulse response or of adaptive filter length (symbol intervals)
Q_n	(4.2)	Complex DFE quantizer input
$\hat{a}_n$	(4.2)	Data symbol decision
N_1	(4.2)	Length of forward filter (symbol intervals)
W_m^*	(4.2)	Forward complex-valued tap coefficient
F_m^*	(4.2)	Feedback complex-valued tap coefficient
N_2	(4.2)	Length of feedback filter (symbol intervals)
$\underline{C}(n)^*$	(4.3)	Adaptive filter tap coefficient vector updated at time nT

Symbol	Equation	Meaning
$\underline{Z}(n)$	(4.3)	Vector of adaptive filter contents at time nT
$N_o/2$	(4.3)	Double-sided white noise power spectral density
d/σ	(4.6)	Effective SNR parameter
$Q(x)$	(4.7)	Integral over tail of gaussian density function
d_{MF}	(4.8)	d parameter for matched filter
d_{MLSE}	(4.11)	d parameter for MLSE receiver
$\{\epsilon_i\}$	(4.11)	Data symbol errors
d_{LB}	(4.13)	Lower bound on d_{MLSE}
C_n, ρ_k	(4.14)	Parameters in calculation of d_{LB}
$\hat{S}(f)$	(4.17)	Power spectrum of sampled channel
$R(mT)$	(4.18)	Autocorrelation function of channel
d_{DFE}	(4.19)	d parameter for DFE receiver
γ	(5.1)	LMS algorithm step size
$e(n)$	(5.2)	Error used for filter adaptation
d_n	(5.2)	Desired output of adaptive filter at time nT
A	(5.3)	Channel autocorrelation matrix
p	(	Number of new complex adaptive filter inputs processed per symbol interval
λ	(5.4)	Exponential weighting factor in FRLS algorithm
$\underline{\hat{h}}(n)^{(1)}$ $\underline{\hat{h}}(n)^{(2)}$	(5.5)	Estimated channel impulse response vectors at time nT

Symbol	Equation	Meaning
$S(n)^{(1)}$	(5.5), (5.22)	Exponentially-weighted sums of squared errors
$S(n)^{(2)}$		
$\underline{a}(n)$	(5.5)	Vector of data symbols at time nT
$y(kT)^{(1)}$	(5.5)	y(kT)
$y(kT)^{(2)}$	(5.5)	y(kT+T/2)
δ	(5.5)	Initialization parameter in FRLS algorithm
$\underline{k}(n)$	(5.7)	FRLS gain vector
$\underline{F}(n)$, $F(n)$	(5.10), (5.28)	Forward predictor vector or matrix
$\underline{B}(n)$, $B(n)$	(5.15), (5.33)	Backward predictor vector or matrix
$f(n)$, $\underline{f}_p(n)$	(5.10), (5.28)	Forward prediction error
$f(n)'$, $\underline{f}_p(n)'$	(5.12), (5.30)	Updated forward prediction error
$\Gamma(n)$	(5.11), (5.29)	Parameter for updating $f(n)'$
$E(n)$, $E_{pp}(n)$	(5.13), (5.31)	Parameter in FRLS algorithm
$\underline{\bar{k}}(n)$	(5.14)	Extended Kalman gain vector
$\underline{g}(n)$, $\mu(n)$	(5.14)	Partitioning of $\underline{k}(n)$
$\Theta(n)$	(5.19)	Estimated channel phase shift at time n
p_1	(5.21)	Number of channel outputs per symbol interval entering DFE
$\underline{\xi}_p(n)$	(5.25)	Latest p inputs to DFE
$\underline{\rho}_p(n)$	(5.26)	Oldest p inputs to DFE
$\underline{x}_p$, $\underline{y}$	(5.32)	Auxiliary vectors
K	(5.37)	Time at which restart is initiated
$\tilde{y}(n)$, $\underline{\tilde{Z}}(n)$, a_n	(5.37)	Adaptive filter inputs during restart

Symbol	Equation	Meaning
u_n	(5.38)	Error in absence of restart
$\underline{Z}(n)^{(-)}$	(5.39)	$\underline{Z}(n) - \tilde{\underline{Z}}(n)$
$\tilde{d}_n$	(5.40)	Modified desired outputs during restart
$\underline{C}(n-1)_{LMS}$	(5.41)	Tap coefficient vector from auxiliary LMS algorithm
MSE(n)	(9.2)	Measured mean squared error at time nT
SNR(n)	(9.3)	Measured SNR at time nT

1. INTRODUCTION

The possibility of realizing a long range (few Km to several thousand Km) link gives the H.F. portion of the spectrum (2-30 MHz) a special place in the world of communications. With a very little expenditure in the form of equipment, time and manpower, a communication link with a moderate to high reliability could be established. The key to such a link lies in the presence of ionized layers between 40 to 500 Km above the surface of the earth. These layers, discovered in the 1920's, were found to possess the property of reflecting (or refracting) the electromagnetic waves, to give the communicator a fairly long range.

The mid-seventies saw sharp rise in the availability of communication satellites for long-distance digital communications systems. However, the vulnerability of the satellite to modern sophisticated weapons, and its longer delays in recovering from the radiation effects of a nuclear explosion, has led to renewed interest in HF channels for military purposes. This is because of the rapid recovery of the ionosphere from nuclear shock, as well as its physical indestructibility. There are also many civilian applications of the HF band for low-cost communication links to distant-remote sites on land or at sea.

In satellite communication, the communicator's primary aim to establish a link is to provide acceptable signal to noise ratio at the receiver; however, for the H.F. communication, in addition to good signal to noise ratio, one has to resort to some form of signal processing at the receiver (or at the transmitter)

to increase the reliability of the link. This study is concerned with reception techniques for relatively high speed (approximately 1 bps or higher per hz of bandwidth) digital communications on HF channels. The specific approach is to simulate receiver processing of recorded digitized signals that resulted from transmitting 2400 bps QPSK-modulated data over actual HF channels. These recordings were made and provided by the Communications Research Centre of the Department of Communications.

Chapter 10 summarizes the major conclusions of the investigation.

2. HF CHANNEL CHARACTERISTICS

Over short distances, HF radio waves propagate between the transmitter and the receiver via three basic modes, i.e., ground waves, tropospheric propagation (LOS) and skywave (resulting in the reflection from the ionosphere. As the transmitter-receiver distance is increased, the ground wave and LOS propagation suffer increased attenuation due to ground conductivity and the earth's curvature respectively. Therefore, for larger distances, only the ionospheric mode of propagation survives.

2.1 The Ionosphere

The literature on ionospheric studies is extensive and several books and conference proceedings are available in the open literature [Bet 67], [Pic 74], [Agar 1979], [YL 72], [Tom 77]. The Consultative Committee for International Radio, CCIR, also publishes periodically on ionospheric predictions.

It is beyond the scope of this report to go into the details of the mechanisms which contribute to the formation of the ionosphere. It is sufficient to say that the sun's radiation, and meteorites travelling through the atmosphere, are major causes of the existence of the ionosphere and physical environmental conditions such as solar flares, and the earth's magnetic fields affect its characteristics. The details of these and other contributors to ionospheric changes are documented in [Pic 74].

The ionosphere has four distinct layers - D, E, F1 and F2 during the day, and in the night only F, formed as a result of F1 and F2 layers combining, is in existence. Table 2.1 summarizes the layer structure.

The heights of these layers fluctuate; also the layers may undergo severe irregularities (or inhomogeneities) due to environmental conditions. These effects lead to severe propagation conditions, an understanding of which is essential in an efficient use of the channel.

Table 2.1

Summary of Ionospheric Layers Structure

Layer	Approximate Height and Layer Thickness	Effective Period	Effect on HF Waves (3-30 MHz)	Possible Transmission Distance by Reflection by the Layer	
				Single Hop Propagation	Multihop Propagation
D	70-100 Km	Day	Absorption	Does not reflect HF waves	
E	100-140 Km	Day	Refraction	Up to 2500 Km	All distances except
F1	150-250 Km	Day	Refraction	Up to 3000 Km	2500-4000 Km
F2	250-500 Km	Day	Refraction	Up to 4000 Km	All distances
F	300-400 Km	Night	Refraction	Up to 4000 Km	All distances

2.2 Multipath Propagation

One of the major sources of problems in HF communications is the multipath effect which arises due to multimode propagation between the transmitter and the receiver. Multiplicity of mode may arise due to the presence of ground, sky, and tropospheric waves at the receiver at short distances or due to refraction of rays of the same wave from E, F1, F2 layers. As a result the signals from various modes of propagation arrive at the receiver with phase delays characteristic of the path lengths. It is generally recognized [WJB 70] that there is usually a relatively

small number of discrete paths through which the wave propagates. Therefore, when an impulse is transmitted, the impulse signal received is due to the superposition of the channel impulse responses with differential delays, resulting in an elongated impulse response or time dispersion. This time dispersion gives rise to intersymbol interference.

If these differential delays, due to a number of discrete paths, remain constant, then the signal processing at the receiver would be relatively easy. However, these differential delays may fluctuate due to solar flares, magnetic storms and sudden ionospheric disturbances (SID). For a time invariant channel presence of differential delay produces fixed inband frequency selective fading of the signals. When the characteristic channel is no longer time invariant, the frequency components which fade wander in the band.

The Sudden Ionospheric Disturbances (SID) may also result in short wave fade-outs (SWF) due to the D-layer. Such fade-outs are relatively rare, but may last for several minutes.

The time dispersion decreases, in general, with the increase in the range due to reduction of propagation paths. Firstly, an increase in the range is generally effected by using a frequency closer to the maximum usable frequency (M.U.F.). Thus the possibility of refraction from E or F1 layers is considerably reduced, so a reduction in time dispersion follows. Secondly, an increase in the range virtually eliminates the ground and tropospheric modes of propagation.

Typical time dispersion for the ranges of 200, 1000, and 2500 Km have been measured to 8, 5 and 3 m sec respectively [WJB

70]. Goldberg [Gol 66] suggested similar figures for the time dispersion, but indicates that a maximum time dispersion occurs for the range of 2500 Km. For a good path and proper frequency selection, the time dispersion can be reduced to approximately 1 msec, which gives a correlation bandwidth of approximately 1 KHz. Even for a single mode of propagation, an irreducible time dispersion of 100 usec has been estimated due to roughness of the ionosphere. This corresponds to the 10 KHz correlation bandwidth of the channel.

2.3 Frequency Dispersion

For a single path propagation mode, a transmitted sinusoid is received as a band of frequencies (known as frequency dispersion) and is due to the time variant nature of the reflecting media. Such a shift in the signal frequencies is caused by the time variant height of the ionosphere layer enforcing the propagation mode. The frequency dispersion is predominantly due to the fast F layer height fluctuations as compared to the E layer fluctuations which are relatively slow. It is hard to measure the frequency dispersion due to the problems associated with the detection of a very small fraction of a Hz. Frequency dispersions of 0.01 to 1 Hz are common. The reciprocal of the frequency dispersion is known as correlation time and is a measure of the fade interval. It is seen that the fade interval may vary between 1 and several tens of seconds, which is much longer than the bit interval of the data over the channel.

2.4 Fading

Due to multiple propagation modes, each with time variant differential delays due to variation of mean path length of the modes, the received signal strength varies with time. Fading rate is defined as the inverse of the period of two consecutive minima and the shortest such period (or rapid fading) is produced by polarization fading as a result of the earth's magnetic field. Fades are more frequent (10 to 15 fades/minute) at dawn and in the evening periods and have a narrower spread. The fades at midday show rather wider spread (0-50 fades/minute) [Mas 82]. The deep fades of 5 or more minutes duration are largely due to increased absorption in the D layer of the ionosphere.

2.5 Delay Distortion

A typical delay vs frequency ionogram is shown in Figure 2.1 [BF 75] and it reveals the non-linear nature of the delay characteristics close to the M.U.F. This produces a rapid change in the group delay with the signal frequency. Inston [Ins 69] has estimated that a typical rate of change of group delay with frequency is approximately 5×10^{-6} usec/Hz. The delay distortion could be reduced by judicious choice of operating frequency.

2.6 Summary

Researchers agree on most of the findings regarding HF ionospheric channel characteristics. The channel is time variant and produces time and frequency spreads. The typical time dispersion is measured to be between 3-8 msec. and depends on the

range. In certain circumstances the channel behaviour is perfect. The frequency spread is in the order of a fraction of a second and the channel is short term stationary. There is usually a small number of discrete modes of propagation typically 1 to 3.

The channel also affects delay distortion when working close to the Maximum Usable Frequency (M.U.F.) and this distortion could be reduced by lowering the operating frequency. However, it may lead to an increase in time dispersion, so a compromise frequency should be sought. Moreover, frequency bands yielding the best transmission conditions may also have the most interference from co-users. Thus it is essential to design transmitters and receivers capable of operating in and adapting to non-ideal propagation conditions on HF channels.

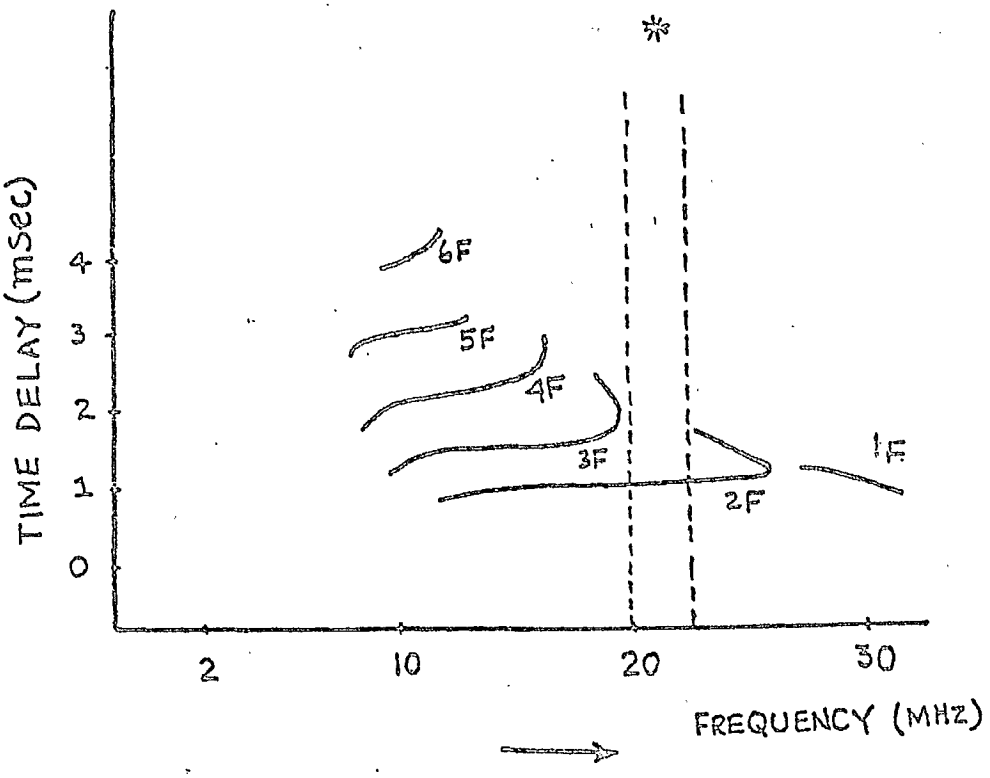

Figure 2.1: Typical Time Delay vs Frequency Characteristic of HF Channel. (nF indicates nth path and * indicates an optimum usable frequency) {Reproduced from [BF 75]}

3. HIGH SPEED SYNCHRONOUS SERIAL DATA TRANSMISSION ON HF CHANNELS

Because of the extent of a typical HF channel's time and frequency dispersion, digital transmission at a bit rate on the same order as or greater than the channel bandwidth is considered "high speed", and requires relatively sophisticated receiver processing. In this study we focus attention on 2400 bps transmission using QPSK modulation over 3-khz-bandwidth HF channels. Higher data rates and alternative modulation formats such as BPSK or multiple-carrier are possible, but the 2400 bps QPSK signal format is very representative of current HF transmission equipment; a 2400 bps data stream could support vocoder-digitized speech.

For a linearly-modulated QPSK data signal passed through a linear channel, the channel's bandpass output waveform can be represented as the real part of a complex waveform;

$$r(t) = \sqrt{2}\ \mathrm{Re}\left[\sum_n a_n\ h_c\ (t-nT)^*\ \exp(j2\pi f_o t) + n_p(t)\right] \qquad (3.1)$$

where $h_c(t)^*$ is a complex-valued baseband impulse response accounting for transmitter filtering, the current channel response and receiver RF or IF filtering. The asterisk denotes complex conjugate. The parameter f_o is the carrier frequency. The complex-value a_n are the data symbols; for the case of QPSK, each a_n takes on the four possible values $(\pm 1\ \pm j)/\sqrt{2}$ where $j=\sqrt{-1}$. The symbol interval is T seconds, so that the baud rate is 1/T complex-valued data symbols per sec. In the case of 2400 bps QPSK, 1/T is 1200 hz. The complex waveform $n_p(t)$ represents additive noise. After a demodulation stage in the receiver

(multiplication by $\sqrt{2}\cos(2\pi f_o t)$ and by $\sqrt{2}\sin(2\pi f_o t)$ and low-pass filtering the baseband channel output can be presented by the complex-valued baseband waveform

$$y(t) = \sum_n a_n h(t-nT)^* + \nu(t) \qquad (3.2)$$

where $h(t)^*$ now includes the low pass filters and $\nu(t)$ is a complex noise waveform. The real and imaginary parts of y(t) are the outputs of the cosine and sine demodulators respectively. The complex baseband impulse response $h(t)^*$ also includes any channel phase shift. The complex representation of passband and baseband signals is more fully described in [Ung 74] and [Fal 76a].

The receiver's demodulator is usually preceded by or includes a AGC (automatic gain control) to minimize the variation in the received signal level caused by severe fading. A symbol timing recovery subsystem is also necessary to ensure that the demodulated signal is sampled with the correct frequency 1/T and phase. The symbol timing problem on HF channels is intensified by the possibility that abrupt changes in the multipath pattern may change the channel's delay equally abruptly. Such an event can cause temporary loss of synchronization.

The demodulating carrier must also be synchronized, at least in frequency, to the transmitted carrier f_o. Frequency differences between transmitter and receiver oscillators, typically on the order of 100 hz or less, must be compensated by the carrier recovery subsystem.

Optimization of the demodulating carrier's phase shift is not so important, since any fixed phase shift may be compensated without penalty by a complex equalizer [Fal 76a] [Fal 76b]. A time-varying phase shift, caused by channel fading, may be regarded as part of the channel's complex baseband equivalent impulse response.

Figure 3.1 shows the "front end" of a synchronous receiver. The complex demodulator output y(t) is assumed to be sampled at a multiple of the symbol rate 1/T which is above the Nyquist rate. Most useful data signals, including those in our simulations, have excess bandwidths of less than 100%, and therefore a sampling rate of 2/T (2 samples per symbol), is appropriate. The resulting samples are the input to the equalizer. Note that the front-end structure of Figure 3.1, including faster-than-Nyquist sampling, causes no performance penalty if the noise is white and gaussian; the sequence of samples of y(t) is a set of sufficient statistics for estimating the sequence of data symbols with minimum error probability [Ung 74], [VH 81]. Sampling and subsequent equalization at the lower rate 1/T is also possible, but in this case, the system performance is more sensitive to the choice of sampling phase, and to channel delay distortion. Reference [GW 81] discusses the advantages of T/2-spaced equalizers over T-spaced equalizers.

The existence of several distinct more or less independent transmission modes (multipath) on an HF channel reduces the likelihood that a deep fade occurs (in which all paths fade simultaneously). However in return for this inherent diversity advantage of multipath, it may introduce severe frequency

selectivity. Attempts to compensate for severe frequency selectivity (implying nulls or near-nulls in the channel's frequency response) with a linear equalizer lead to noise enhancement and poor performance [MP 73], [Pro 75], [Mes 74]. Thus a nonlinear equalization technique such as decision feedback equalization (DFE) or maximum-likelihood sequence estimation (MLSE) is necessary. The effective duration of the complex baseband channel impulse response to be equalized is typically in the range of 2 to 8 msec. For a 2400 bps QPSK system with a symbol rate of 1200 hz, this amounts to an impulse response pan between 1 and 10 symbol intervals.

Significant time variability in the channel's impulse response over a period of several tens or hundreds of symbol intervals necessitates fast and accurate adaptation of the equalizer's parameters to the channel. The simplest LMS type of equalizer adaptation algorithm very effective for slowly-varying channels such as telephone channels [WH 60]. However there is some question as to its tracking capability for typical HF channels [HGDP 80], [Hsu 82]. In recent years filter adaptation algorithms have been developed, based on recursive least squares estimation criteria, which in a sense offer the fastest possible convergence to the optimal set of filter parameters in a time-invariant situation. These fast algorithms have the potential for fulfilling the fast-tracking requirements of HF channel equalization.

The adaptive algorithms for the HF channel equalizer, and possibly also for carrier and timing synchronization, use the

receiver's decisions on the transmitted data symbols as a reference. The effect of occasional decision errors should have a negligible effect on adaptation. However occasionally, "catastrophic" fades can occur, which cause a long sequence of errors and during which the equalizer "loses track" of the channel. An important system design question concerns "crash recovery" measures which minimize the time spent in recovering from such a catastrophic fade.

In Chapters 4, 5 and 6, we discuss the application of nonlinear equalization methods, fast filter adaptation methods, and synchronization techniques respectively to high-speed digital transmission on HF channels. A modified fast recursive least squares algorithm is introduced and its application to channel impulse response estimation is described. Chapter 7 describes the simulated receiver processing. Chapter 8 compares the attainable performance of DFE and MLSE equalization on actual HF channels, based on the results of channel impulse response measurements. Statistical characterization of HF channel impulse response properties, relevant to equalizer design and performance, are also reported. Chapter 9 describes the simulation of an adaptive DFE receiver on actual HF channels. Chapter 10 provides a summary and conclusions of this study.

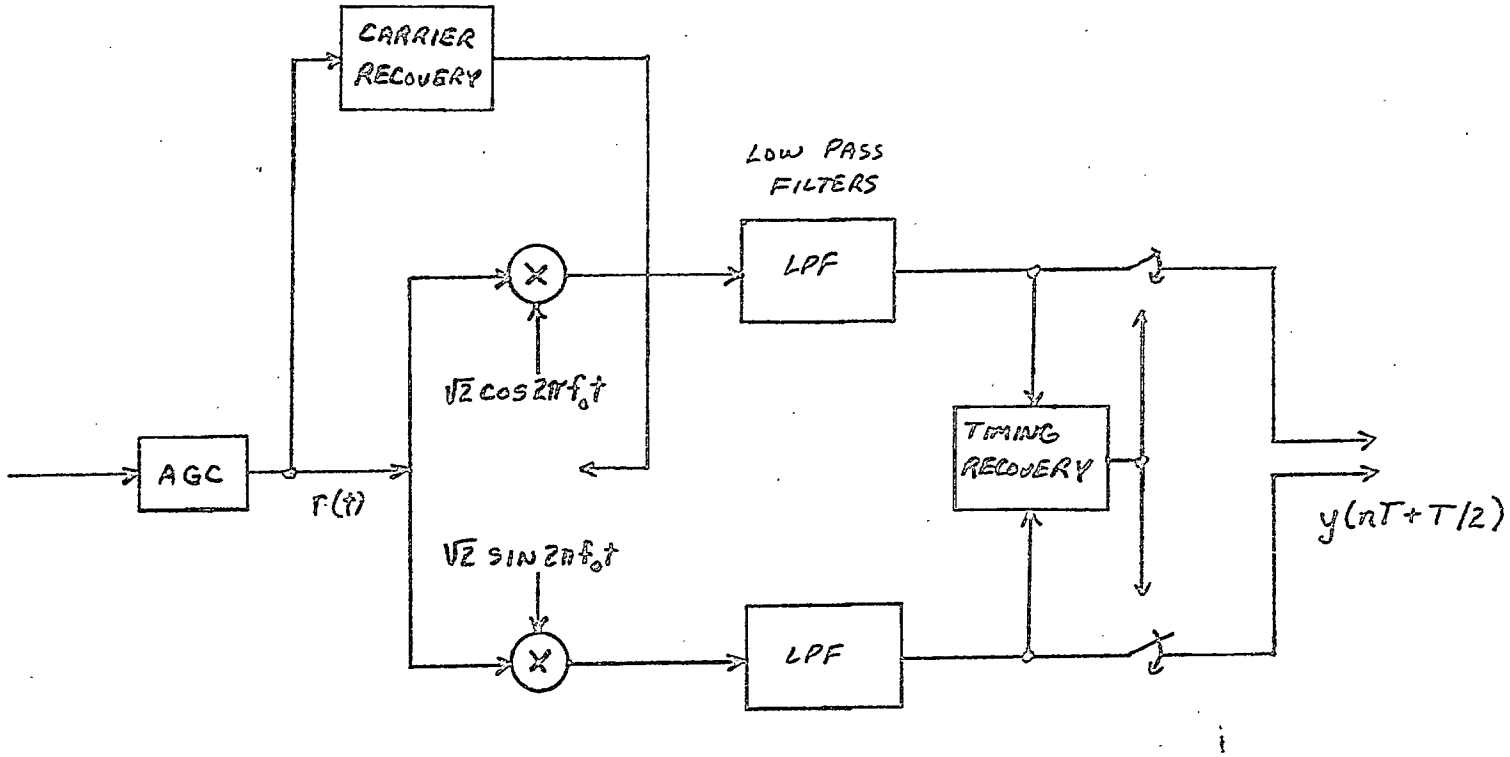

FIG. 3.1 RECEIVER FRONT END

4. CHANNEL EQUALIZATION

For high speed serial digital transmission over fading HF channels, one is forced to consider adaptive equalization techniques for channels with severe linear distortion. Adaptation problems are deferred till the next chapter. In this chapter we discuss appropriate equalization techniques.

Linear equalization, while effective for telephone channels, can incur a significant noise enhancement penalty when used to compensate for intersymbol interference on more severely distorted channels [Pro 75], [Mes 74]. In particular, a linear equalizer tends to amplify the channel noise at those frequencies most attenuated by the channel, in an attempt to produce a flat overall frequency response. Consequently nonlinear equalization methods such as decision feedback equalization (DFE) and maximum-likelihood sequence estimation (MLSE, also known as the Viterbi Algorithm) appear to be more appropriate for the HF channel.

4.1 MLSE Equalization

If the channel noise is assumed to be gaussian, then the receiver that is optimum in the sense of extracting the most likely sequence of a priori equiprobable data symbols from the received waveform y(t) is a MLSE receiver. Forney [For 72] first showed the application of this algorithm to channel equalization. A variation of the algorithm, and its extension to passband modulated data was proposed by Ungerboeck [Ung 74]. A version of the MLSE receiver which uses Nyquist-rate sampling and requires no channel-dependent analog filter is described in [VH 81]. Note

that these versions of the MLSE algorithm differ only in their implementation; each would extract the same maximum-likelihood sequence of data symbols from a receive waveform.

Assuming that 2/T is above the Nyquist rate, the complex baseband waveform (3.2) can be sampled at the rate 2/T without degradation. Then the MLSE receiver determines the <u>maximum-likelihood</u> sequence of data symbols $\{a_k\}$ which minimizes, up to time n, the running sum [VH 81].

$$J_n = \sum_{k=0}^{n} \left| \sum_{m=0}^{N-1} h(mT)^* a_{k-m} - y(kT) \right|^2 + \sum_{k=0}^{n} \left| \sum_{m=0}^{N-1} h(mT+T/2)^* a_{k-m} - y(kT+T/2) \right|^2 \tag{4.1}$$

where NT is the time duration of the channel's impulse response. The MLSE algorithm must obviously know or have an accurate estimate of the 2 NT samples of the channel impulse response $h(t)^*$ at T/2 second intervals.

Ungerboeck's MLSE receiver requires a matched filter at its input, while Forney's requires a "whitened matched filter", which, in the case of white noise, has a Nyquist-equivalent frequency response uniform in magnitude (therefore causing no noise enhancement) and tends to yield an overall sampled impulse response that is minimum-phase. It was pointed out by Price [Pri 72] and Forney [For 72] that this whitened matched filter is the same as the front end filter of an infinite-length zero-forcing decision feedback equalizer. MLSE receivers employing adaptive decision-directed estimation of <u>a priori</u> unknown channel impulse

responses were studied in [MP 73] and [Ung 74]. Figure 4.1 shows a block diagram of such an adaptive MLSE receiver.

The computational and storage requirements of the MLSE receiver increase exponentially with the duration of the channel's impulse response. For a QPSK (four-phase) system in which the impulse response of the channel plus transmit and receive filters spans N symbol intervals, the number of distinct channel states (which is also proportional to the number of memory locations and MLSE algorithm operations required per output data symbol) is 4^N. The metric J_n is computed and stored for each state in each symbol interval, as is the most likely sequence of data symbols leading to each state. The MLSE algorithm's delay in releasing reliable data decisions (prior to where the paths merge) is typically on the order of 5 times the channel's memory.

Complexity considerations limit the application of the MLSE algorithm to short-impulse-response channels. Adaptive receiver structures which pre-equalize the channel output so as to create an overall impulse response of short duration were described and evaluated in [FM 73], [Mes 74], and [FM 76a], [FM 76b]. Another approach, explored in [McL 80], called for ignoring all but a short, judiciously chosen portion of the channel impulse response. The ignored portion contributes intersymbol interference. This approach results in only a small degradation if most of the energy in the impulse response is concentrated within a few symbol intervals. It was found to yield good results for 2400 kpbs data transmission on a fading HF channel under the assumption that the effective impulse response duration

was less than about 2.5 msec [CTLL 82]. However, the possible occurrence of longer impulse responses (up to say 8 msec) or the use of higher bit rates would yield a less attractive performance/complexity tradeoff for this approach.

The pre-equalization approach mentioned earlier can be employed with an adaptively-adjusted [FM 73], [Mes 74] or a fixed [FM 76a, b] overall impulse response. Because of the very wide variation of the HF channel, an adaptively-adjusted short overall impulse response would be preferable. Several authors have advocated a short decision feedback equalizer impulse response as an ideal overall impulse response [Mes 74], [DC 78]. The pre-equalizer in this case is the forward filter part of an adaptive decision feedback equalizer (DFE) with only a few (say less than 5) feedback taps. The feedback tap coefficients then constitute the overall impulse response used by the MLSE algorithm. The forward filter approximates a whitened matched filter, the opimum front-end of Forney's MLSE receiver [For 72]. It is important that for QPSK signaling, the DFE forward and feedback tap coefficients be allowed to be complex. If the feedback taps are constrained to be real, poor performance can result [FM 76b].

A related MLSE receiver with a DFE front end was discussed in [LH 77]. In this case the overall impulse response of the channel and forward DFE filter is shortened by estimating and subtracting the intersymbol interference due to all but the few most recent data symbols before processing with the MLSE algorithm. This estimation and subtraction is carried out by a

conventional DFE making preliminary decisions. In this system the MLSE performance is affected (adversely) by any preliminary errors made by the DFE.

4.2 DFE (Decision Feedback Equalization)

Figure 4.2 shows a block diagram of a decision feedback equalization (DFE) receiver. The forward filter is a transversal filter whose inputs are samples of the complex baseband channel output sampled either at T/2- or T- second intervals. The feedback filter is a T-spaced transveral filter whose inputs are previous data symbol decisions $\hat{a}_n$. The input at time n to the quantizer is

$$Q_n = \sum_{m=0}^{2N_1-1} W_m^* \, y(nT-mT/2) + \sum_{m=1}^{N_2} F_m^* \, \hat{a}_{n-m} \tag{4.2}$$

where $\{W_m^*\}$ are $2N_1$ complex forward tap coefficients and $\{F_m^*\}$ are N_2 complex feedback tap coefficients. Equation (4.2) can also be expressed as a scalar product of two complex partitioned vectors

$$Q_n = \underline{C}^* \, \underline{Z}(n) \tag{4.3}$$

where the asterisk stands for the complex conjugate transpose and

$$\underline{C}^* \equiv (W_o^*, W_1^*, \ldots W_{2N_1-1}^* \,\vdots\, F_1^*, F_2^*, \ldots F_{N_2}^*) \tag{4.4}$$

and

$$\underline{Z}(n)^* \equiv (y(nT)^*, y(nT-T/2)^*, \ldots y(nT-N_1T+T/2)^* \,\vdots\, \hat{a}_{n-1}^*, \ldots \hat{a}_{n-N_2}^*) \tag{4.5}$$

The forward filter tends to produce an overall causal sampled impulse response (with as much energy as possible in the first sample). The freedom from noise enhancement and consequent superiority of decision feedback equalization over linear equalization was shown in [Pri 72], [Sal 73] and [FF 73]. A series of papers by Monsen [Mon 71], [Mon 73], [Mon 74], [Mon 77] established its value in fading dispersive radio channels. A potential problem in decision feedback equalization is error propagation-feedback of erroneous decisions affecting later decisions. An upper bound on the error-multiplicative effect of error propagation reported in reference [DMM 74] indicates that error propagation is not an overwhelming problem if the number of feedback tap coefficients is small; the multiplicative factor in the bound is 2^{N_2} .

4.3 Comparison of DFE and MLSE

Under the assumptions that the channel impulse response is known to the receiver, the additive noise is gaussian, and that no prior decision errors have been made, the three types of equalization are ranked in order of increasing error probability as: (1) MLSE, (2) DFE, and (3) linear equalization. For comparison purposes, an ideal MF (matched filter) or "one-shot" receiver, consisting only of a matched filter, yields the lowest possible error probability in the case where only a single symbol is ever sent; i.e. zero intersymbol interference. Thus the theoretical rankings are:

(1) MF (One-shot) receiver (no isi)

(2) MLSE receiver

(3) DFE receiver

(4) Linear equalization receiver

↓ increasing error probability

However, the relative differences in performance depend critically on the actual channel impulse response. If the overall impulse response of the channel plus matched filter satisfies the Nyquist criterion, all four have the same error probability. In general, the more non-uniform is the amplitude-versus-frequency response of the channel, the greater is the spread in error probabilities of the above four systems. One of our goals has been to make a comparative evaluation of the theoretical error performance of systems (1), (2) and (3) for actual HF channels, based on their measured impulse responses.

Under the assumption that the channel noise is gaussian and white with double-sided power spectral density $N_0/2$, the theoretical error probability per complex-valued QPSK data symbol is approximately (for high signal-to-noise ratio) [For 72], [Ung 74], [Pri 72]

$$P_e = 2Q\ (d/\sigma) \tag{4.6}$$

where d/σ is an "effective signal-to-noise ratio" parameter characteristic of each system and

$$Q(x) \equiv \frac{1}{\sqrt{2\pi}} \int_x^{\infty} \exp\ (-y^2/2)dy \tag{4.7}$$

The application of (4.6) to the MLSE system is approximate, neglecting a constant in front of Q [For 72], [Mes 74], [Ung 74]. Equation (4.6) applied to DFE and linear equalizer systems assumes that they are optimized with the zero-forcing criterion; i.e. a sufficient number of tap coefficients is employed to minimize the noise variance subject to zero intersymbol interference at the decision point [Pri 72].

For the MF receiver, d/σ is the ratio of the received signal power to the noise power in a bandwidth 1/T, with

$$d_{MF} = \left[\frac{1}{T} \int_{-\infty}^{\infty} |h(t)|^2 \, dt\right]^{1/2} \tag{4.8}$$

where $h(t)^*$ is the channel's complex baseband impulse response. Also,

$$\sigma = \sqrt{N_o/T} \tag{4.9}$$

We have obtained estimates of the impulse response $h(t)^*$ of real HF channels at T/2-second sampling instants. From Parseval's relationship [Pro 83] then,

$$d_{MF} = \left[\frac{1}{2} \sum_i |h(iT/2)|^2\right]^{1/2} \tag{4.10}$$

For an ideal MLSE receiver, the parameter d_{MLSE} is half the <u>minimum distance</u> [For 72], [Mes 73], [Ung 74].

$$d_{MLSE} = \min_{[\varepsilon_0, \varepsilon_1, \ldots} \frac{1}{2T} \sum_{m_1 \geq 0} \sum_{m_2 \geq 0} \varepsilon_{m_1} \varepsilon_{m_2}^* \int_{-\infty}^{\infty} h(t-m_1T)^* \, h(t-m_2T) dt]^{1/2} \tag{4.11}$$

where the $\{\varepsilon_i\}$ are possible complex symbol errors

ε_0 = one of $\{\sqrt{2}, j\sqrt{2}, \sqrt{2} + j\sqrt{2}\}$

ε_i = one of $\{0, \pm\sqrt{2}, \pm j\sqrt{2}, \pm\sqrt{2} \pm j\sqrt{2}\}$ for $i>0$

For the T/2-sampled impulse response, corresponding to (4.10) we have

$$d_{MLSE} = \left[\min_{\epsilon_0,\epsilon_1 \cdots} \frac{1}{4} \sum_{m_1 \geq 0} \sum_{m_2 \geq 0} \epsilon_{m_1} \epsilon_{m_2}^* \sum_i h(iT/2-m_1T)^* \, h(iT/2-m_2T)\right]^{1/2} \tag{4.12}$$

Calculation of d_{MLSE} is a form of integer minimization problem. It is equivalent to the MLSE algorithm itself. The values of d_{MLSE} were computed for HF channels by searching (4.12) over ever-longer error sequences, giving a sequence of upper bounds, and comparing the results to a series of lower bounds, as described in [Mes 73]. The search stopped when the upper and lower bounds were within 1% of each other, at which point their average was taken as d_{MLSE}.

The lower bound for error sequences of length K+1 symbols [Mes 73] is given by

$$d_{LB} = \left[\min_{\epsilon_0,\epsilon_1, \cdots \epsilon_k} \sum_{n=0}^{K} \frac{1}{2} \left| \sum_{m=0}^{n} \epsilon_m \, C_{n-m} \right|^2 \right]^{1/2} \tag{4.13}$$

where the $\{C_n\}$ are given recursively by

$$C_n = \frac{2}{n} \sum_{m=0}^{n-1} (n-m) \, \rho_{n-m} \, C_m \qquad n \geq 1 \tag{4.14}$$

with $C_o \equiv \exp(\rho_o)$ (4.15)

and $$\rho_k \equiv \int_{-1/2T}^{1/2T} \frac{1}{2} \log_e (\hat{S}(f)) \exp(j2\pi fkT) df \tag{4.16}$$

$$S(f) \equiv T \sum_m R(mT) \exp(-j2\pi fmT) \tag{4.17}$$

$$R_m \equiv \frac{1}{T} \int_{-\infty}^{\infty} h(t)\, h(t+mT)^* \, dt. \qquad (4.18)$$

For sampled impulse responses, (4.18) is replaced by

$$R(m) = T/2 \sum_i h(iT/2)\; h\,(iT/2 + mT)^*$$

The parameter d for the DFE receiver is

$$d_{DFE} = 1/\sqrt{T}\; C_o \qquad (4.19)$$

where C_o is given by (4.15)-(4.18) [Mes 73] i.e.

$$d_{DFE} = \frac{1}{\sqrt{T}} \exp\left[\frac{T}{2} \int_{-1/2T}^{1/2T} \log_e (\hat{S}(f))df\right]. \qquad (4.20)$$

A similar d parameter can be defined for an ideal linear zero-forcing equalizer, but is not considered further here, because of its poor performance on channels with severe distortion.

The aforementioned formulas give the minimum error probabilities for <u>ideal</u> receivers in the presence of white gaussian noise. Their relative performance depends on the d parameter. As alluded to earlier it can be shown that [Pri 72], [Mes 73]

$$d_{MF} \geq d_{MLSE} \geq d_{DFE}$$

While these formulas do not take into account imperfections such as finite numbers of tap coefficients, non-gaussian, non-white

noise, inaccurate or time-varying channel reponse estimates, synchronization errors, etc., they do provide a convenient basis for comparison of inherent performance limits for each receiver technique, as well as a comparison with the zero-intersymbol-interference matched filter performance. They are used as a basis of comparison of the performance available from MLSE and DFE in Chapter 8.

As mentioned earlier, the DFE receiver, while offering the same or worse performance than the MLSE receiver, detects data symbols with much lower complexity than an ideal MLSE receiver if the channel's impulse response can be longer than about 3 or 4 symbol intervals. A non-ideal MLSE receiver, for which the channel impulse response has been shaped or equalized to one with a shorter duration, may include a DFE as its front end. The greater complexity of the MLSE receiver's decision-making algorithm may be partly compensated by the somewhat lower complexity of its adaptive channel estimation filter relative to the complexity of the adaptive filters in a DFE receiver. This will be apparent in the next chapter.

Another issue that affects the performance of the MLSE receiver is its sensitivity to errors in estimating the channel parameters: impulse response and phase shift. A comparative evaluation of DFE and MLSE receivers on voiceband telephone channels illustrated that for multilevel QAM-partial-response modulated systems, the DFE receiver is more robust to the impairment of carrier phase estimation errors and time-varying carrier phase shift [FM 76a,b]. A more recent study of non-partial response BPSK systems showed a lack of sensitivity of

MLSE performance to these factors. The relative sensitivity of QPSK systems should lie between these two extremes, and will depend on the channel's impulse response. In fact, an analysis of the decrease in d_{MLSE} due to a carrier phase error Δ, similar to that reported in [FM 76a] for multilevel QAM systems, was done for a QPSK system assuming a duobinary (partial response class I) channel response. The term d_{MLSE} was diminished only by a factor $(1-2 \sin \Delta)$ in the worst case. This contrasts with a factor $(1-10 \sin \Delta)$ for a 16-point QAM constellation found in [FM 76a]. We may conclude that the effects of carrier phase errors on the performance of MLSE QPSK-modulated systems is moderate; however carrier phase errors can have a rather large effect on performance for multi-level QAM systems.

The effect of errors in estimating the channel's impulse response was reported in reference [MP 73]. It was shown that the approximate effect of these errors is to increase the noise variance by the mean squared error in estimating the channel output samples with the slightly incorrect estimated channel impulse response.

An issue related to the MLSE receiver's performance sensitivity to channel parameter estimation errors is its tracking ability in estimating the impulse response and/or carrier phase of a time-varying channel. The estimate of the channel impulse response is updated adaptively using receiver decisions on the transmitted data symbols, as outlined in the next section. The MLSE detection algorithm achieves its optimality at the expense of delayed receiver decisions; a

typical delay in releasing reliable data is 20 to 30 symbol intervals. The estimated impulse response from an adaptation algorithm which uses these delayed receiver decisions, is delayed an equal amount; in effect the adaptation algorithm provides an estimate of the channel's impulse response which is 20- to 30-symbol intervals "older" than that which would be provided in a DFE or other receiver which yields decisions with little or no delay. An HF channel's impulse response can change in a period of 20- to 30-symbol intervals. Thus the decision delay of the MLSE algorithm may have the effect of increasing the additive noise, through the increased error in the decision-directed estimate of the channel impulse response

This problem of delayed channel response estimates in an adaptive MLSE receiver may be dealt with in three ways:

(1) It may be ignored, in the hope that the typical channel change is 20 to 30 symbol intervals (17 to 25 msec. at a symbol rate of 1200 hz) is negligible.

(2) Linear or polynomial extrapolation of the estimated impulse response may be employed [CM 81]. Here, extrapolation error becomes a problem.

(3) Preliminary decisions, say from a front-end decision feedback equalizer may be employed by the channel response adaptation algorithm. This is likely the most practical solution if the MLSE receiver is implemented with a DFE front end. However, it may be sensitive to DFE errors.

In summary, the choice between decision feedback equalization and maximum-likelihood sequence estimation for digital transmission on HF channels involves weighing the MLSE receiver's theoretically superior performance against the DFE receiver's lower detection complexity and its use of non-delayed decisions for adaptation. Our study of HF channel response parameters described in Chapter 8 is intended to shed light on these factors.

The receiver simulations reported in Chapter 9 are of a DFE receiver. As we have seen, a DFE may be used in its own right or as the front-end of a MLSE receiver. Thus the DFE receiver simultations may also be applicable to a type of MLSE receiver.

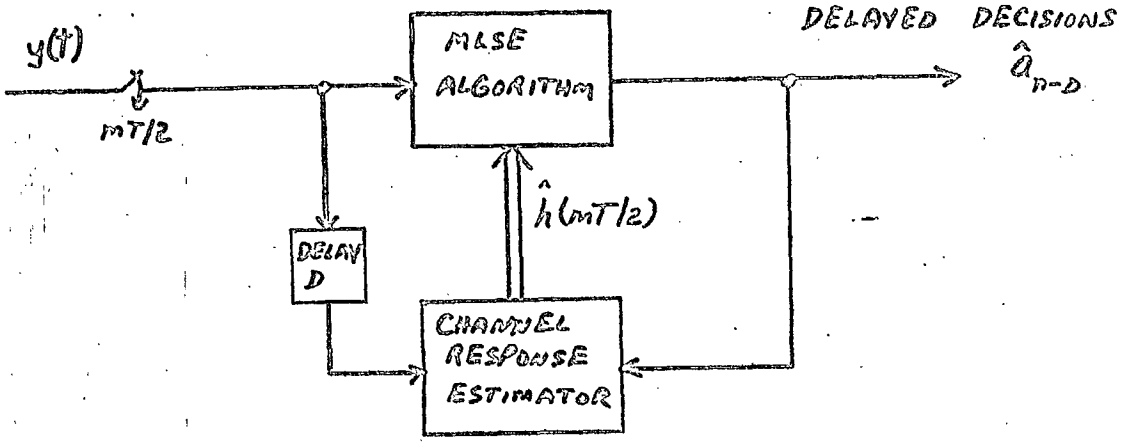

FIG. 4-1 ADAPTIVE MLSE RECEIVER

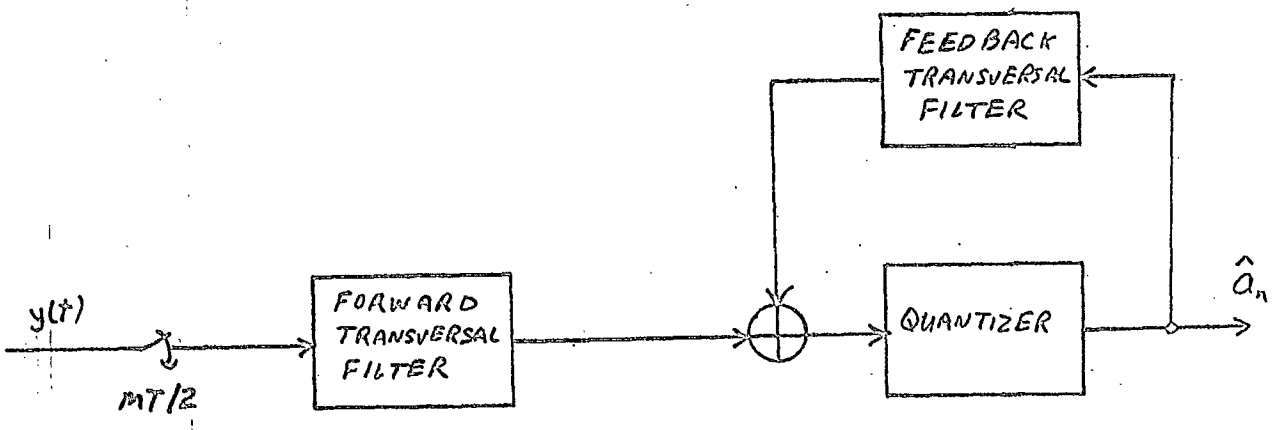

FIG. 4-2 DECISION FEEDBACK EQUALIZATION RECEIVER

5. ADAPTATION TECHNIQUES

The extent and rapidity with which the fading HF channel varies distinguishes it from most other types of bandlimited dispersive channels used for data communication. Previous studies [Mas 82], [CTLL 82], [HGDP 80] have indicated that the ability of the adaptive equalization algorithm to track the time-varying channel response is at least as important as the choice of the equalization method itself.

5.1 The LMS Algorithm

The most commonly employed equalizer adaptation algorithm for voiceband telephone and other channels is the LMS algorithm or variations of it [WH 60], [WMLJ 76], [Ung 72], [Pro 75], [GBS 71], [FM 76a, b], which can be applied to linear equalizers, DFE's or MLSE pre-equalizers or to channel impulse response estimation. If the samples stored at the N taps of a transversal adaptive filter are represented by the N-dimensional vector $\underline{Z}(n)$ at time n, if the corresponding tap coefficient vector is $\underline{C}(n)^*$, and if the desired filter output is d_n, then the coefficient vector is updated in the LMS algorithm as follows:

$$\underline{C}(n+1) = \underline{C}(n) + \gamma\, e(n)^*\, \underline{Z}(n) \qquad (5.1)$$

where

$$e(n) = d_n - \underline{C}(n)^*\, \underline{Z}(n) \qquad (5.2)$$

and γ is a positive constant called the adaptation step size.

For stationary inputs and small enough γ this algorithm can be shown to converge eventually to the coefficient vector $\underline{C}$ that minimizes $\langle |e(n)|^2 \rangle$, the mean-square of $|e(n)|$. The speed with

which it converges depends on γ and also on the spread in the eigenvalues of the positive definite autocorrelation matrix [WMLJ 76], [Ung 72]

$$A \equiv < \underline{Z}(n)\ \underline{Z}(n)^* > \qquad (5.3)$$

The LMS algorithm of (5.1) and (5.2) is of the same form for each type of equalizer. For a linear equalizer, the components of the vector $\underline{Z}(n)$ are complex samples of the baseband channel output at either T- or T/2-second intervals. For a decision feedback equalizer $\underline{Z}(n)$ is a partitioned vector consisting of both sampled channel outputs and previous receiver decisions as in equations (4.4) and (4.5). In both of these equalizers, the desired output d_n is the receiver's most recently-decided data symbol $\hat{a}_n$. In the case of channel impulse response identification as employed in a MLSE receiver, the components of $\underline{Z}(n)$ are the receiver's most recent decisions $\hat{a}_n$ (possibly delayed by the MLSE algorithm), and d_n is the correspondingly delayed complex channel output sample y(nT).

In the LMS algorithm the step size γ must be inversely proportional to the number of coefficients N for a reasonable steady state mean squared error but small values of γ limit the ability of the LMS algorithm to track variations in the optimal coefficient vector [WMLJ 76]. Thus if the impulse response of the adaptive filter, used for example as a channel estimator for an MLSE receiver, is quite short (i.e., N is small), the LMS algorithm may be an adequate adaptive filter algorithm for fading HF channels [CM 81], [CTLL 82]. However previous simulation studies have indicated that longer adaptive filters, used for

example as linear equalizers, DFE's or pre-filters for MLSE receivers, may be able to use faster adaptation algorithms to advantage, at least for reasonably high signal-to-noise ratios [HGDP 80].

5.2 Recursive Least Squares Algorithm

Filter adaptation algorithms with faster tracking capability than the LMS algorithm are available for channel response estimation and equalization. These recently developed faster algorithms require roughly an order-of-magnitude increase in the number of arithmetic operations per processed sample, relative to the LMS algorithm, but they appear to be within the capabilities of existing or near-future VLSI signal-processing devices for signal bandwidths limited to 3 or 4 khz.

In particular a recursive least squares adaptation algorithm yields at any time nT that coefficient vector $\underline{C}(n)$ which minimizes a weighted sum of squares of the errors

$$\sum_{k=0}^{n} \left| \underline{C}(n)^* \, \underline{Z}(k) - d_k \right|^2 \lambda^{n-k} \qquad (5.4)$$

where λ is a positive constant equal or less than unity used for exponential weighting of the past. In the sense of this exact error minimization criterion then, the recursive least squares estimation algorithm makes the best possible use of all the data $\{\underline{Z}(k), d_k\}$ up to time n; therefore in this sense it converges and tracks "as fast as possible". The solution to this minimization problem can be put in a recursive form, simplifying it, but still requiring storage and manipulation of N-by-N matrices. In its recursive form the least squares adaptation algorithm is a

special use of a Kalman algorithm. The first application of the recursive least squares (RLS) or Kalman algorithm to the adaptation of an equalizer was by Godard [God 74], with extensions by Gitlin and Magee [GM 77]. Hsu et al [HGDP 80] found that RLS adaptation of a DFE for a simulated fading HF channel allowed the channel variations to be tracked satisfactorily most of the time, and the tracking performance was far superior to that of the simpler LMS algorithm.

The complexity (number of arithmetic operations) of the RLS adaptation algorithm applied to adaptive transversal filters can be markedly reduced by computational techniques related to those used in the Levinson algorithm for adaptive linear prediction [MLK 76]. The resulting reduced-complexity transveral filter algorithm, called the fast recursive least squares algorithm (FRLS) or "fast Kalman" algorithm [LMF 78], [FL 78], produces exactly the same optimum coefficient vector $\underline{C}(n)$ at each time n (assuming infinite precision arithmetic) but with storage and computational requirements proportional to N rather than to the N^2 requirements of the RLS algorithm. The next two sections show the application of the FRLS algorithm to the adaptation of a channel estimation filter and of a fractionally-spaced decision feedback equalizer.

Lattice filters are an alternative to transversal filters for adaptive equalization or channel estimation. Figure 5.1 shows a transversal filter and a lattice filter. Each of these filters is FIR (finite-length impulse response) and with the proper choice of filter coefficients, each can have the same

impulse response. The lattice coefficients k_{fi} and k_{bi} are adapted so as to minimize the mean squared values of each of the signals $e_f(i,n)$ and $e_b(i,n)$, which can be interpreted as i^{th} order forward and backward prediction errors, respectively. This minimization tends to de-correlate the N backward prediction errors $e_b(i,n)$ [VM 76], [MV 78], [Mak 78]. This de-correlation effect speeds the convergence of adaptive lattice filters. LMS-type adaptation algorithms can be used for the lattice coefficients, in which case $k_{fi} = k_{bi}$ for all i. The LMS joint adaptation of the lattice coefficients and the coefficients F_i for linear equalization has been carried out [MV 78], [SA 78], and found to yield faster convergence than LMS adaptation for the transversal filters at the expense of more multiplies and divides per sample.

A FRLS adaptation algorithm exists in several forms for lattice filters; in fact, it can be shown to perform the same minimization of (5.4) and therefore offers the same convergence and tracking performance as FRLS transversal filter adaptation [MLNV 77], [Mor 77], [ML 79], [Shi 82].

The application of FRLS adaptation of lattice filters for linear equalization has been described in [SP 81]. The extension to adaptive decision feedback equalization was given in [She 80] and [LP 82]. [LP 83] describes the application of a lattice DFE to fading HF channels. A prescription for the FRLS algorithms applied to adaptive DFE's with a <u>transversal</u> structure is found in [FL 78].

A unifying description, derivation and computer-simulation evaluation of FRLS algorithms for adapting transversal and

lattice linear equalizers with complex tap coefficients and fractional tap spacing on telephone channels has been provided in a paper by Mueller [Mue 81]. Comparable lattice and transversal FRLS algorithms were shown to exhibit virtually identical convergence rates. However, the number of complex multiplications per iteration required by the FRLS adaptive lattice algorithm is greater than that required by the FRLS adaptive transversal algorithm: the latter requires

$$N(p^3+6p) + 5/3\ p^3 + 2p^2 + 4/3\ p$$

while the former requires

$$N(13/3\ p^3 + 7p^2 + 11/3\ p) - 4p^3 - 5p^2 - 2p$$

where p is the number of new complex received samples processed per symbol. The above number of multiplications for FRLS transveral adaptive filters also holds for decision feedback equalizers [FL 78]: in this case p is 1 plus the number of samples per symbol interval processed by the forward filter. A FRLS lattice DFE processing one received sample per symbol (p=2) described in [LP 83] has approximately $18N_1 + 39N_2$ multiplications and divisions, where N_1 and N_2 are the numbers of forward and feedback tap coefficients respectively. Thus, from the standpoint of minimizing complexity, FRLS transversal adaptive filters appear superior to FRLS lattice adaptive filters.

A major consideration in addition to the tracking ability for time-varying channels of a fast adaptive filter algorithm is numerical stability. Numerical roundoff errors pose potential problems for <u>any</u> recursive least squares adaptation algorithm,

transversal or lattice, which minimizes (5.4), since according to (5.4) this minimization explicitly or implicitly forms and inverts a N by N matrix whose elements are found by accumulating weighted sums of all previous filter inputs. Previous simulation studies have reported that the FRLS adaptation algorithm tends to become unstable (the coefficients "blow up"), especially for λ less than unity [Mue 81], [HGDP 80], [Hsu 82], [CK 83]. More stable (i.e. blowing up after a much longer time) is the much more computation-intensive RLS algorithm. The most stable reported recursive least squares transversal adaptive filter is the "square-root Kalman" filter [Hsu 82], but even in this case, it was considered necessary to re-initialize the algorithm about once every 100 symbol intervals to avoid instabilities due to roundoff errors. It is worth noting that the relatively slow-converging simple LMS adaptive transversal filter does not fall prey to numerical stability resulting from round-off error. However digital implementation of the LMS adaptation algorithm must be carefully designed to avoid problems due to bias in some types of digital arithmetic [GMW 82].

Among the lattice adaptive filters the FRLS lattice has been found to exhibit better numerical stability than its FRLS transveral counterpart [Mue 81]. Still more stable is a normalized version of the FRLS lattice [Fri 82], which unfortunately is more computation-intensive, requiring square roots as well as multiplications and divisions.

It is unfortunate that the FRLS or "fast Kalman" adaptation algorithm, which is the least computation-intensive of all the equally-fast-converging RLS and FRLS algorithms, is also the most

numerically unstable. A recent study of this type of algorithm suggests modifications to it which may improve its numerical stability and even decrease its complexity somewhat [CK 83]. These modifications will be incorporated and discussed in the next section.

While the RLS and square-root Kalman transversal adaptive filters or the various lattice adaptive filters have been advocated for equalization of fading HF channels [HGDP 80], [Hsu 82], [LP 83], primarily for their numerical stability properties, we have focussed our attention on the simpler FRLS transversal adaptive filters and (for comparison purposes) the simplest LMS transversal adaptive filters. Even the LMS lattice adaptation algorithm requires more computations than the FRLS transversal filter. Moreover the adaptative lattice algorithms all require many more divisions than do the transversal filter algorithms; thus their complexity if implemented with most existing or contemplated digital signal processing devices is even greater.

Our remedy for the numerical stability problem of FRLS transversal filters is periodic re-initialization. We describe new restart procedures which guarantee smooth re-initialization of the adaptive algorithm without introducing any significant performance-degrading transients. These restart procedure appear to make the FRLS transversal filter algorithm viable for adaptive equalization of time-varying channels such as the fading HF channel.

5.3 Adaptive Channel Impulse Response Estimation

The MLSE receiver which finds the most likely data symbol sequence by minimizing the running sum (4.1), requires an estimate of the channel's impulse response $h(t)^*$, sampled at intervals of T/2, using T/2-spaced samples of the complex baseband channel output and prior receiver decisions as shown in Figure 4.1. Since for every data symbol a_k, there are two complex channel outputs y(kT) and y(kT + T/2), it is convenient to consider two sets of T-spaced channel outputs {y(kT)} and {y(kT + T/2)}, and two corresponding sets of T-spaced estimated channel impulse response samples $\{h(kT^*)\}$ and $\{h(kT + T/2^*)\}$.

In accordance with the weighted sum of squared errors criterion (5.4), an FRLS channel response estimation algorithm yields that N-dimensional vector $\hat{\underline{h}}(n)^{(1)}$ which minimizes

$$S(n)^{(1)} \equiv \sum_{k=0}^{n} |\hat{\underline{h}}(n)^{(1)*}\, \underline{a}(k) - y(kT)^{(1)}|^2\, \lambda^{n-k} + \delta\lambda^n |\hat{\underline{h}}(n)^{(1)}|^2 \tag{5.5a}$$

and (independently) that N-dimensional vector $\hat{\underline{h}}(n)^{(2)}$ which minimizes

$$S(n)^{(2)} \equiv \sum_{k=0}^{n} |\hat{\underline{h}}(n)^{(2)*}\, \underline{a}(k) - y(kT)^{(2)}|^2\, \lambda^{n-k} + \delta\lambda^n |\hat{\underline{h}}(n)^{(2)}|^2 , \tag{5.5b}$$

where N is the chosen duration in symbol intervals of the estimated response, δ is a small positive constant and the vectors are defined as

$$\hat{\underline{h}}^{(1)}(n)^* \equiv (h(0)^*,\ h(T)^*, \ldots\ \ h((N-1)T)^*) \tag{5.6a}$$

$$\hat{\underline{h}}^{(2)}(n)^* \equiv (h(T/2)^*,\ h(T+T/2)^*, \ldots\ \ h((N-1)T+T/2)^*) \tag{5.6b}$$

$$\underline{a}(k)^* \equiv (a_{k-1}{}^*,\ a_{k-2}{}^*, \ldots\ \ a_{k-N}{}^*) \tag{5.6c}$$

and

$$y(kT)^{(1)} \equiv y(kT) \tag{5.6d}$$

$$y(kT)^{(2)} \equiv y(kT + T/2) \tag{5.6e}$$

The superscripts on the channel impulse response vector and channel output samples denote one of the two possible sampling clock phases 0 or T/2. Henceforth these superscripts will be suppressed for convenience. The δ terms in (5.5a) and (5.5b) prevent any problems arising from singularities or near-singularities during initial startup.

The FRLS transversal filter, or "fast Kalman" algorithm applied to the adaptation of a channel impulse response vector $\underline{h}(n)^*$ consists of two parts [FL 78], [Mue 81], [CK 83].

Part 1

Initialization at n=0:

$\underline{\hat{h}}(0)$ = all-zero vector, $a_n = 0$ for $n \leq 0$. (5.7a)

At $n \geq 1$:

$$\underline{\hat{h}}(n) = \underline{\hat{h}}(n-1) + e(n)^* \underline{k}(n) \tag{5.7b}$$

where

$$e(n) = y(nT) - \underline{\hat{h}}(n-1)^* \underline{a}(n) \tag{5.8}$$

is the complex-valued error in approximating y(kT) by $\underline{h}(n-1)^*\underline{a}(n)$. The N-dimensional complex vector $\underline{k}$ is the "Kalman gain vector" and is updated in part (2). Again we point out that $\underline{\hat{h}}(n)$, and y(kT) and are understood to have superscript (1) or (2).

Part 2

Initial conditions at n = 0:

$\Gamma(0) = 1$ (a scalar) (5.9a)

$\underline{k}(0) = \underline{0}$ (5.9b)

$\underline{F}(0) = \underline{0}$ (N-dimensional forward prediction vector) (5.9c)

$\underline{B}(0) = \underline{0}$ (N-dimensional backward prediction vector) (5.9d)

$E(0) = \delta$ (a positive real number, which prevents singularities during start-up). (5.9e)

Then the vector $\underline{k}(n)$ is updated at time nT as follows ($n \geq 1$):

Forward prediction error:

$$f(n) = a_n + \underline{F}(n-1)^* \underline{a}(n) \tag{5.10}$$

Forward prediction update:

$$\underline{F}(n) = \underline{F}(n-1) - f(n)^* \underline{k}(n-1) \tag{5.11}^*$$

Updated forward prediction error:

$$f(n)' = \Gamma(n-1) f(n) \tag{5.12}$$

$$E(n) = \lambda E(n-1) + f(n)\, f(n)'^* \tag{5.13}$$

Extended Kalman gain (a N+1 - dimensional vector):

$$\bar{\underline{k}}(n) = \begin{bmatrix} E(n)^{-1} f(n)' \\ \hline \underline{k}(n-1) + \underline{F}(n)\, E(n)^{-1} f(n)' \end{bmatrix} \tag{5.14a}$$

which is re-partitioned as

$$\bar{\underline{k}}(n) = \begin{bmatrix} \dfrac{\underline{g}(n)}{\mu(n)} \\ \hline - \end{bmatrix} \tag{5.14b}$$

---

* Equations (5.11) and (5.18) represent a slightly different but mathematically equivalent formulation of the original FRLS algorithm [FL 78] suggested by Cioffi and Kailath [CK 83], which improve its numerical stability.

where $\underline{g}(n)$ is a N-dimensional vector and $\mu(n)$ is a scalar.

Backward prediction error:

$$b(n) = a_{n-N} + \underline{B}(n-1)^* \underline{a}(n) \tag{5.15}$$

Backward prediction update:

$$\underline{B}(n) = [\underline{B}(n-1) - \underline{g}(n)\ b(n)^*]\ [1-\mu(n)b(n)^*]^{-1} \tag{5.16}$$

Finally, $\underline{k}(n)$ is updated:

$$\underline{k}(n) = \underline{g}(n) - \underline{B}(n)\,\mu(n) \tag{5.17}$$

and $\Gamma(n)$ is updated:

$$\Gamma(n) = [\Gamma(n-1) - f(n)'^*\ E(n)^{-1}\ f(n)'][1-\mu(n)^* b(n)]^{-1} \tag{5.18}$$

A variation of this adaptation algorithm can be employed if it is desired to estimate the carrier phase shift separately from the complex channel impulse response. In this case rather than minimizing expression (5.5) we minimize

$$\sum_{k=0}^{n} \left|\hat{\underline{h}}(n)^*\ \underline{a}(k) - y(kT)\ \exp(-j\Theta(k))\right|^2 \lambda^{n-k} + \delta\lambda^n \left|\hat{\underline{h}}(n)\right|^2 \tag{5.19}$$

where $\Theta(k)$ is the estimated phase shift at time kT. Then in equation (5.8) $y(nT)$ is replaced by $y(nT)\ \exp(-j\Theta(n))$, and $\Theta(n)$ can be updated using a variation of the phase-updating algorithm used in [Fal 76a]:

$$\Theta(n) = \Theta(n-1) - \mathrm{Im}\left[\frac{\hat{\underline{h}}(n-1)^*\ \underline{a}(n)\ \exp(j\Theta(n-1))}{y(kT)}\right] \tag{5.20}$$

If $|y(kT)| < .001$, $\Theta(n) = \Theta(n-1)$.

In this way, the channel's impulse response and carrier phase estimate can be jointly estimated. If (5.20) is not employed, then the channel's phase shift is implicitly a complex factor in the complex impulse response estimate $\hat{\underline{h}}(n)$. Simulations of the FRLS impulse response estimation algorithm with (5.20) yielded

little improvement. Consequently subsequent simulations did not explicitly estimate phase angle as in (5.19) and (5.20).

5.4 Adaptive DFE

As shown in Figure (4.2) and as indicated by equation (4.2) a decision feedback equalizer processes $p_1 N_1$ incoming complex baseband samples with a linear transversal filter, whose output is combined with a linear combination of N_2 previous receiver decisions and then passed to a quantizer for a decision on the current symbol a_n. The integer p_1 is the number of incoming samples per symbol interval. p_1 is 1 for a T-spaced forward filter and 2 for a T/2-spaced filter. The input during the n_{th} symbol interval is expressed as $Q(n) = \underline{C}(n-1)^* \underline{Z}(n)$, where the partitioned vectors $\underline{C}$ and $\underline{Z}$ are defined in (4.4) and (4.5). They are N-dimensional, where

$$N = p_1 N + N_2 \tag{5.21}$$

An FRLS algorithm for adapting the tap coefficient vector $\underline{C}(n)^*$ minimizes the weighted sum of squared errors plus an exponentially decreasing term proportional to the magnitude squared of $\underline{C}(n)$.

$$S(n) = \sum_{k=0}^{n} |\underline{C}(n)^* \underline{Z}(k) - \hat{a}_k|^2 \lambda^{n-k} + \delta\lambda^n |\underline{C}(n)|^2 \tag{5.22}$$

where $0 < \lambda \leq 1$. Then analogous to (5.7) $\underline{C}(n)$ is updated as follows:

Part 1 of the DFE Adaptation Algorithm

$$\underline{C}(n) = \underline{C}(n-1) + e(n)^* \underline{k}(n) \tag{5.23}$$

where

$$e(n) = a_n - \underline{C}(n-1)^* \underline{Z}(n) \tag{5.24}$$

and the N-dimensional complex vector $\underline{k}(n)$ is updated as described in Part (2) below. Initially $\underline{C}(0)$ = the all-zero vector $\underline{0}$ and it is assumed that all channel outputs $y(nT)$ and $y(nT + T/2)$ and data symbols $\hat{a}_n$ are zero for $n \leq 0$.

At time nT, we can regard the p_1+1 newest inputs to the DFE (p_1 channel output samples and the latest receiver decision) as a p-dimensional vector $\underline{\xi}_p(n)$ where $p = p_1 + 1$. For example for a T/2-spaced forward filter p=3 and

$$\underline{\xi}_3(n) = \begin{pmatrix} y(nT+T) \\ y(nT+T/2) \\ \hat{a}_n \end{pmatrix} \tag{5.25}$$

while the p oldest inputs that have just left the DFE are represented by the p-dimensional vector $\underline{\rho}_p(n)$ which in the case $p_1=2$ is

$$\underline{\rho}_3(n) = \begin{pmatrix} y(nT - N_1T+T) \\ y(nT - N_1T+T/2) \\ \hat{a}_{n-N_2} \end{pmatrix} \tag{5.26}$$

Part (2) of the DFE Adaptation Algorithm

The forward and backward predictor vectors of (5.10) and (5.16) respectively are now replaced by N-by-3 matrices F(n) and B(n). The forward and backward prediction errors of (5.10), (5.12) and (5.15) are replaced by p-dimensional vectors $\underline{f}_p(n)$, $\underline{f}_p(n)$, and $\underline{b}_p(n)$ respectively. The quantity $\mu(n)$ is now a p-dimensional vector $\underline{\mu}_p(n)$, and E(n) becomes a p-by-p matrix $E_{pp}(n)$, whose initial value is δ times the p-by-p identity matrix I_{pp} Initial conditions at n=0:

$$\Gamma(0) = 1 \quad \text{(a scalar)} \tag{5.27a}$$

$$\underline{k}(0) = \underline{0} \quad \text{(N-dimensional vector)} \tag{5.27b}$$

$$F(0) = [0] \quad \text{(N-by-p forward predictor)} \tag{5.27c}$$

$$B(0) = [0] \quad \text{(N-by-p backward predictor)} \tag{5.27d}$$

$$E_{pp}(0) = \delta I_{pp} \tag{5.27e}$$

Then vector $\underline{k}(n)$ is updated as follows for $n \geq 1$

$$\underline{f}_p(n) = \underline{\xi}_p(n) + F(n-1)^* \underline{Z}(n) \tag{5.28}$$

$$F(n) = F(n-1) - \underline{k}(n-1) \underline{f}_p(n)^* \tag{5.29}$$

$$\underline{f}_p(n)' = \Gamma(n-1) \underline{f}_p(n) \tag{5.30}$$

$$E_{pp}(n) = \lambda E_{pp}(n-1) + f(n) f(n)'^* \tag{5.31}$$

For the DFE the equivalent of expression (5.14a) and (5.14b) appears somewhat more complicated, but is no more difficult to implement. The detailed derivation is [LMF 78] and [FL 79]. The result is a N-dimensional vector $\underline{g}(n)$ and a p-dimensional vector $\underline{\mu}_p(n)$ formed as follows (and as exemplified in Figure 5.2 for the case p=3).

(a) First form a p-dimensional vector

$$\underline{x}_p \equiv E_{pp}(n)^{-1} \underline{f}_p(n)' \tag{5.32a}$$

and a N-dimensional vector

$$\underline{y} \equiv \underline{k}(n-1) + F(n) \underline{x}_p \tag{5.32b}$$

(b) Set first p_1 components of $\underline{g}(n)$ = first p_1 components of $\underline{x}_p$

(c) Set next $p_1N_1 - p_1$ components of $\underline{g}(n)$ = first $p_1N_1 - p_1$ components of $\underline{y}$.

(d) Set first p_1 components of $\underline{\mu}_p(n)$ = components $(p_1N_1 - p_1 + 1)$, through p_1N_1 of $\underline{y}$.

(e) Set component (p_1N_1+1) of $\underline{g}(n)$ = component p of $\underline{x}_p$.

(f) Set components (p_1N_1+2) through N of $\underline{g}(n)$ = components (p_1N_1+1) through $(N-1)$ of $\underline{y}$

(g) Set component p of $\underline{\mu}_p$ = component N of $\underline{y}$.

Note that the transformations (b) through (c) are also followed in changing $(\underline{\xi}_p(n), \underline{Z}(n))$ to $(\underline{Z}(n+1), \underline{\rho}_p(n))$. Then backward prediction error is:

$$\underline{b}_p(n) = \underline{\rho}_p(n) + B(n-1)^* \underline{Z}(n+1) \qquad (5.33)$$

Backward predictor update:

$$B(n) = [B(n-1) - \underline{g}(n)\ \underline{b}_p(n)^*][I_{pp} - \underline{\mu}_p(n)\underline{b}_p(n)^*]^{-1} \qquad (5.34)$$

Update of $\underline{k}(n)$:

$$\underline{k}(n) = \underline{g}(n) - B(n)\ \underline{\mu}_p(n) \qquad (5.35)$$

Update of $\Gamma(n)$:

$$\Gamma(n) = [\Gamma(n-1) - \underline{f}_p(n)^* \underline{x}_p][1 - \underline{\mu}_p(n)^* \underline{b}_p(n)]^{-1} \qquad (5.36)$$

5.5 FRLS Algorithm Restart Procedures

Initial simulations of the FRLS adaptation algorithm applied to channel impulse response estimation and to DFE adaptation confirmed earlier findings: eventually the algorithm became unstable, and tap coefficients assumed unreasonable values. Running in single precision on a 36-bit Honeywell level 66 computer (28-bit mantissa including sign), a FRLS 10-tap-coefficient adaptive channel estimation algorithm typically became unstable after about 600 symbol intervalswith λ=.93. A double precision version typically went unstable after about 2000 symbol intervals. A single-precision FRLS DFE with 30 T/2-spaced forward tap coefficients and 10 feedback coefficients also went unstable, after about 600 symbols intervals with λ=.97.

As a remedy to the problem of instability due to accumulated roundoff errors we propose re-starting (re-initializing) the FRLS

algorithm at periodic intervals which are less than the typical time to become unstable. When a restart is initiated, the internal variables in part 2 of the FRLS algorithm are re-initialized - as in equation (5.9) for the adaptive channel impulse response estimator or as in equation (5.27) for the adaptive DFE.

For an N-parameter adaptive filter following a restart, the normal evolution of these internal variables, including the vector $\underline{k}(n)$ is disrupted for about N to 2N iterations. The disruption to $\underline{k}(n)$ would tend to cause a dissruption to the adaptive filter tap coefficient vector $\hat{\underline{h}}(n)$ updated as in (5.7) and (5.8) or to $\underline{C}(n)$ updated as in (5.23) and (5.24). However the effect of this dis ruption and the consequent impairment of the FRLS algorithm's tracking ability due to the re-initialization of the internal variables may be minimized by adapting the filter as specified by (5.7b) - (5.18) or (5.23) - (5.36), but not using its output. Instead during the restart interval (N to 2N iterations following initiation of restart), the output is taken from an auxiliary LMS-adapting filter whose tap coefficients were initialized to those of the FRLS filter just before the restart. The FRLS restart interval is sufficiently short that the momentary reliance on the slower-adapting LMS algorithm should cause little reduction in the adaptive filter's tracking capability.

Following a restart at time KT, all inputs y(kT), y(kT+T/2) and a_k are taken to be zero for $k \leq K$. In other words, for $n \geq K$, the N-dimensional input vector for purposes of adaptation is taken to be $\tilde{\underline{Z}}(n)$ whose components consist of

$$\tilde{y}(kT),\ \tilde{y}(kT-T/2),\ \tilde{a}_k = \begin{cases} y(kT),\ y(kT-T/2),\ a_k \text{ respectively} \\ \qquad \text{for } k \geq K \\ 0 \qquad \text{for } k \leq K. \end{cases} \tag{5.37}$$

However the use of the truncated input vectors $\underline{\tilde{Z}}(n)$ rather than the actual input vectors $\underline{Z}(n)$, which is necessary for the re-initialization of the FRLS adaptation algorithm may slow down its ability to track channel time variations during the restart period somewhat. The tracking ability may be improved by modifying the desired adaptive filter outputs d_n during the restart period (the d_n are channel output samples for the channel estimation algorithm and are receiver decisions for the DFE). To see how the $\{d_n\}$ should be modified we note that if there were no restart just prior to time nT, then we could express d_n as

$$d_n = \underline{C}(n)'^{*}\ \underline{Z}(n) + u_n \tag{5.38}$$

where u_n is an error due to noise and random data, and where $\underline{C}(n)'$ is the value $\underline{C}(n)$ would have in the absence of restart. Now define the N-dimensional vector

$$\underline{Z}(n)^{(-)} \equiv \underline{Z}(n) - \underline{\tilde{Z}}(n) \tag{5.39}$$

i.e. $\underline{Z}(n)^{(-)}$ contains only the components of $\underline{Z}(n)$ which occurred prio to n=K. Thus

$$d_n \backsim \underline{C}(n)'^{*}\ \underline{Z}(n)^{(-)} = \underline{C}(n)'^{*}\ \underline{\tilde{Z}}(n) + u_n \tag{5.40}$$

Since the restarted FRLS algorithm only has the vectors $\underline{\tilde{Z}}(n)$ available, and since the adapted tap coefficient vector $\underline{C}(n)$

should ideally approach $\underline{C}(n)'$, equation (5.40) suggests that during the restart period, the desired outputs used for FRLS adaptation should be during the restart interval

$$\tilde{d}_n = d_n - \underline{C}(n-1)_{LMS}^{*}\ \underline{Z}(n)^{(-)} \qquad (5.41)$$

where $\underline{C}(n-1)_{LMS}$ is the current set of tap coefficients from the auxiliary LMS algorithm. Note that when n exceeds K by a number of symbol intervals at least equal to the filter's memory, $\underline{Z}(n)^{(-)}$ is zero, and $\tilde{d}_n = d_n$. This modification to the $\{d_n\}$ was tested in our simulations. Also tried was an alternative modification:

$$\tilde{d}_n = \begin{cases} \underline{C}(n-1)_{LMS}^{*}\ \tilde{\underline{Z}}(n) & \text{during restart interval} \\ d_n & \text{after restart interval} \end{cases} \qquad (5.42)$$

Both variations (5.41) and (5.42) were first simulated in the channel impulse response estimation algorithm described in section 5.3, processing recorded baseband waveforms resulting from transmission of 2.4 kbps data through real HF channels. In these simulations, $\hat{\underline{h}}(K)$ was initialized to zero during each restart and an auxiliary LMS algorithm was used to generate output and modified desired outputs. Figure 5.3 illustrates the behaviour of both variations of the restart procedure as well as of an uninterrupted FRLS algorithm (which would eventually succumb to numerical instability) following restarts at 300 and at 615 iterations.

The relevant parameters were:

- N=10 complex tap coefficients
- restart at intervals of K=315 symbol intervals

- restart interval (time in which auxiliary LMS algorithm takes over)

  = 15 symbol intervals

- λ = .93

- δ = .1 (input data symbols all have unit magnitude)

- LMS adaptation parameter γ = .05

The channel used in this particular simulation was designated MDA006. It exhibited little or no time-variability, so the LMS and FRLS algorithms yielded similar performance. Figure 5.3 shows that the FRLS/LMS restart algorithm using equation (5.42) maintains a slightly higher (by less than 1dB) signal-to-noise ratio (ratio of desired output to the algorithm's error in estimating it) than the FRLS/LMS restart algorithm using equation (5.41). Furthermore the momentary dip relative to the uninterrupted FRLS algorithm is less than 1dB.

Figure 5.4 is for channel 'MDA 011', which is characterized in this time interval by occasional rapid deep fades and relatively low noise. In this figure, there is a sudden fade at about the 1680th symbol interval, which appears to last on the order of 20 to 40 msec. In the figure the SNR of the LMS algorithms as well as periodically-restarted FRLS algorithms with two different values of λ, .93 and .96 are shown. (The smaller is λ the faster the algorithm can track but the more "noisy" it is). It appears that this fade is so sudden and disappeared so quickly, that none of the three adaptation algorithms had time to change the tap coefficients significantly before the fade ended. Thus all three algorithms behave similarly. However, the FRLS algorithm with λ =.93

apparently allowed a greater change in its coefficients, with the result that it "strayed from the course" more than the other algorithms.

These simulations demonstrate that the FRLS algorithm can be re-initialized periodically with little or no disruption to the useful filter output signal in order to forestall numerical instability problems.

Figure 5.5 shows a record of the SNR fluctuations observed in adaptive channel impulse response estimation during 700 symbols intervals (about 583 msec.) on another channel, MDA010. Note that the FRLS and LMS algorithms appear to track equally well (or equally poorly) during this interval. Note too the more than 10-dB variation in SNR in this interval as a result of fading.

Figures 5.6 and 5.7 shows the cumulative probability distribution of the measured signal-to-noise ratio (SNR) for channel identification on channels MDA011 and MDA010 respectively. These results show that LMS-tracking of the channel's impulse response with a parameter $\gamma = .05$ may result in at least as high a SNR as FRLS-tracking with $\lambda = .93$.

5.6 More on the Numerical Stability of the FRLS Algorithm

Cioffi and Kailath have recently reported a study of FRLS algorithms [CK 83] with particular emphasis on their numerical stability problems and properties. They found that a tendency toward numerical instability can be related to algorithm initialization and also to the existence of a large steady state mean squared error, due for example to noise. A modified

initialization for the case where $\delta=0$ is given, which may be useful when the steady state mean squared error is small. The propensity toward numerical problems in systems with relatively large steady state mean squared error is especially relevant to equalizer adaptation for HF channels, since as we shall see in Chapter 8, the signal-to-noise ratio for such channels can be quite modest.

Cioffi and Kailath also give a mathematical reformulation of the FRLS adaptation algorithm (equations (5.11) and (5.18) and equations (5.30) and (5.36)) which improves its numerical stability somewhat. Further improvements are obtained by placing restrictions on some of the interval variables in the FRLS algorithm. It can be shown [LMF 78], [Mue 81], [CK 83] that the scalar factor $\Gamma(n)$ is real-valued and that it must be lower-bounded by zero and upper-bounded by 1. It can also be shown [CK 83] that the factor $(1-\underline{\mu}(n)^* b(n))$ in equation (5.18) and the factor $(1-\underline{\mu}_p(n)^* \underline{b}_p(n))$ in equation (5.36) is real and also bounded between zero and 1. In finite-word-length digital computation these constraints may eventually be violated if not enforced. In practice the above quantities can be checked on each iteration, and if they violate the above properties they are forced to be real and to be bounded by zero and 1. It has been observed [CK 83] that it is usually the bound

$$1-\underline{\mu}_p(n)^* \underline{b}_p(n) \leq 1$$

which is violated first, and we have found this to also be true in our simulations in the absence of period restart. Forcing

this quantity to 1 when the above bound is violated, or to a small positive quantity if the lower bound is violated, delays the onset of instability, but does not prevent eventual instability if periodic restarting is not applied. In our FRLS simulations of the DFE receiver, $\Gamma(n)$ is forced for be real, but the other constraints are not applied.

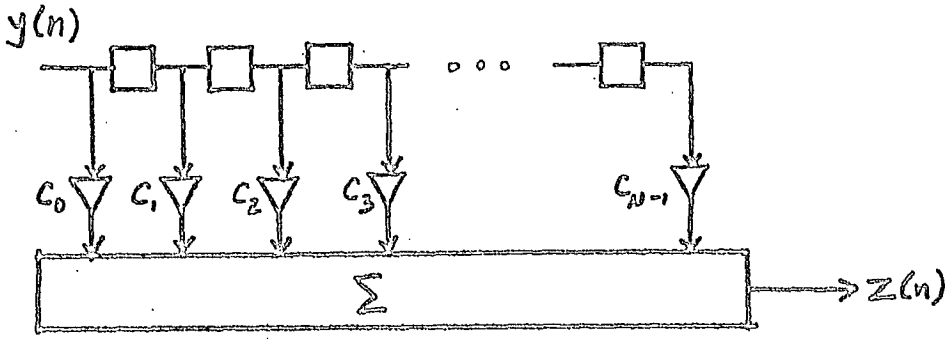

(a) TRANSVERSAL FILTER (BOXES ARE ONE-SAMPLE DELAYS)

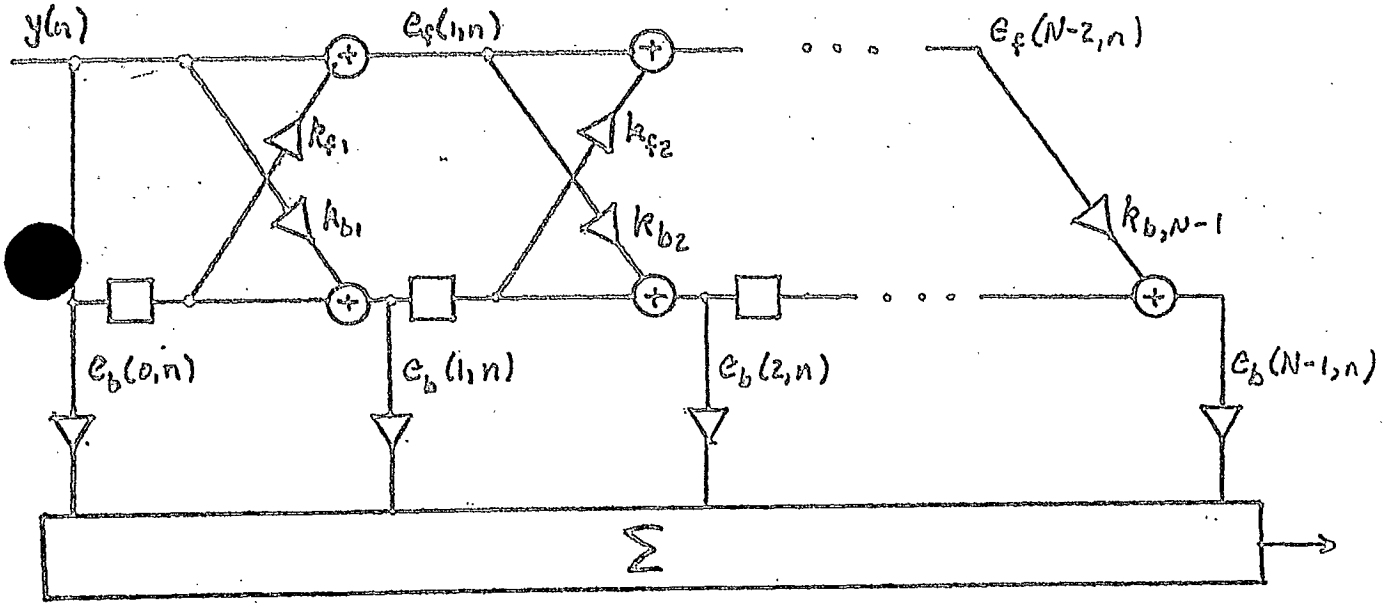

(b) LATTICE FILTER

FIG. 5.1 TRANSVERSAL AND LATTICE FILTER STRUCTURES

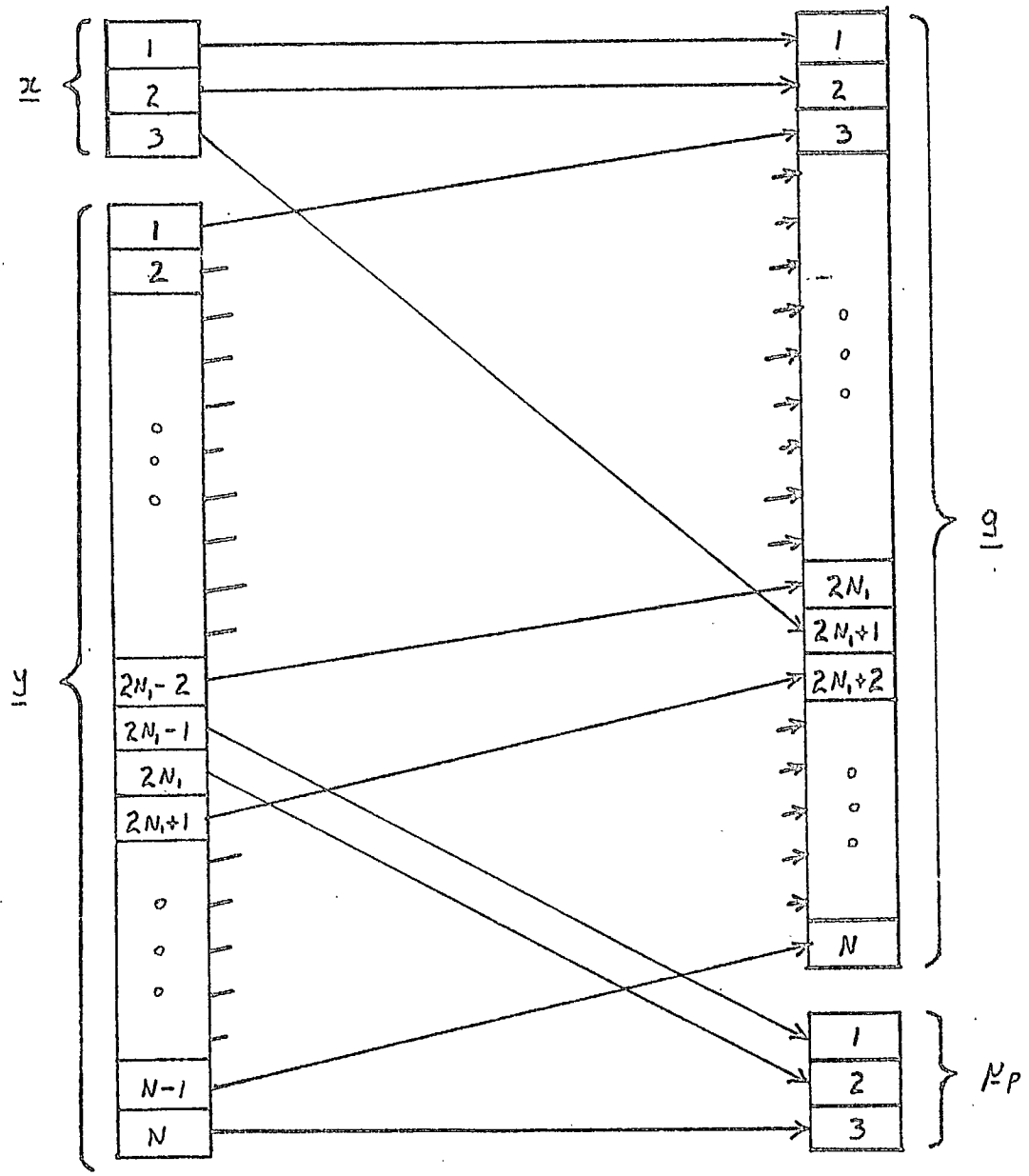

FIG. 5.2 FORMATION OF $\underline{g}$ AND N_p FOR FRLS ALGORITHM FOR DFE WITH $p = 3$.

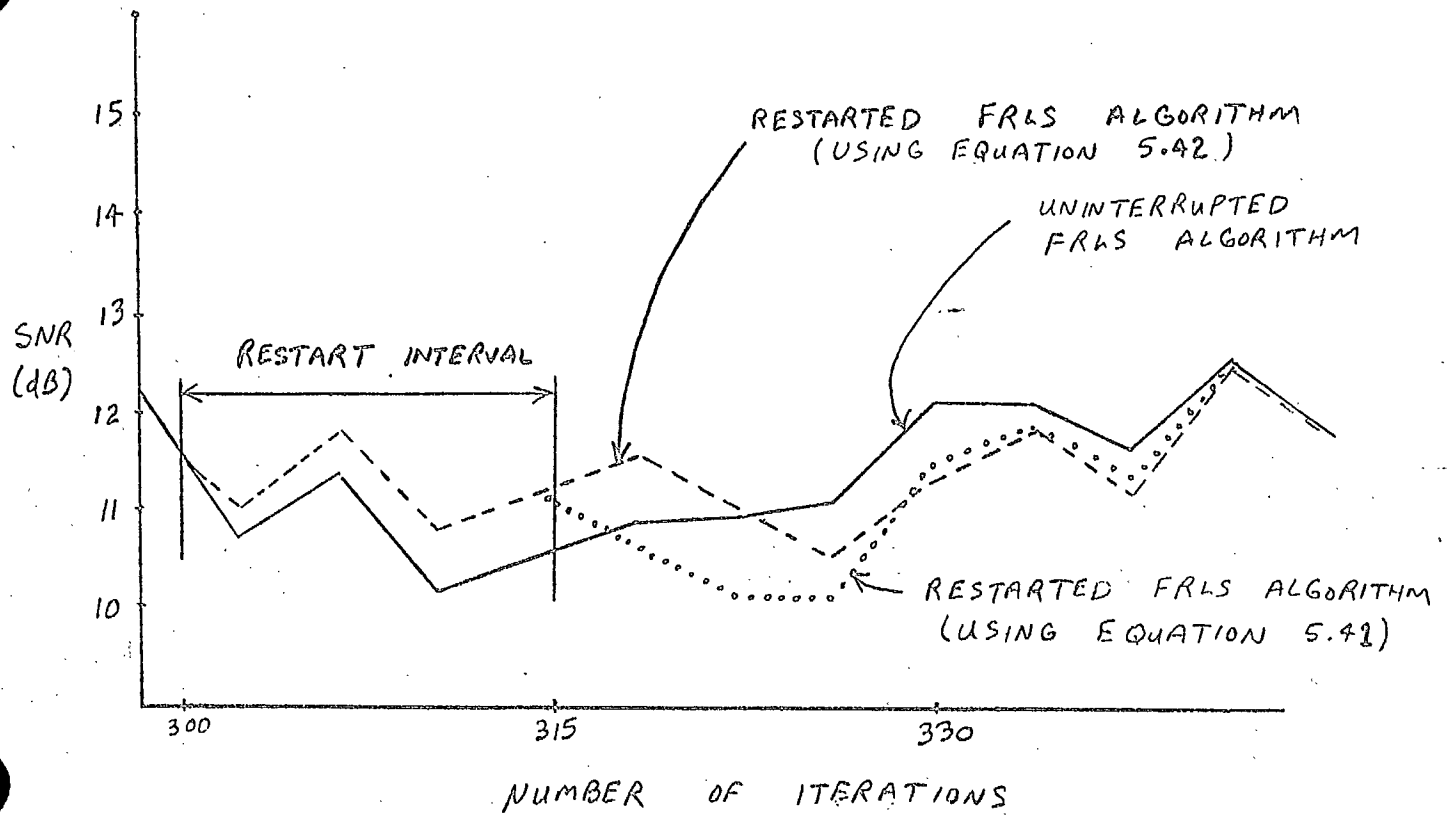

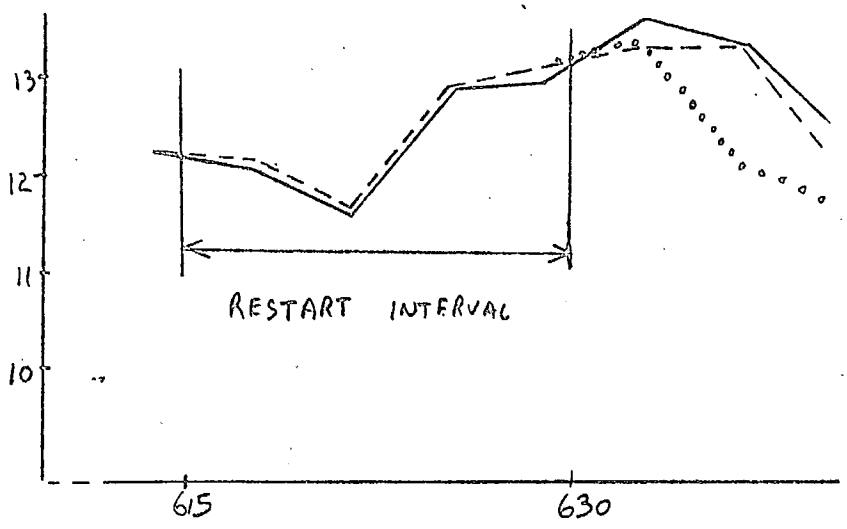

FIG. 5.3 RESTARTED CHANNEL RESPONSE ESTIMATION ALGORITHMS FOR CHANNEL MDA 006.

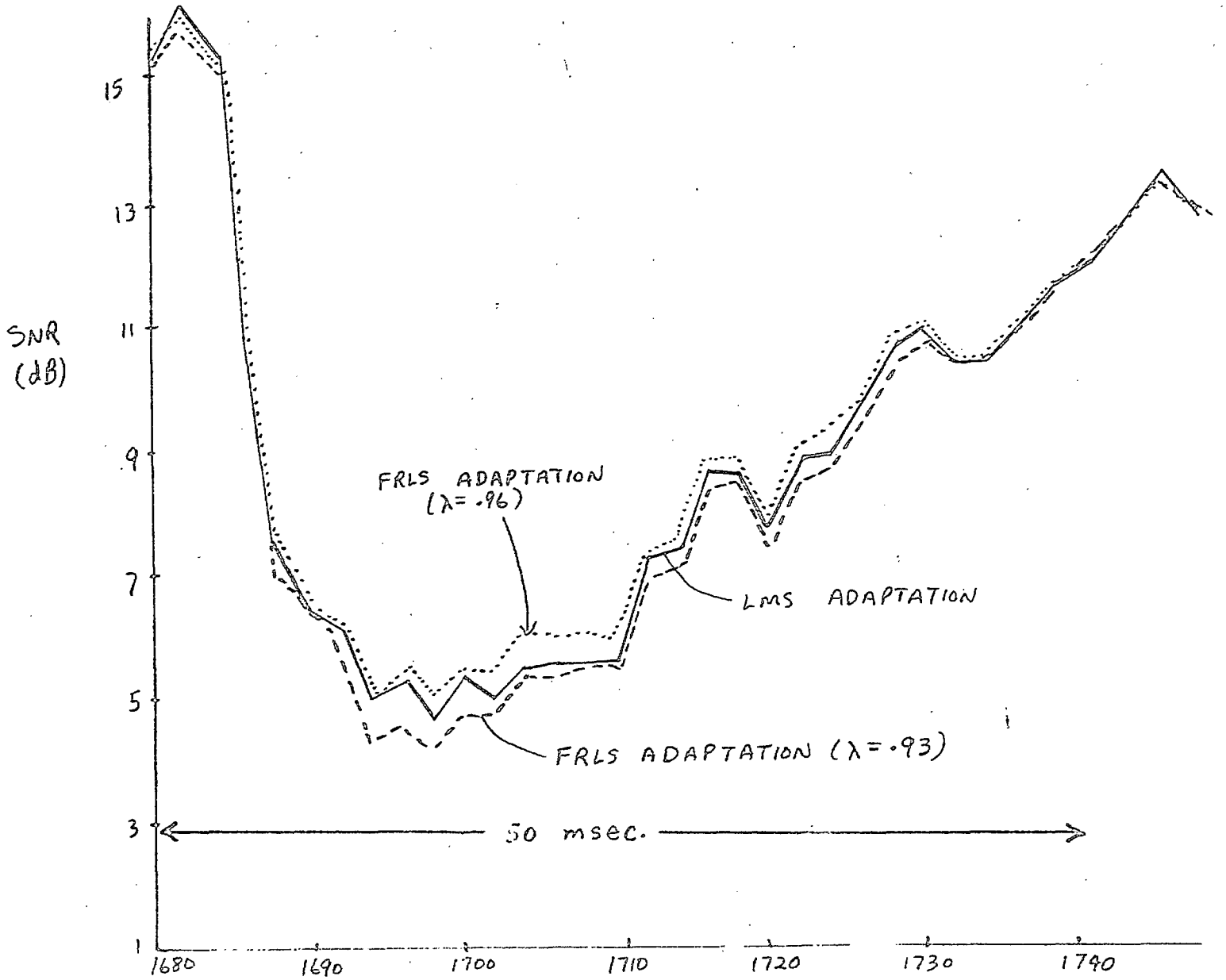

FIG. 5.4 FRLS AND LMS ADAPTATION ALGORITHMS (CHANNEL MDA011) DURING A FAST FADE

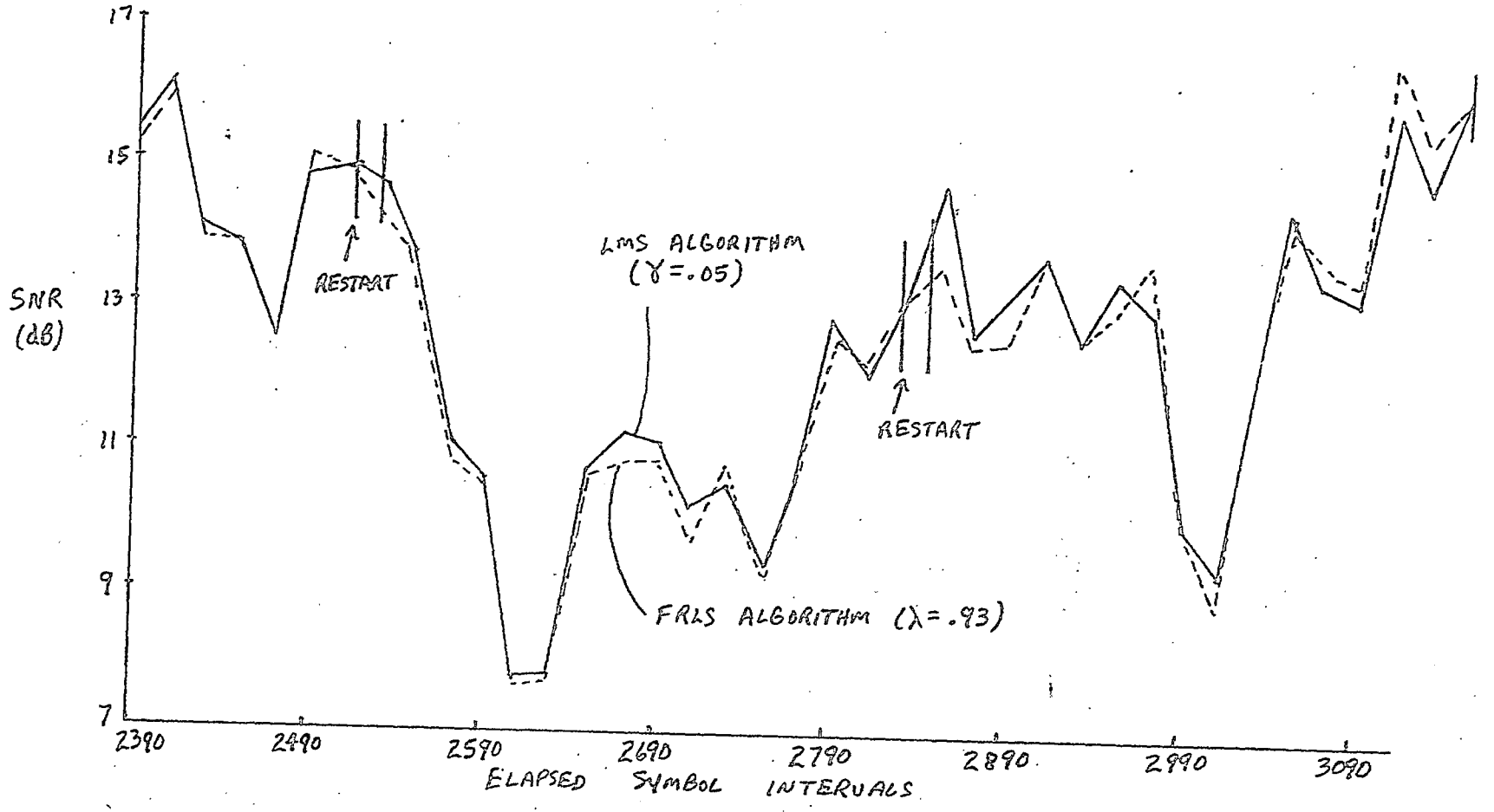

FIG. 5.5 FRLS AND LMS ADAPTATION ALGORITHMS (CHANNEL MDA 010)

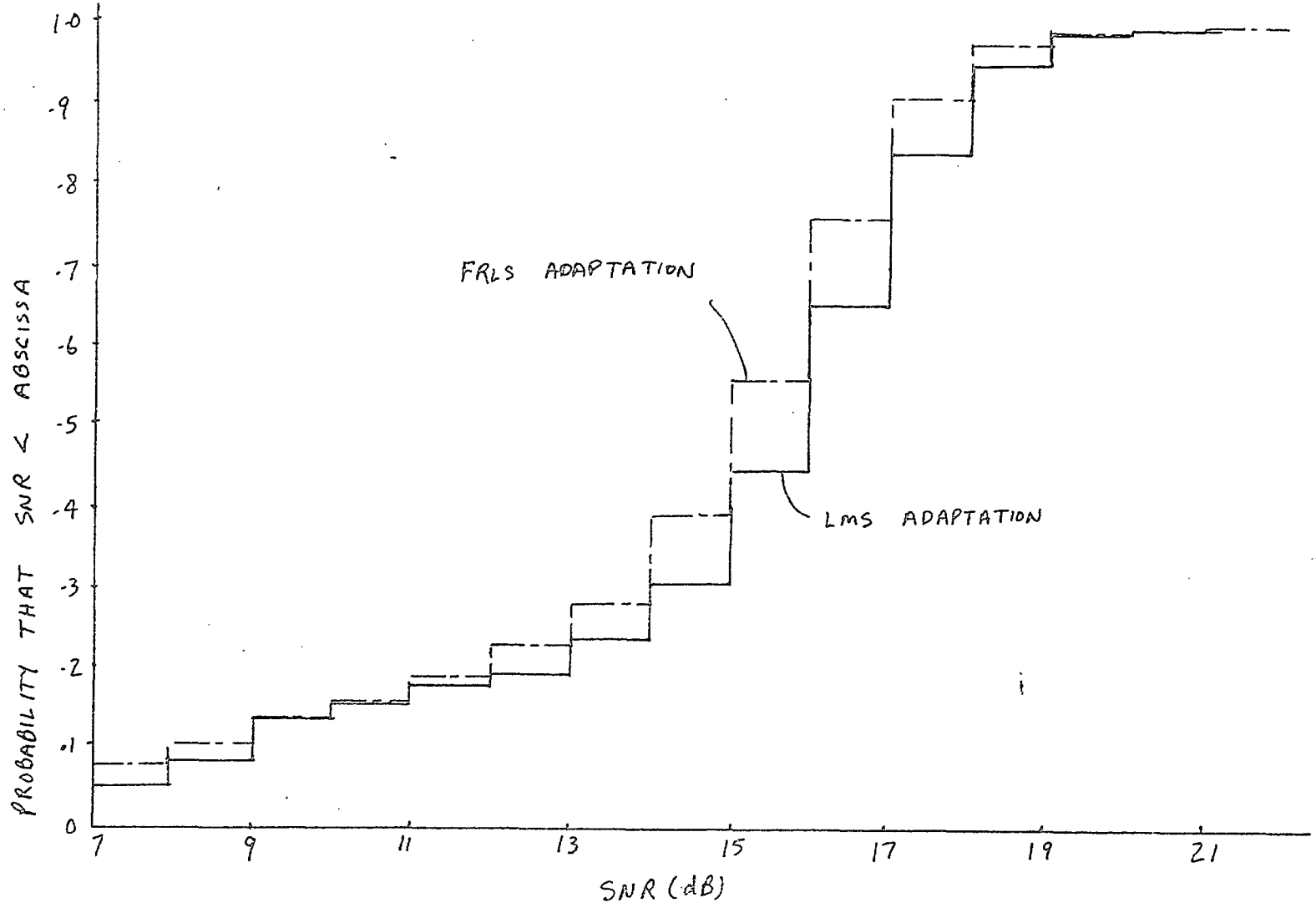

FIG. 5.6 SIGNAL-TO-NOISE RATIO STATISTICS FOR FRLS AND LMS ADAPTATION ALGORITHMS ON CHANNEL MDA 010

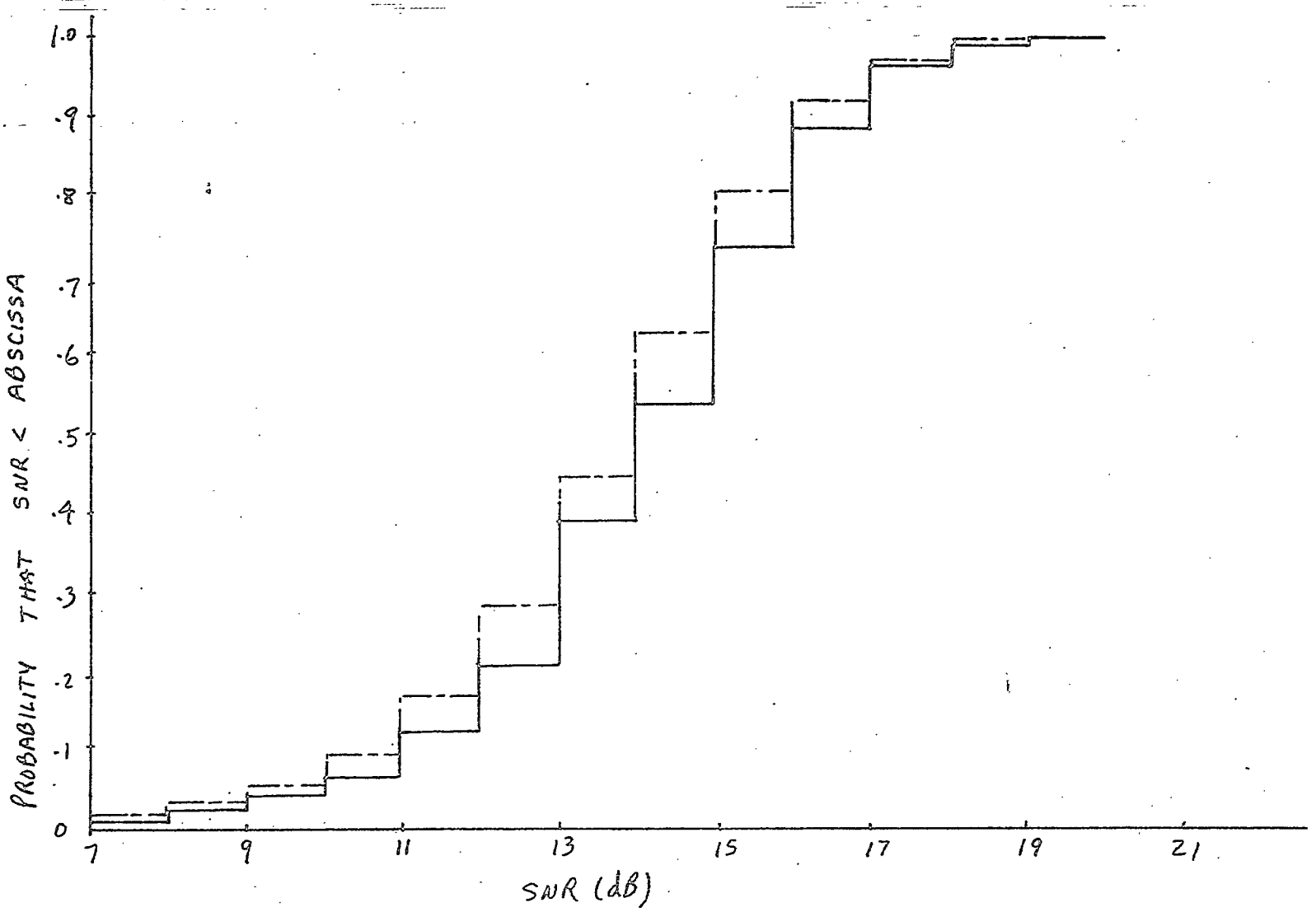

FIG. 5.7 SIGNAL-TO-NOISE RATIO STATISTICS FOR FRLS AND LMS ADAPTATION ALGORITHMS ON CHANNEL MDA 011

6. CARRIER AND TIMING SYNCHRONIZATION

6.1 Introducton

In a HF channel the unknown phase of the received signal consists of several components:

- constant phase shift due to the unknown propagation delay
- variable phase due to the changes in the channel response; which may include sudden changes in channel delay
- linear phase shift due to a frequency difference between the transmit and receiver oscillators
- slowly varying Doppler frequency

and - rapid fluctuations of the phase with a small magnitude due to system noise (phase jitter)

Some or all of these components could be observed during the intervals where the signal is present. These intervals are intermitted with deep fading intervals where a total loss of the received signal is encountered. The fading periods are usually long enough to cause total loss of the timing information as well as everything else.

The problem of timing and carrier synchronization should be approached in a way that takes into account the entire receiver structure. In our case the receiver consists of an adaptive equalizer which attempts continuously to estimate and match the channel parameters including its time-varying delay. Therefore, it is reasonable to assume that as long as the phase error time variation is no faster than that of the channel itself; it can be tracked and compensated for by the adaptive equalizer. So, the

equalizer does in part the syncrhonization function. Basically, there are two approaches in dividing the synchronization function between the equalizer and the synchronizer; these are:

(i) Individual circuits for synchronization and equalization; in that case one should build a synchronizer that corrects those phase error components that cannot be tracked by the equalizer; and

(ii) Jointly adaptive equalization and carrier recovery

Intuitively, the second approach appears to be superior to the first one; but this statement should be qualified by taking into account the channel characteristics and the added complexity to an already complicated equalizer.

Since the main thrust of this work is directed towards a comparative performance evaluation of different equalization methods, then the first approach will be followed.

At this point, we re-examine the various phase error components to determine which part of the synchronization will be done by the equalizer and which part would need a separate circuit. We divide the phase error components into three categories:

(i) Errors that could be corrected by the equalizer

(ii) Errors that can be best dealt with by a separate synchronizer

and (iii) Errors that are difficult to deal with by either the equalizer or the synchronizer.

The phase errors that could be corrected by the equalizer are those which are in-step with the variations of the complex channel impulse response; provided, of course, that the equalizer

itself is tracking these changes. This category includes: constant or slowly varying unknown delays as well as small Doppler frequency variations.

Large phase errors due to a fixed frequency off-set between the transmit and receive oscillators cannot usually be tracked by the equalizer. Fortunately, such an error can be easily handled by a simple AFC circuit. The same argument is applicable to Doppler frequency shifts (which may vary with time). Then, the major function of the synchronizer is to track the frequency detuning of the received signal and is to remove any frequency offset that might cause large phase variation which would unduly strain the equalizer performance.

An example of phase error components which should probably be left alone is abrupt phase changes. The reason is that such sudden changes in the channel response delay would be expected to accompany corresponding changes in other parameters of the response which would upset the equalizer. Then, there is little to be gained by tracking the phase information while the main part of the receiver is inoperable. Such rapid variations were observed in the recorded data with the results of either upsetting the equalizer or being ignored by it.

Fast phase jitter which is induced by the system noise and is characterized by small magnitudes and rapid variations may be best handled by a Costas loop or similar circuit.

The previous discussion seems to indicate that the most suitable approach for synchronization at this point of the investigation is to implement a separate circuit for phase

locking and to augment this circuit by an AFC circuit for rapid compensation of frequency errors. The problem of carrier synchronization is discussed in section 6.2, and the problem of timing (clock) recovery is discussed in section 6.3.

6.2 Carrier Frequency/Phase Synchronization

In view of the assumption that the adaptive equalizer will correct the phase variations resulting from changes in the channel delay, the three basic requirements of the carrier synchronization circuit becomes:

(i) Frequency tracking;

(ii) Fast recovery of the carrier frequency/phase at the beginning of the transmission or after a fade interval;

and (iii) Reduction of the noise-induced phase jitter.

The three requirements are listed in descending order based on their relative importance.

A small frequency error between the received and local carriers manifests itself as a continuous rotation of the equalizer tap coefficients. Such rotation was observed in the data used in the simulation study. However, the observed frequency offset was small and an attempt to correct it has resulted in a very small improvement in performance (< 1dB).

It is believed that there are two reasons for such a small frequency error: (1) highly stable oscillators were used to produce the data; and (2) the relatively small distance between the transmitter and receiver. Under more typical conditions the frequency error could be tens of cycles per seconds and variable.

Even when stable oscillators are used over longer distances, the Doppler effect could be substantial.

Fortunately, the frequency tracking is relatively a simple problem and there are several techniques to accomplish it. The received QPSK signal (without noise) can be written as:

$$r(t) = A \cos (2\pi f_o t + \theta(t)) \tag{6.1}$$

where $\theta(t)$ is assumed to consist of the phase modulation $\theta_o(t)$ and a frequency error term ($2\pi\Delta f t$); i.e.

$$\theta(t) = 2\pi\Delta f t + \theta_o(t) \tag{6.2}$$

To get rid of the modulation phase $\theta_o(t)$, the received signal should be passed through a 4th power device. The fourth harmonic of the received signal is:

$$r_1(t) = k A \cos (2\pi(4f_o)t + 2\pi(4\Delta f)t + 4\theta_o(t)) \tag{6.3}$$

The $4\theta_o(t)$ term is now a multiple of 2π and can be set to zero at all times. Figure 6.1 shows a general form of a frequency error detector for QPSK signals. The block diagram shown in the figure represents a very fast method to estimate the frequency error and make it available to the adaptive equalizer. The scheme can be modified to track the frequency of the received carrier as shown in Figure 6.2.

A second modification of the system shown in Figure 6.2 allows it to aquire and track the phase as well as the frequency of the received carrier. This is shown in Figure 6.3.

The operation of the circuit shown in Figure 6.3 goes through two stages: (i) Frequency acquisition, followed by (ii) Phase acquisition. During the frequency acquisition stage, the phase comparator goes through several cycle slippings due to the large phase error and the singular points in the phase transfer function. During a complete cycle the error signal contains positive and negative halves, and because the phase changes rapidly compared to the LPF time constant, the two halves will cancel each other. Therefore, the frequency comparator will dominate the VCO timing during this state producing a signal proportional to the frequency error. The output of the integrator will, in effect, sweep the VCO frequency driving it closer to the received frequency. As the frequency error decreases so does the signal at the integrator output, and when the two frequencies are nearly equal the role of the frequency comparator diminishes. At that point the phase acquisition starts. Now the phase error signal is slow enough for the LPF to track it and correct the phase of the VCO signal. It has been reported [EWH 81] that the inclusion of a frequency comparator in a PLL reduces the acquisition time significantly in the presence of an initial frequency error.

Some examples of the phase and frequency comparators are the Bidirectional Shift Register (BSR) and the three cell asynchronous delay line (ADL) [ED 82]. A generalized treatment of these kinds of comparators is given in [Obe 71], where they are viewed as combinations of Up-Down Counters (UDC).

Another type of frequency comparator is the Rotational Frequency Comparator (RFC) [Mes 79] which is based on comparing

the zero crossing relative locations in the two signals being compared. A schematic diagram of such a comparator is shown in Figure 6.4. The different situations encountered by the comparator are shown in Figure 6.4a, where f_2 ($\sim 4f_o$) denotes the frequency of the received signal and f_1 is the VCO frequency. The phasor diagram of f_1 and f_2 at two instants $1/f_2$ seconds apart is shown in Figure 6.4b. It is readily seen that the angle of rotation of f_2 is 2π, while the angle of rotation of f_1 is $2((f_1/f_2)-1)$ which is counter-clockwise if $f_1>f_e$ and clockwise if $f_1<f_2$. Therefore detecting the sign of the frequency offset is equivalent to determining the direction of rotation, while the magnitude is related to the angle of rotation.

A full cycle of the VCO output and its quadrature component is shown in Figure 6.4c and the cycle is divided into four quadrants A, B, C and D. Each of these quadrants is defined uniquely by the logical levels of the two carrier components. When the loop is in lock, the low-to-high transition of the incoming signal takes place in the same quadrant all the time. In the presence of a frequency offset, the transition will change quarters with time in a direction which depends on the sign of the frequency offset. The frequency of this change is directly related to the frequency error, in absolute value. An implementation of the comparator is shown in Figure 6.4d. In this implementation the VCO output and its quadrature components are sampled with the rising edge of the received signal. Two consecutive pairs of samples are stored in the D flip-flop's. Gate G_1 generates a narrow pulse whenever $Q_1Q_2Q_3Q_4=1101$

indicating that a transition from the quadrant B to C has taken place. Similarly, Q_2 generates a pulse whenever a transition from C to B occurs. Therefore, the output of Q_1 carries a pulse train only when $f_1 > f_2$ while Q_2 remains low. The frequency of occurance of these pulses is directly proportional to the frequency offset. The transfer characteristic of this comparator is shown in Figure 6.4e. The train of pulses coming out of Q_1 and Q_2 could be converted into a voltage signal proportional to the frequency offset (with the proper sign) as shown in Figure 6.4f. The main advantage of the RFC described above is the simplicity of implementation.

Another simple method that can be used to extract the frequency offset from the 4th harmonic of the received signal is given in [Par 70] and is shown in Figure 6.5.

Using equation (6.3), it is easy to show that A(t) and B(t) at the output of the two LPF's are:

$$A(t) = 1/2\ A \cos [8\pi\Delta f t] \tag{6.4}$$

$$B(t) = -1/2\ A \sin [8\pi\Delta f t] \tag{6.5}$$

and that the comparator output C is:

$$C = A^2/4\ (8\pi\Delta f) \tag{6.6}$$

This circuit was first proposed in 1970 by Park, but was somehow ignored because of the difficult implementation using analog discrete components. However, a digital version can now be implemented using some of the recently available digital signal processor chips.

6.3 Time Synchronizer

The extraction of timing information from the received signal can be accomplished by either operating on the received signal directly or by using the estimated channel response.

In the first case, there are many standard techniques that can be used to recover the clock from a modulated signal and to track that clock. The complexity of these techniques depends on the characteristics of noise and time disturbances in the channel. In general, a slowly varying channel can be tracked with simple PLL's, while abrupt time changes of the channel delay requires more elaborate designs.

Among the most common types of clock synchronization are:

i) The Nonlinear Bit Synchronizer

The widely used nonlinearities are the second order, fourth order, delay and multiple, absolute value and log [cosh(x)]. This technique has been discussed in several references, e.g. [WL 69], [Spi 77] and [Gar 79]. The technique has the advantages of simplicity and fast aquisition. On the other hand, the timing jitter due to noise may be unacceptable under low signal-to-noise conditions.

ii) In-Phase and Mid-Phase Bit Synchronizer

This is sometimes called the "Data Transition Tracking Loop" (DTTL). It has been first suggested by Lindsay and Transworth [LT 68] and investigated in [Sim 69] and [HA 70]. The technique is based on estimating the In-phase and Mid-phase of data transitions. The In-phase estimator determines the polarity of the data transition if and when they occur, while the Mid-phase determines the magnitude of

the timing error. An advantage of this technique is that during long periods between data transitions, the discriminator does not allow any noise to perturb the loop; it "holds" the last valid estimate.

iii) Early-Late Gate Synchronizer

This is also referred to as the absolute-value bit synchronizer (AVBS). It uses an early and a late integrate and dump channels. Its main advantage is having an absolute value operation, which makes it bit-independent. It was found in [Sim 70]. That his technique provides a 3 dB improvement in noise jitter over the DTTL and that it is also superior in terms of the mean time to first cycle slip; however, its aquisition time is longer than that of the DTTL.

Probably, for the purpose of this study, it is better to stay with the simple nonlinearity bit synchronizer, basically because of its fast aquisition performance, and in view of the fact that the adaptive equalizer will track the timing phase variation once aquisition is achieved it seems that there is very little to gain by adaptive more sophisticated timing recovery loops.

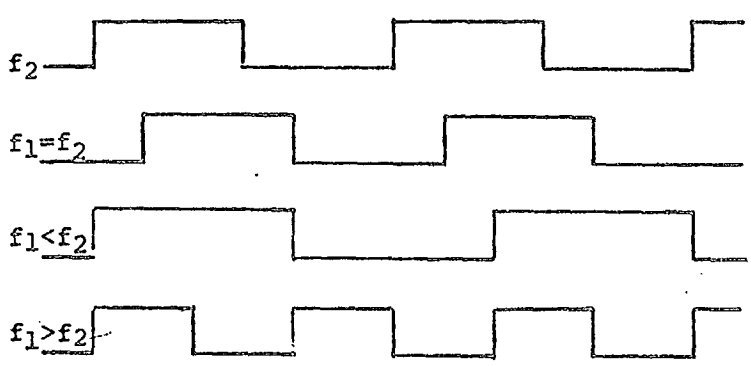

(a)

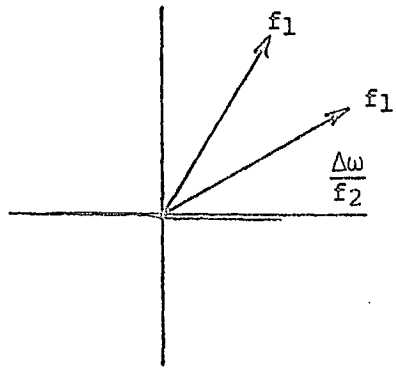

(b)

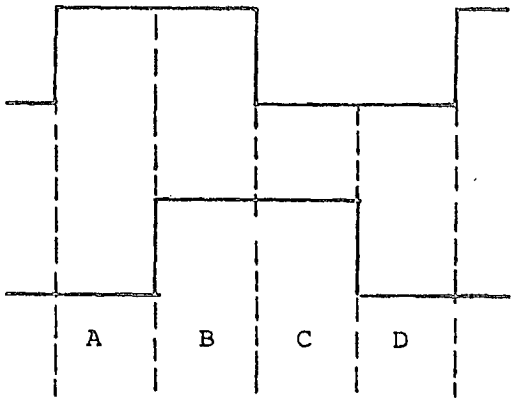

(c)

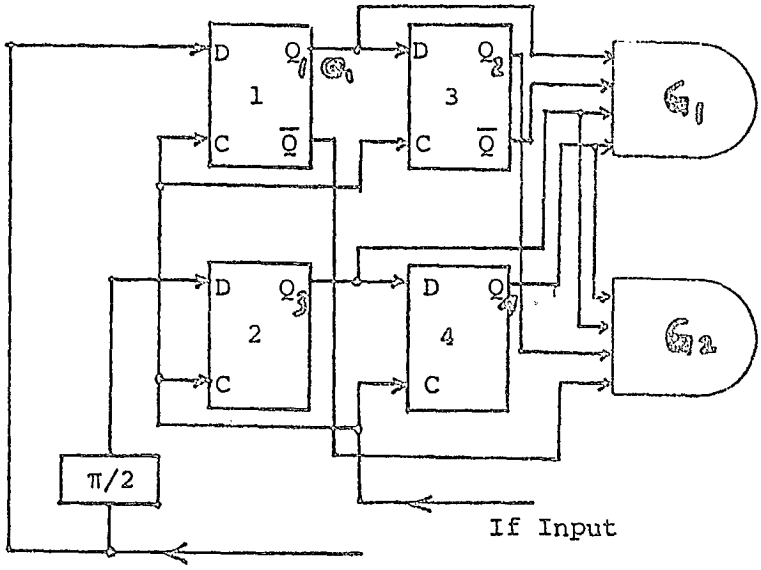

(d)

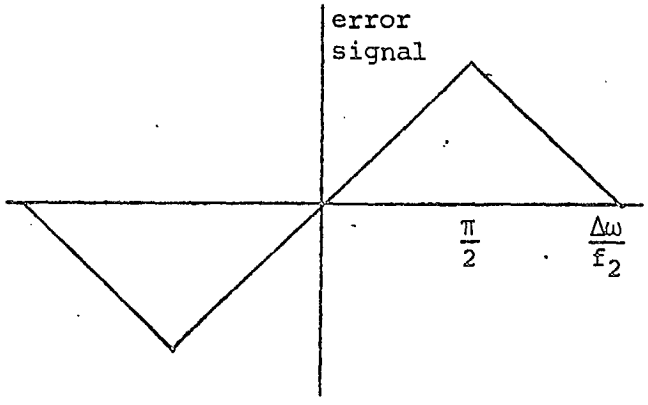

(e)

FIG. 6.4 Rotational Frequency Comparator

(a) Different Signals Encountered by F.C.*
(b) Phase or Diagram
(c) In-phase and Quad. Carrier
(d) Implementation of F.C.
(e) Error Characteristic
(f) Signal Filtering

*F.C. = Frequency Comparator

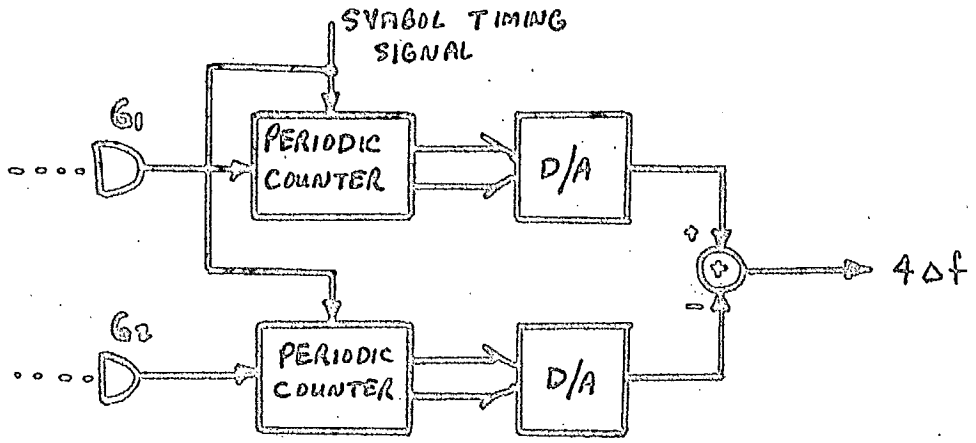

FIG. 6.4 (f)

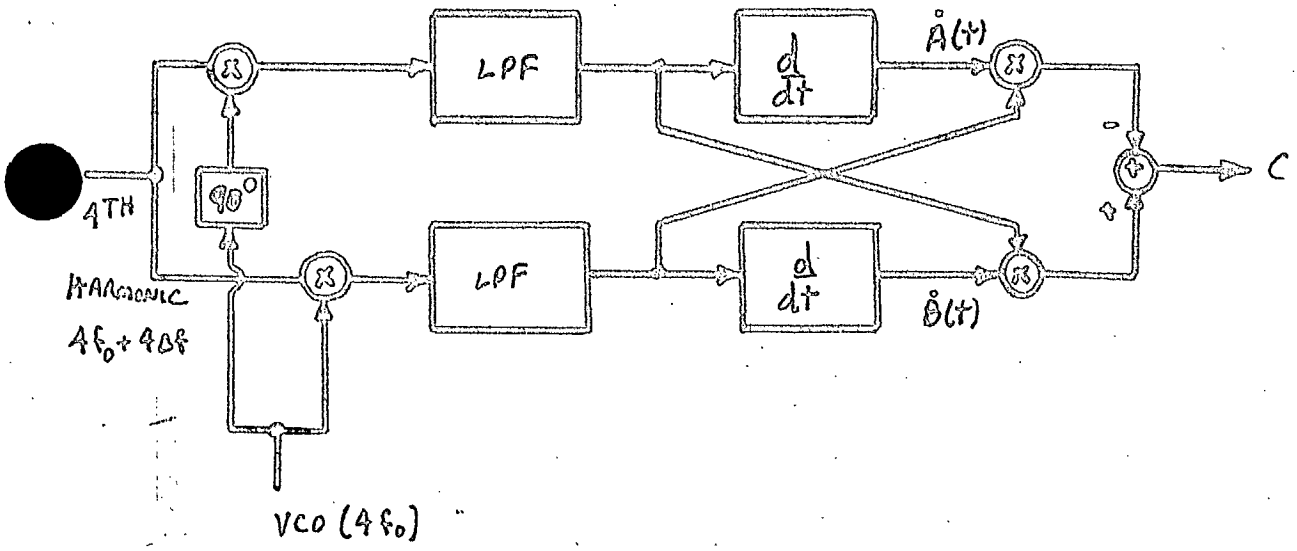

FIG. 6.5 SIMPLE FREQUENCY COMPARATOR

7. COMPUTER PROCESSING OF THE RECORDED WAVEFORMS AND SIMULATIONS

Our experimental investigation was based on computer simulation of receivers which process digitally-recorded received waveforms from real HF channels. These recordings were made and provided to us by the Communications Research Centre. We describe the channels and their characteristics in the next chapter. In this chapter we describe the transmitted signals and the software that was developed to process the recorded signals.

7.1 The Transmitted Signals*

The transmitted signals were generated by QPSK-modulating a length 1023 pseudo-random bit pattern. The PN-sequence generator is shown in Figure 7.1. For the recorded channel signals used in this study, successive bit pairs resulted in 45°, 135°, 225° or 315° phase shifts as shown in Figure 7.1. Preceding this repetitive PN-generated pseudo-random data sequence is a fixed data sequence consisting of two parts: the first is a 1200-symbol sequence, each symbol advanced 135° from the preceding one; the second is 1200 symbols of a repetitive 17-symbol "Frank sequence". In our processing of the recorded signals we ignored these preliminary data sequences, and instead used a correlation technique to detect the start of the 1023-bit PN pattern from the demodulated signal.

The generated symbol rate derived from a Cs beam frequency standard, was 1201.739 hz. Thus with 2 bits per symbol in the

---

* Information for this section was kindly provided by D. Clark and R. Jenkins of the Communications Research Centre.

QPSK carrier frequency was 1505.107 hz, also derived from the Cs QPSK modulation format the true bit rate was 2403.478 bps. The beam standard. The approximately 2.4 khz-bandwidth signal thus generated was subsequently up-converted to the desired RF frequency in the HF band.

7.2 Reception, Recording and Signal Processing

The modulated signals were transmitted over several HF channels, whose characteristics are described in the next chapter. The received voiceband signals were sampled and digitized to 12 bits and were recorded in digital form by CRC using a PDP11/23 minicomputer. The receiver had a AGC with a 20 msec. attack time and about 250 msec. decay time. The sampling rate used for recording was 9600.000 hz, again controlled by a Cs beam standard. Several tapes were recorded, each containing the output of a different channel; i.e. as defined by time of day and RF frequency.

Since the data recorded on the tapes was to be processed with a Honeywell level 66 computer with a CP6 generating system, a data reformatting procedure was necessary and is described in Appendix A. For processing on the CP6 system, the taped data was transferred to a disk file using a job file listed in Appendix A.

The front end of the receivers simulated on the CP6 system included sine and cosine demodulation followed by low pass filtering as shown in Figure 3.1. In this stage of processing the original sample rate of recording, 9600 hz; i.e. about 8 times the baud rate, was used. However, this rate was not an

exact multiple of the transmitted baud rate, although both rates were extremely stable due to the Cs beam frequency standards. It was therefore necessary to re-sample the recorded signal at a rate 8 times the transmitted baud rate. This required sampling rate was 9613.912 hz, while the recording sampling rate was 9600.000 hz. Thus the original receiver clock "slips" one T/8 sample approximately once every 86 symbol intervals.

Figure 7.2(a) shows a block diagram of the "front-end" of the simulated receiver. Received samples $r(k'T'/8)$ are read from the disk file containing the recorded waveform and demodulated into baseband in-phase and quadrature components represented by samples of the real and imaginary parts respectively of a complex waveform y(t) taken every $T'/8$ seconds where $T'/8$ is the sampling period used in recording the received signal, (0.1042 msec.). Interpolation was applied to the sampled demodulated baseband in-phase and quadrature signals in the block labelled "RE-SAMPLING". Since their bandwidth is less than 1/10 of the 9.6 khz sampling rate, simple linear interpolation was adequate for the re-sampling process [SR 73].

The indices k' of the current received samples needed for linear interpolation are computed by the interpolation software. The frequency f_o used for demodulation is the transmitted carrier frequency 1505.107 hz. The lowpass filters shown in Figure 7.2(a) are identical raised cosine filters with a 6 dB frequency of 600 hz and a 20% rolloff. They are implemented by the FFT overlap-add method. For simulation of the DFE receiver a 1200 hz bandwidth was used.

The output of the re-sampling block is the complex waveform y(t) sampled at t=kT/8 where T is the transmitter's symbol interval 0.83213 msec. and k is the transmitted sample index. The relationship between k and k' and between k'T'/8 and kT/8 is shown in Figure 7.2(b). The output samples of y(t) are further decimated by a factor of 4 so that the sampling frequency of the complex signal y(t) used for channel impulse response estimation and equalization is 2/T.

Figure 7.3 shows the correlation signal processing which locates the beginning of the 1023-bit pseudo-random sequence. The complex transversal filter in this figure correlates the demodulated complex baseband signal with values known to occur at the beginning of the sequence.

The adaptive channel impulse response estimation algorithm and the adaptive decision feedback equalizer that were simulated processed the complex-valued re-sampled demodulated signal {y(nT+mT/2), (m=0 or 1)}. The DFE simulation is described in Chapter 9.

Estimated channel impulse responses at regular periodic time intervals were extracted using the FRLS channel estimation algorithm described in section 5.3. The number of impulse response samples N was 10, λ was 0.93 and δ was 0.1. The FRLS restart procedure described in section 5.5 was invoked every 315 symbol intervals. At each restart, the filter coefficients estimated by the FRLS algorithm were reset to zero, and the modified desired outputs of equation (5.42) were used. An auxiliary LMS algorithm with γ=.05 provided the output tap coefficients during each restart interval, which lasted 15

symbol intervals.

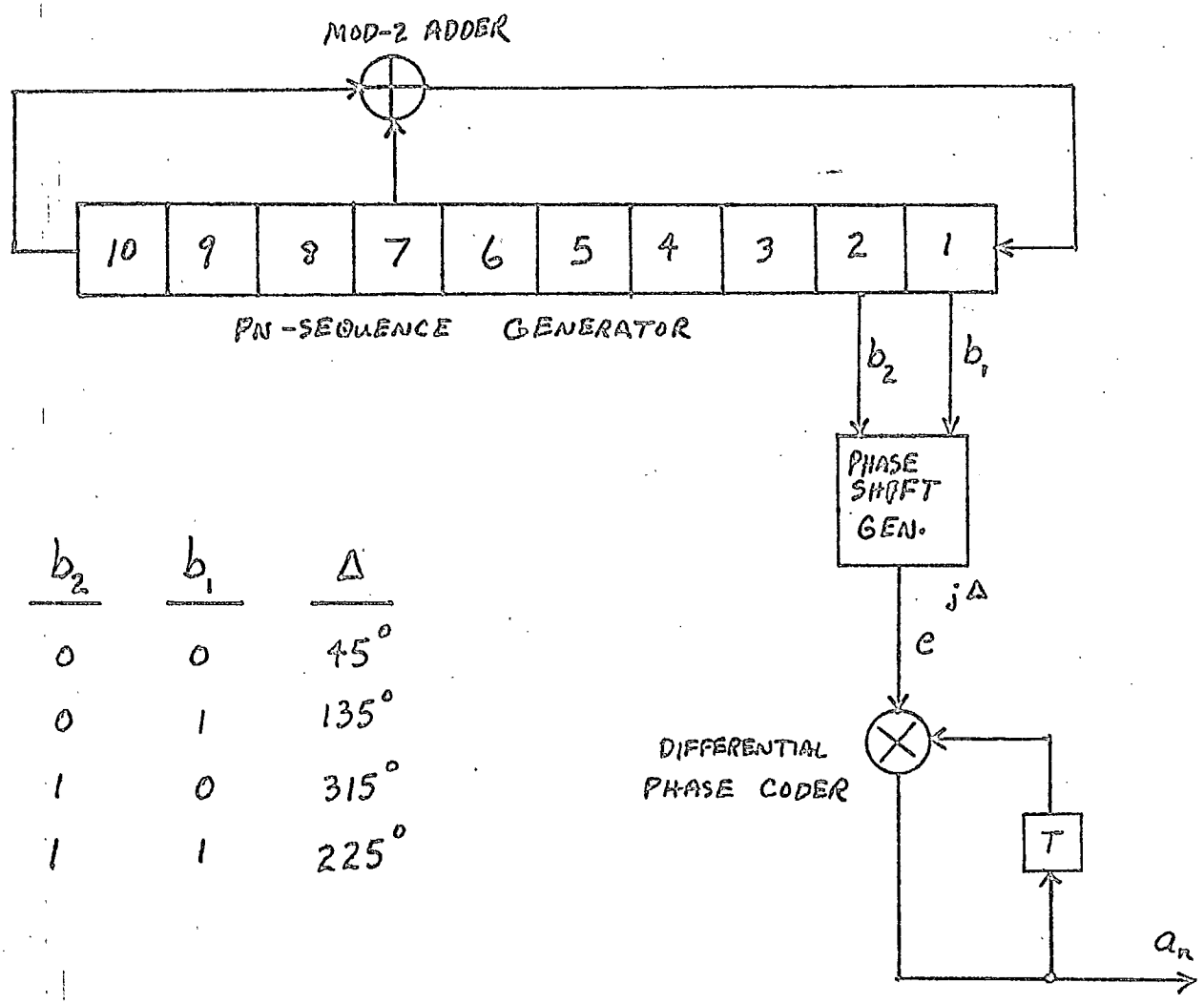

b_2	b_1	Δ
0	0	45°
0	1	135°
1	0	315°
1	1	225°

FIG. 7-1 "PSEUDO-RANDOM DATA SYMBOL GENERATOR

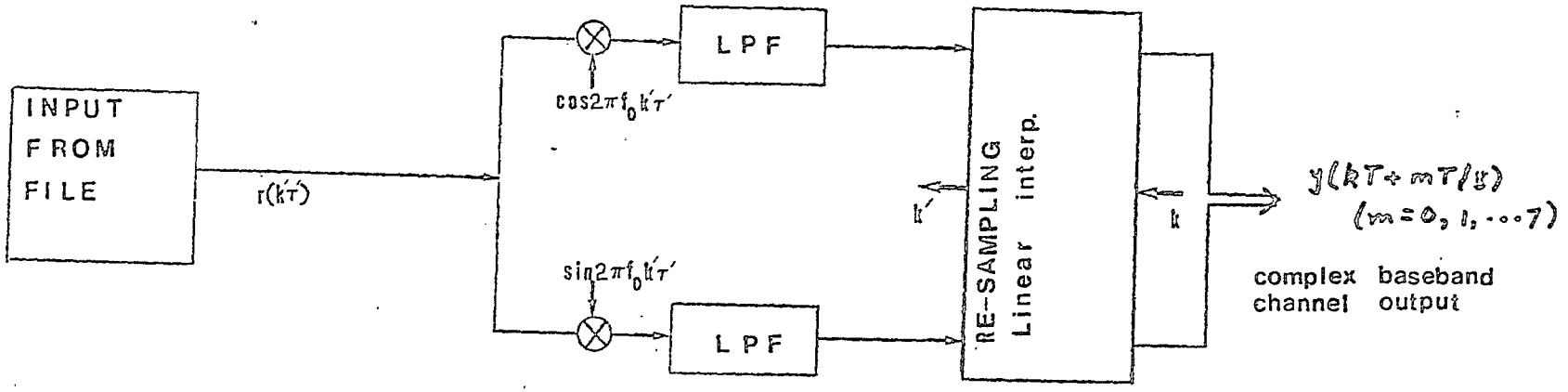

FIG. 7.2(a) SIMULATED RECEIVER FRONT END

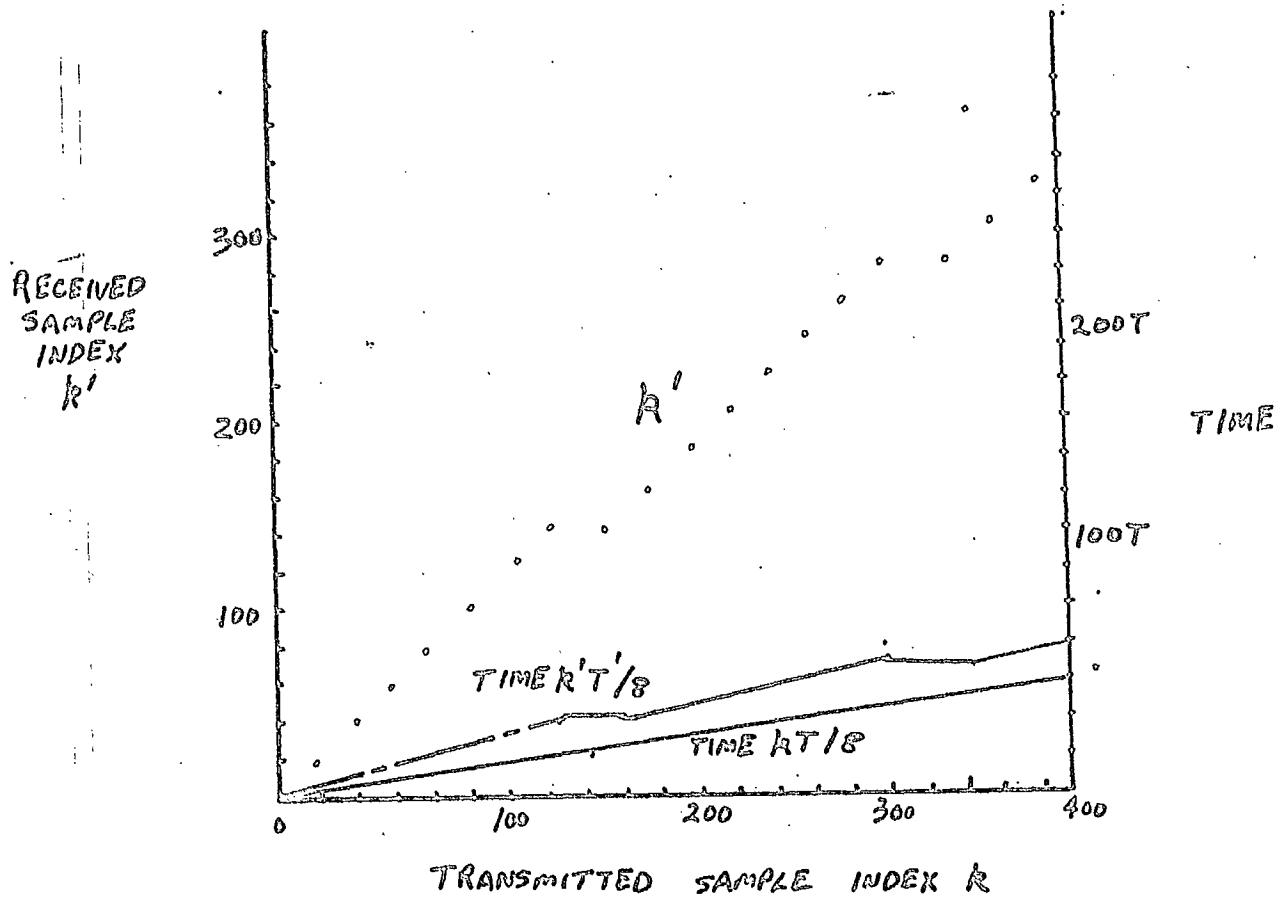

FIG. 7.2(b) RELATIONSHIP BETWEEN TRANSMITTED AND RECEIVED SAMPLE INDICES AND TIMES

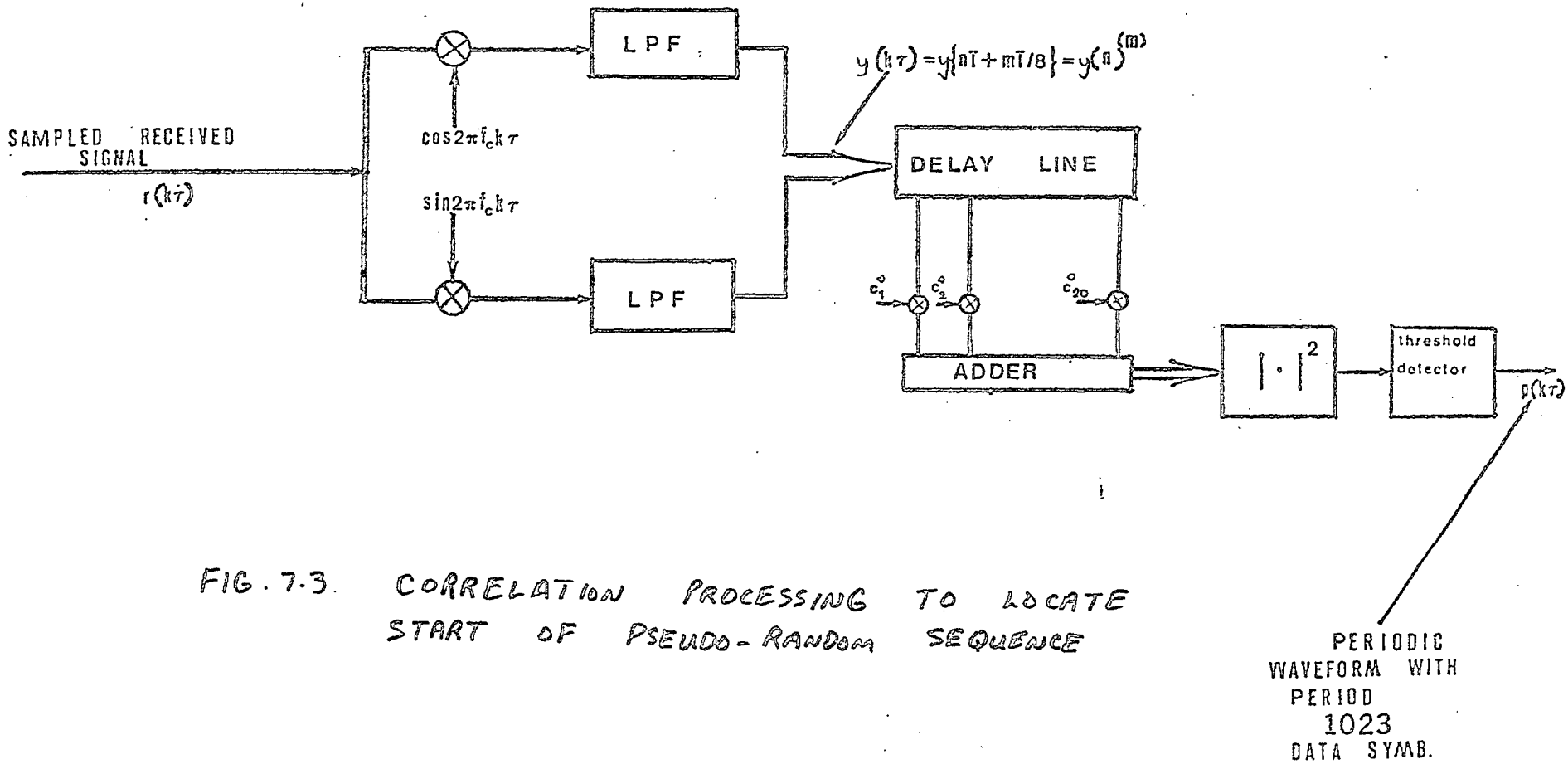

FIG. 7.3 CORRELATION PROCESSING TO LOCATE START OF PSEUDO-RANDOM SEQUENCE

8. CHANNEL CHARACTERIZATION BASED ON IMPULSE RESPONSE ESTIMATES

8.1 Introduction

For an efficient use of HF channel (or in fact any channel), estimates of the channel parameters characterizing the channel are essentially required. Where the channel under consideration is time variant, definite values cannot be assigned to the important parameters and statistical characterization becomes the normal course of action. The HF channel falls into this category and here in this chapter, the channel characterization for the specific application of adaptive equalization to combat intersymbol interference is brought under discussion. Due to peculiarity of the application i.e. a desire to combat intersymbol interference due to multipath propagation, the typical characterization parameters such as delay and doppler spreads are not considered here, instead statistics of the channel impulse response and its influence on the performance of the equalization techniques described in Chapter 4 will be described.

The channel is characterized in the form of impulse response length statistics, the magnitude of the impulse response and statistics of impulse response variability. The impulse response length, as mentioned earlier in the report, plays an important role in the selection of the number of taps required in the equalization filter, and hence directly influences the complexity of the equalization algorithm. Similarly, the impulse response variability rate over a given numbers of symbol intervals, determines how fast the algorithm should be to track the channel

with a minimum of noise arising out of tap adjustment errors.

For the given channel, performance of MLSE and DFE receivers will be compared with the upper bound performance given by a matched filter receiver. By studying these aspects, recommendations could be made about the suitability of a particular receiver.

8.2 Observation of Channel Behaviour While Recording the Data

In order to correlate the statistical results with some physical propagation mechanisms, it is worthwhile to describe the behaviour of the channel when the data was being recorded. This may provide us with some subjective interpretation of the results. The data was obtained by CRC from measurements of 1200 baud QPSK signals transmitted from Cobden to the CRC Laboratories at Shirley Bay over a path of about 60 km. In all, data was collected on six tapes at various times of the day, December 8, 1981. The signals were received via skywave without any significant groundwave component. The observed subjective characteristics are listed in Table 8.1.

From Table 8.1, it seems that tapes MDA007, 008, 010, and 011 will provide sufficient data to cover a variety of impairments in the channel behaviour and evaluation of their statistical behaviour will provide an insight into the physics of ionosphere. The data on tape MDA009 is accompanied by a strong interfering signal makes it unique in the sense that it provides enough academic curiosity to study for effectiveness of channel equalization when both multipath fading and interference are

present. However, this particular tape has not been used for channel characterization and such a task has been reserved for future studies.

Table 8.1

Subjective Characteristics of the Recorded Tapes

The average signal to noise ratio at the receiver input (for transmitted power of 16 watt) ≃ 18 dB. All tapes with 1200 baud-QPSK signals.

Tape No.	Power Transmitted (Watts)	Frequency (MHz)	Transmitted Time (Local Time)	Features/Characteristics
MDA006	16	7.5555	11:40	strong, steady and clear signal
MDA007	1	7.5555	14:20	increased baseband noise, sufficient fading noticed
MDA008	16	7.5555	14:50	good signal strength strong fading fade rate ≃ 0.3 Hz
MDA009	16	11.623	15:00	presence of strong interference in the nature of pulses at rate 10 per second was noted
MDA010	16	5.2675	16:00	deep slow fading ($\geq$ 20dB fades) with very strong signal. fade rates ≃ 0.15 Hz
MDA011	16	5.2675	17:40	strong signal with deep (down to noise level) rapid fades were observed (fade rate ≃ 0.5 Hz)

8.3 Impulsive Response Characteristics

It is mentioned earlier that the length of the averaged impulse response and its variation over certain given time intervals are two important statistical parameters for deciding on a particular equalization technique to be employed. The data on the tapes MDA010 and MDA011 has been analyzed for the mean magnitude of the impulse response, distribution of the impulse response duration, and distribution of percentage change in the impulse response over various time intervals.

8.3.1 Channel Impulse Response Characterization

It has been mentioned in Chapter 7, section 7.2 of this report that how using the impulse response identification program files of channel complex impulse responses $\underline{h}(n)$ every 25 symbol intervals, with 2 samples per symbol intervals were obtained. These files have been used to estimate the minimum span of M symbol intervals that contain at least a predetermined percentage of energy in the impulse response.

8.3.2 Averaged Magnitude of the Impulse Response

The mean magnitude of the impulse response is obtained by first estimating the magnitude of the impulse response over 25 symbol intervals and then averaging the results over 10,000 or 20,000 symbol intervals. For tapes MDA010 and MDA011 are plotted in Figures 8.1 and 8.2. Table 8.2 shows the summary of the findings.

Table 8.2

Impulse Response Mean Magnitude

Tape No.	No. of Paths	Magnitude of Secondary Paths Relative to the Primary	Approximate Height of the Reflecting (or Refracting) Layer Relative to the Primary Paths
MDA010	3	-9 dB; - 16 dB	250 Km; 500 Km
MDA011	3	-6 dB; - 14 dB	275 Km; 500 Km

The entries in the last column give relatively large values for the distances between three propagation paths which is a physical impossibility unless the primary impulse response peak is obtained via a direct communication path. If that is so, then looking at the time intervals between the primary and secondary paths, it is reasonable to imagine that the second and third paths arrive at the receiver via F_1 and F_2 layers. MDA011 has a stronger secondary peaks which should give higher intersymbol interference. Going over Table 8.1, it is noted that subjectivily fades for MDA011 were deeper with higher fade rate. Intuitively, stronger secondary peaks could be responsible for deeper fades.

8.3.3 Impulse Response Duration Distribution

Here we get a minimum span of M symbols such that the associated energy with the M symbol intervals S´ is more than or

equal to some fraction of total energy S. The distributions of the impulse response duration for MDA010 and MDA011 arranged over 10,000 symbols intervals are shown in Figures 8.3 and 8.4. It is clear that distributions of the impulse response duration are dependent on the fraction of total energy considered for such measurements. However, it seems to make a very little difference in the impulse response distribution if the averaging time is varied between 25 to up to 300 symbol intervals. Table 8.3 lists the findings of this analysis.

Table 8.3

Impulse Response Duration Distribution

Tape	MDA010		MDA011			
Energy Level Considered	0.97	0.99	0.96	0.97	0.98	0.99
Mean (Symbols)	4.66(25) 4.69(100)	6.59(50) 6.72(200)	4.456(100)	4.81(75) 4.88(300)	5.53(50) 5.52(200)	6.64(25) 6.29(150)
Median (Symbols)	4 (25) 4 (25)	6.31(50) 6.33(200)	3.875	4.68(75) 4.68(300)	5.37(50) 5.37(200)	6.48(25) 6.46(150)
Standard Deviation (Symbols)	1.3326(25) 1.3924(25)	1.31(50) 1.298(200)	1.000	0.869(75) 0.917(200)	0.87(50) 0.988(200)	0.799(25) 0.71(150)

The figures in brackets denote averaging interval in symbol periods.

Considering the median values of the impulse duration, it is clear that the median changes very little over the averaging interval for the same energy levels. For examples for the tape MDA010 the median value of impulse response is 4 and 6.31 symbols for 97% and 99% of energy levels respectively. Similarly for the tape MDA011 for the same energy levels the median impulse response durations are 4.81 and 6.48. It is evident that complexity of the algorithm (number of mathematical operations) could be reduced by considering truncated impulse response. For example a reduction factor of 16 and 4 will result for tape MDA010 and MDA011 respectively if the energy requirements are cutdown from 0.99 to 0.97. However, such reduction in the impulse response energy will result in an increase in the residual intersymbol interference which will reduce the percentage eye opening and more errors will result [MCL 80]. It would be of some interest to study the relationship between percentage eye opening with reduced impulse response energy levels and to find a suitable limit of such reduction which will result in an acceptable minimum of percentage eye opening of 0.8.

8.3.4 Distribution of relative Change in Estimated Impulse Response

It is of primary interest to estimate relative change over certain time interval [in symbol intervals], so that the requirement of the channel tracking algorithm could be established. The relative change in estimates of impulse response over say 50 symbols intervals may be calculated from the files of impulse response estimates, as given below.

$$\text{relative change in \%} = \frac{|\hat{\underline{h}}(n) - \hat{\underline{h}}(n-50)|}{1/2(|\hat{\underline{h}}(n)| + |\hat{\underline{h}}(n-50)|}$$

It cannot, however, be estimated that to what extent phase jitter and frequency offset is responsible for such relative change.

The relative changes in the impulse response estimates for the channels MDA010 and MDA011 have been plotted in Figures 8.5 and 8.6. These changes in estimates are over 25, 50, 75, 100, 150 and 200 symbol intervals. From the curves it could be stated:

(a) The relative change per symbol interval is nearly constant over probability ranges of 0.25 to 0.80. The median relative change is estimated to be 0.33% per symbol interval for MDA011 and 0.220% per symbol interval for MDA010. The channel corresponding to MDA011 is varying approximately one and a half times as fast as MDA010.

(b) The probability density function of the percentage for tape MDA010 seems to have much longer tail as compared to MDA011. This is confirmed by comparing the standard deviations for the MDA010 and MDA011 which are 4.7 and 2.9 respectively. This means that though rate of change of channel MDA010 may be slower on the average, but when it starts to change it probably goes through an extensive change. Table 8.1 indicates similar phenomenon that the tape MDA010 has slower rate, but has deeper fades. This is being confirmed here.

For a quick reference the results on the percentage changeare summarized in Table 8.4.

Table 8.4

Relative Change of the Channel Impulse Response

Tape No.	MDA010	MDA011
Mean	18.82% (25) 22.8 % (50) 30.0 % (100) 44 % (200)	17.58%(25) 16.8% (50) 20.02%(100) 68.0% (200)
Median	12.0 % (25) 15.6 % (50) 28.4 % (100) 44.0 % (200)	12.6% (25) 19.4% (50) 33.4% (100) 66.4% (200)
Standard Deviation	9.4 % (25) 9.6 % (50) 9.2 % (100) 9.4 % (200)	5.64% (25) 5.80% (50) 6.32% (100) 10.24%(200)

8.4 System Performance Comparisons Based on Impulse Response Estimates

It has been mentioned in section (4.3), that relative difference in performance of DFE and MLSE receiver critically depends on the actual channel impulse response. One of the aims of this study is to compare the performance of the two receivers when the channel impulse response is available. Such comparison could be made by comparing the performance with an ideal Matched Filter [MF] which yields lowest error probability.

It is also mentioned that the error probability is given by

$$P_e = 2\,Q\,(d/\sigma)$$

where (d/σ) is effective signal to noise ratio and

$$Q(x) = \frac{1}{\sqrt{2\pi}} \int_{-\infty}^{x} \exp(-y^2/2)dy$$

For the three receivers i.e. MF, DFE and MLSE, the receiver performance can be evaluated on the basis of (d/σ) and d andσ can be estimated from the impulse response estimations (equations 4.8-4.12). Here, in this section the cumulative distributions of $(d_{min}/\sigma)_{MLSE}$ are obtained as outlined in section 4.3. The performance comparison of the three receivers for the channels MDA010 and MDA011 are shown in Figures 8.7 and 8.8 in the form of probability distribution of (d_{min}/σ) dB. Here it could be said that given the channel as it is, the DFE receiver which is a suboptimum receiver always performs worse than VA or MLSE receiver. It is evident from the Figures 8.7 and 8.8. It is clear that the margin in the performance of the two receivers is greater at (d_{min}/σ)dB of less than say 5 dB and 10 dB for channels MDA010 and MDA011 respectively, at lower end of (d_{min}/σ) Perhaps such an improvement is required for real life systems as need to get improvements arises only when channel behaviour is at its worst. For a good channel one may not need complex equalizations. Beyond these values of (d_{min}/σ) of 5 and 10 dB mentioned above the VA is better than DFE by less than a dB for MDA010 and 1 dB for MDA011. It seems that the relative complexity of MLSE receiver outweighs the advantage over DFF.

It is noted that performance of MLSE receiver is identical with matched filter receiver for MDA011 but deviates (to a very small extent) for MDA010. These results reflect the performance of the three receivers for particular channel impulse responses. Looking at these curves it is not possible to get any feel about

the channel behaviour. It is however possible to pinpoint the effect of a particular type of channel impairments on the performance of the DFE and MLSE receivers by examining the channel impulse response at the instances when receiver performance degrades below a certain (d_{min}/σ) threshold. Software for such a study has been written and this particular aspect will be studied in future.

8.4.1 DFE and MLSE Receiver Performance Comparison

The joint probability densities of (d_{min}/σ) for the two receivers have been plotted and these are shown in Figures 8.9 and 8.10 for the two channels MDA010 and MDA011. The numbers in the joint probability distribution print out shows the number of occurances for particular values of (d_{min}/σ) for MLSE along ordinate and DFE along the absissa. If the performance of the two receivers were identical, then all the numbers would lie along the diagonal drawn. If the majority of the number of occurances lies in the upper left of the diagaonal, then the MLSE receiver performs better, vice versa will show the DFE receiver behaves better. It again shows better performance of MLSE by relatively small margins. The performance differential is not too much though.

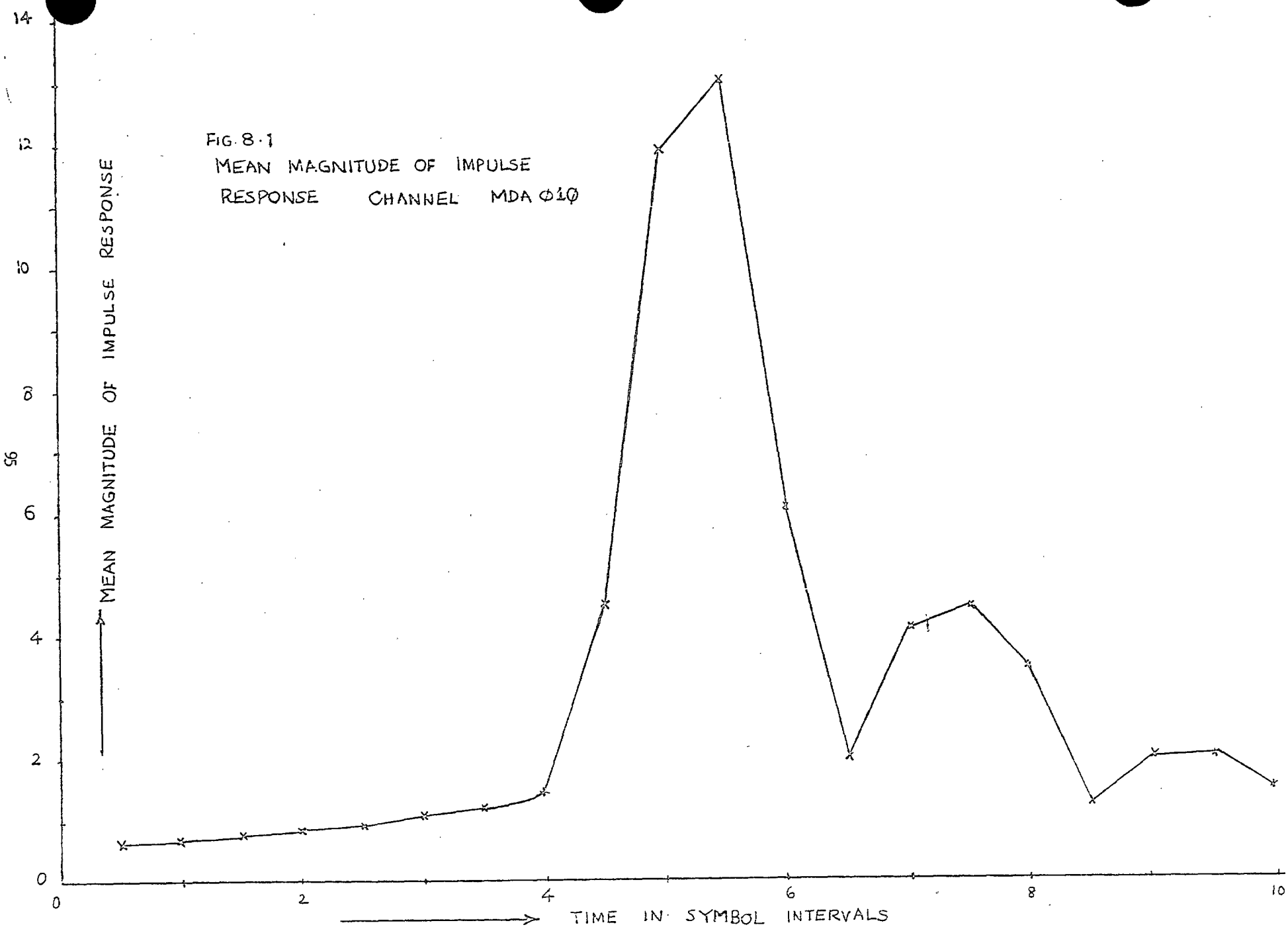

FIG. 8·1
MEAN MAGNITUDE OF IMPULSE RESPONSE CHANNEL MDA Φ1Φ

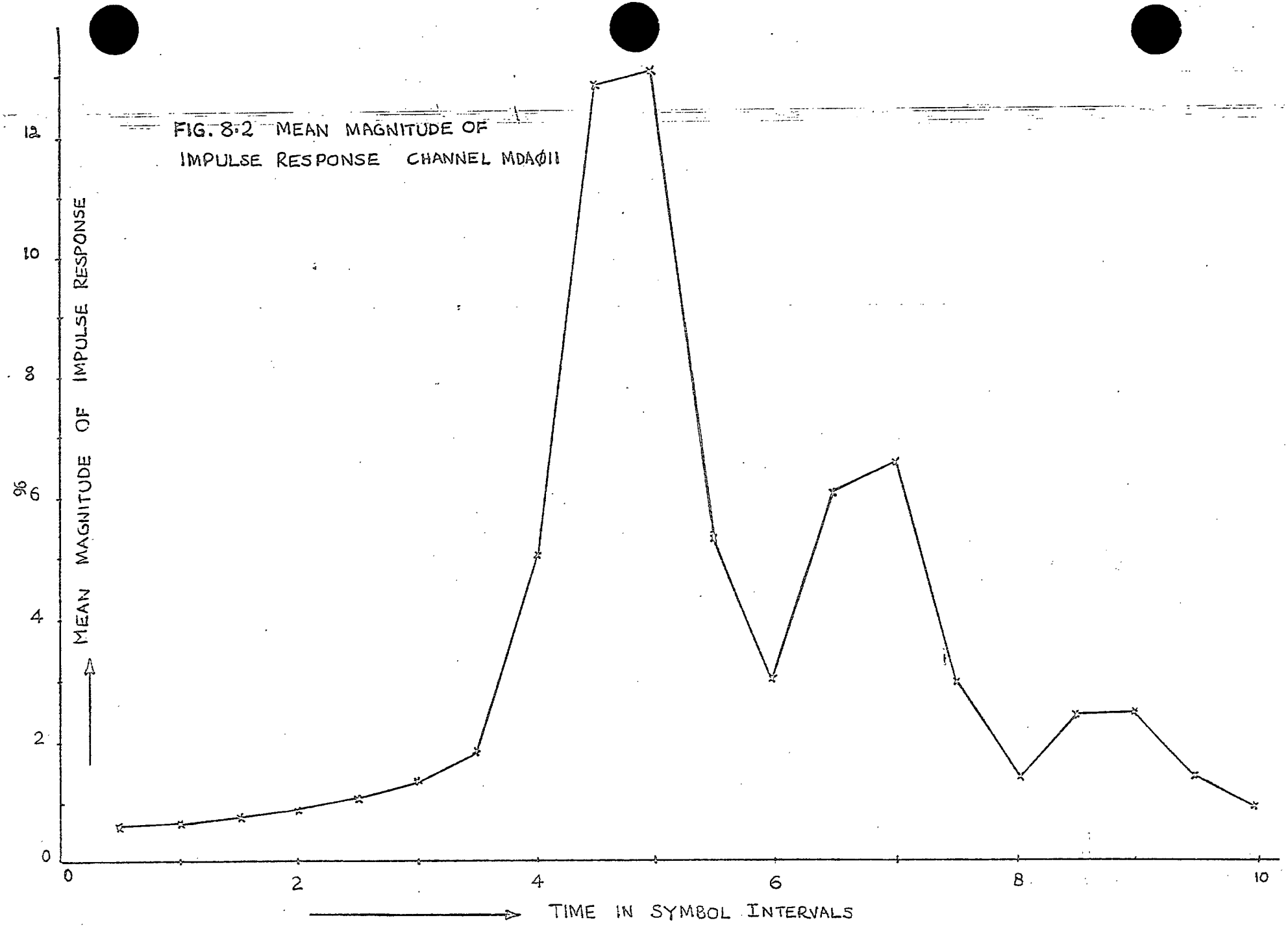
FIG. 8-2 MEAN MAGNITUDE OF IMPULSE RESPONSE CHANNEL MDAΦ11
MEAN MAGNITUDE OF IMPULSE RESPONSE
96
0
2
4
6
8
10
12
0
2
4
6
8
10
TIME IN SYMBOL INTERVALS

FIG. 8.3 IMPULSE RESPONSE LENGTH PROBABILITY DISTRIBUTION

CHANNEL MDAØ1Ø

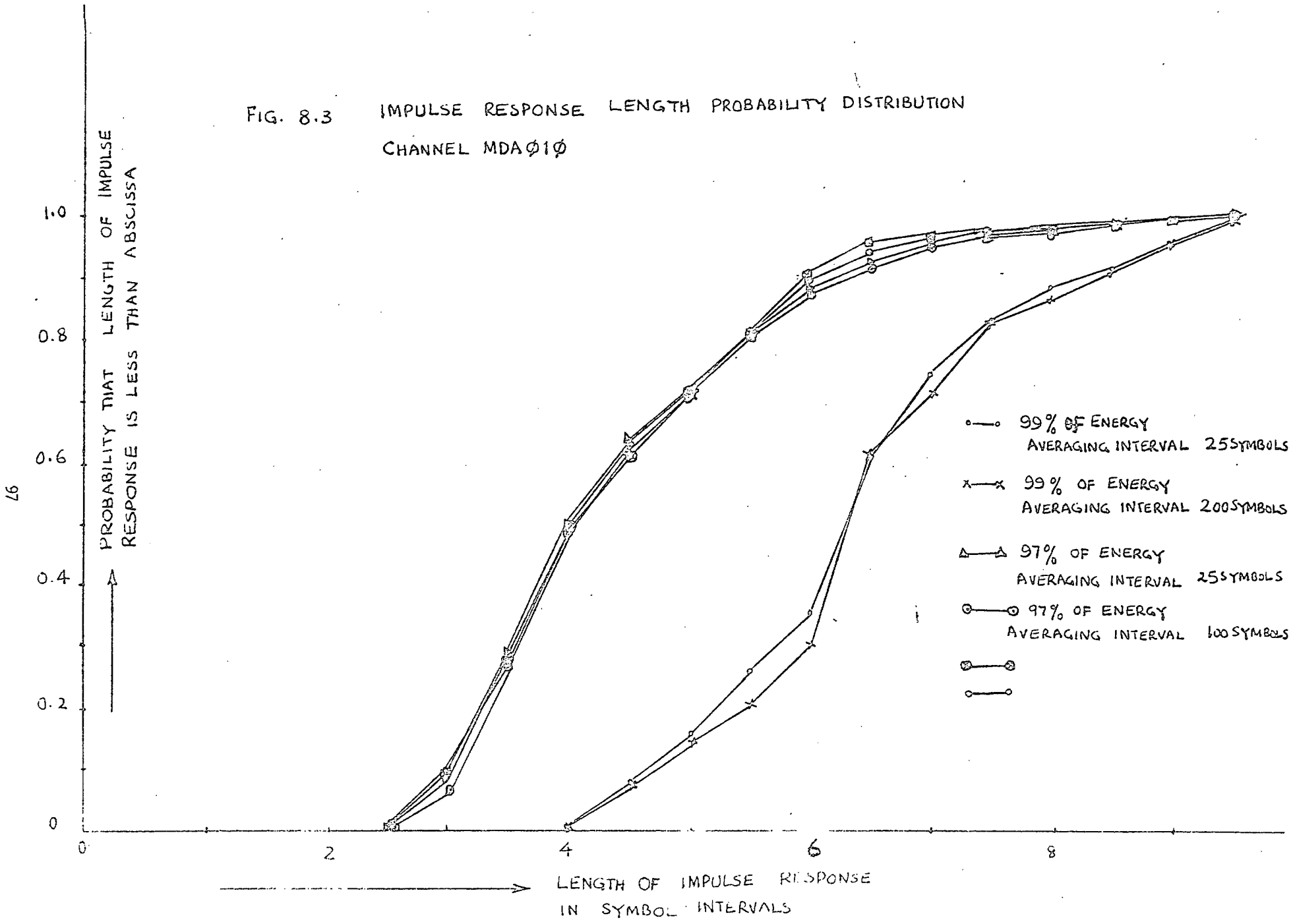

FIG 8.4 — IMPULSE RESPONSE LENGTH PROBABILITY DISTRIBUTION CHANNEL MDA Ø11

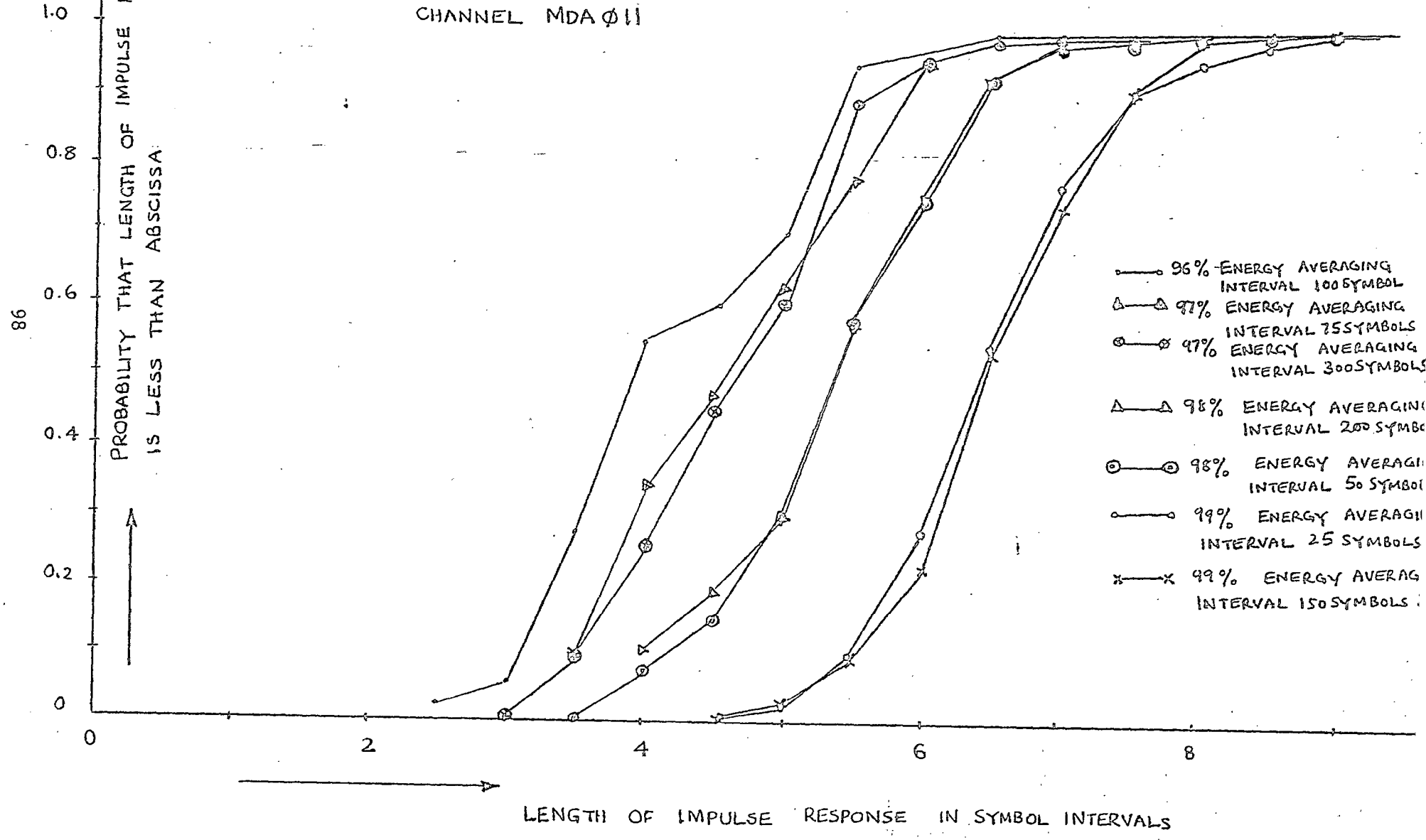

FIG 8.5 PROBABILITY DISTRIBUTION OF PERCENTAGE CHANGE CHANNEL MDA ØIØ

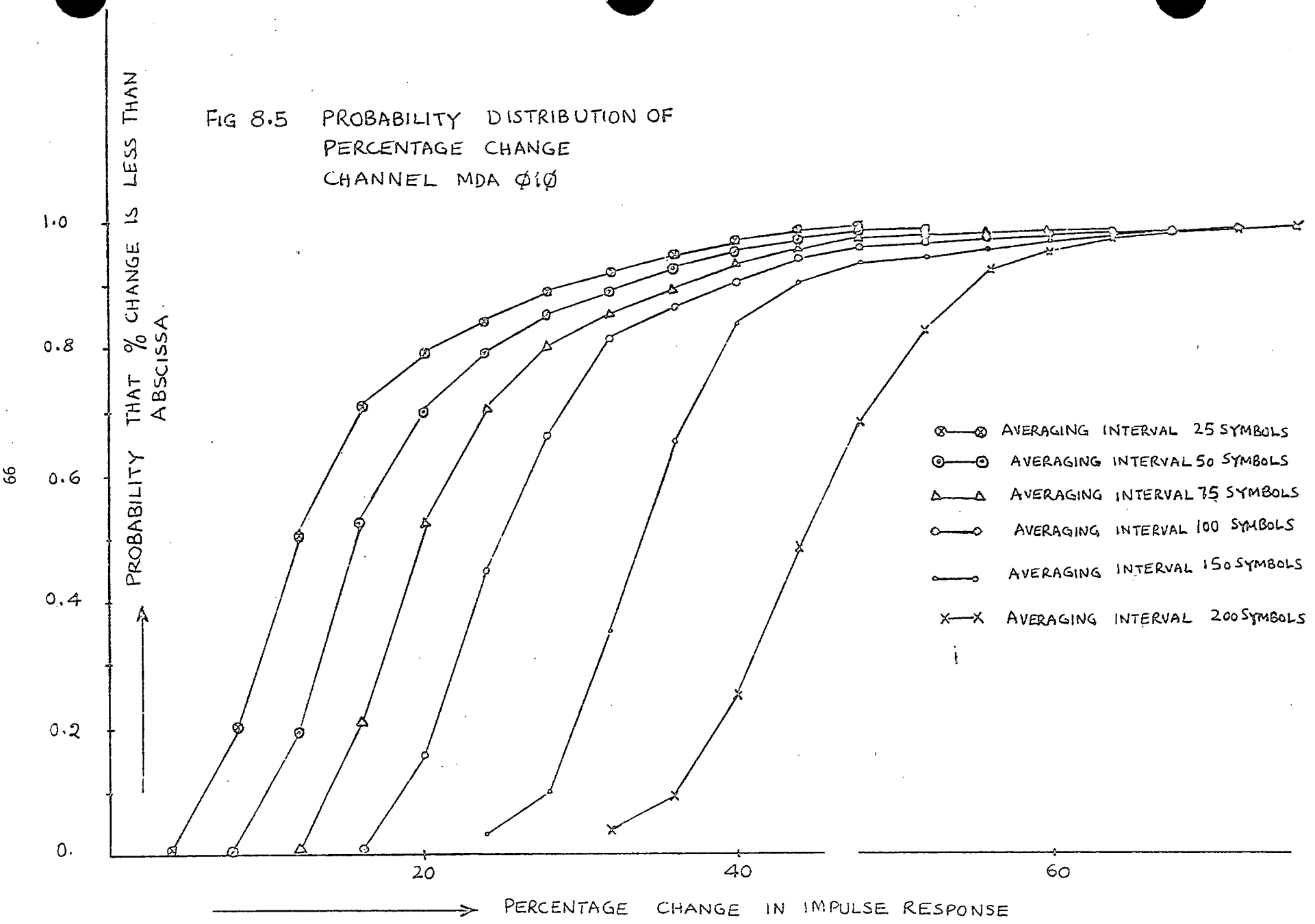

FIG. 8.6 PROBABILITY DISTRIBUTION OF PERCENTAGE CHANGE CHANNEL MDA Ø11

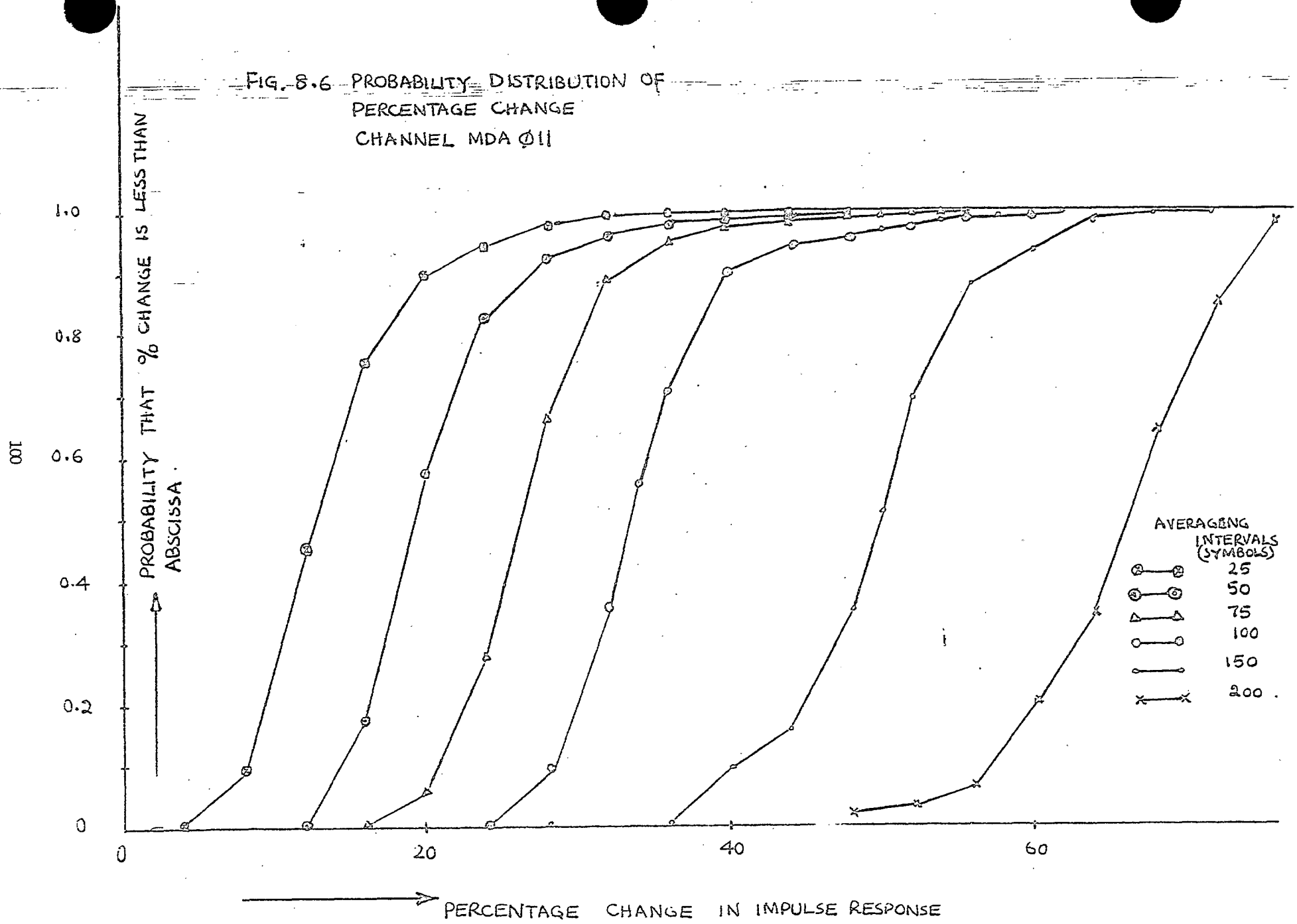

100

FIG. 8.7 PROBABILITY DISTRIBUTION OF $(d_{min}/\sigma)_{dB}$ CHANNEL MDA $\phi 1 \phi$

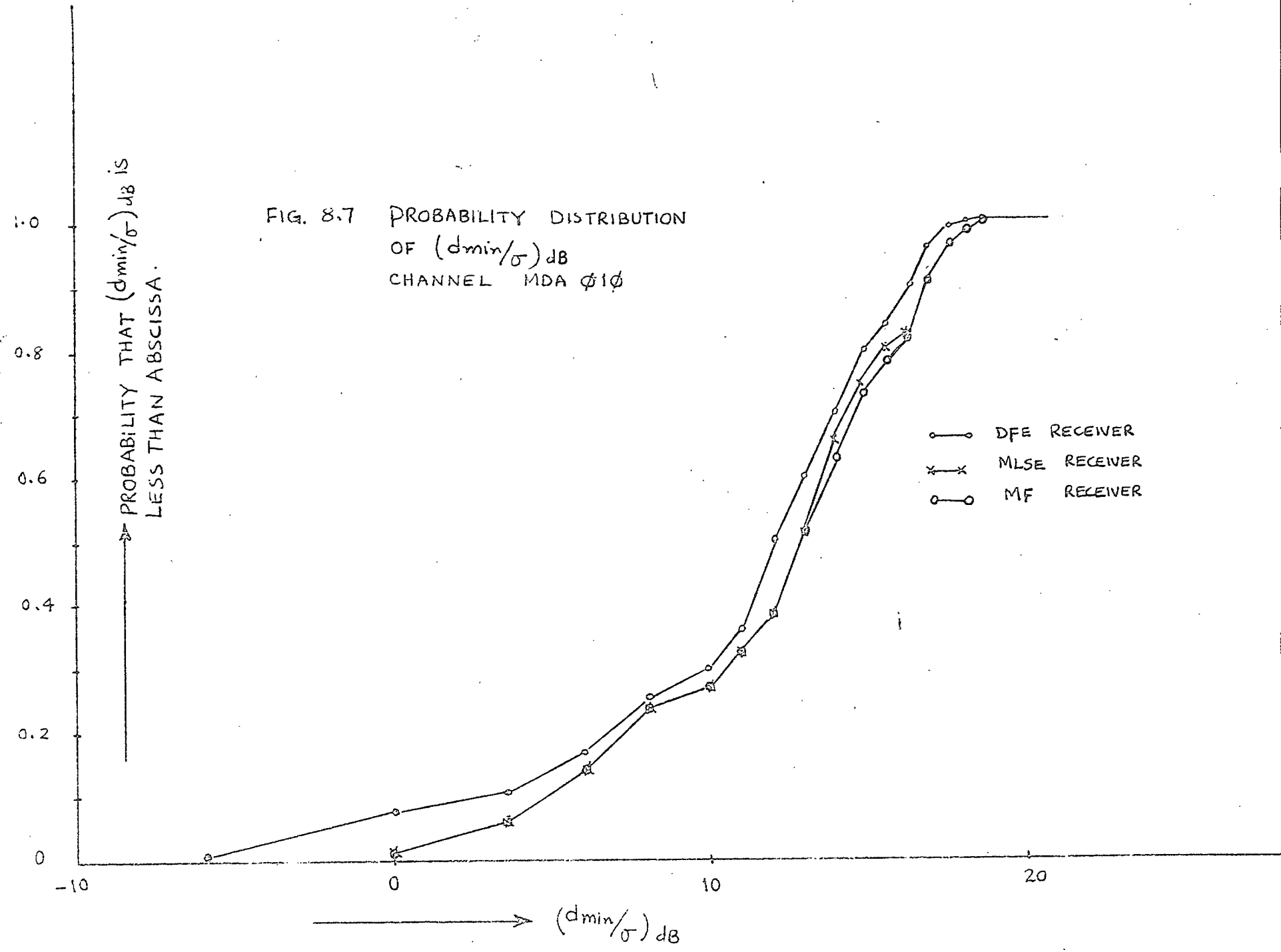

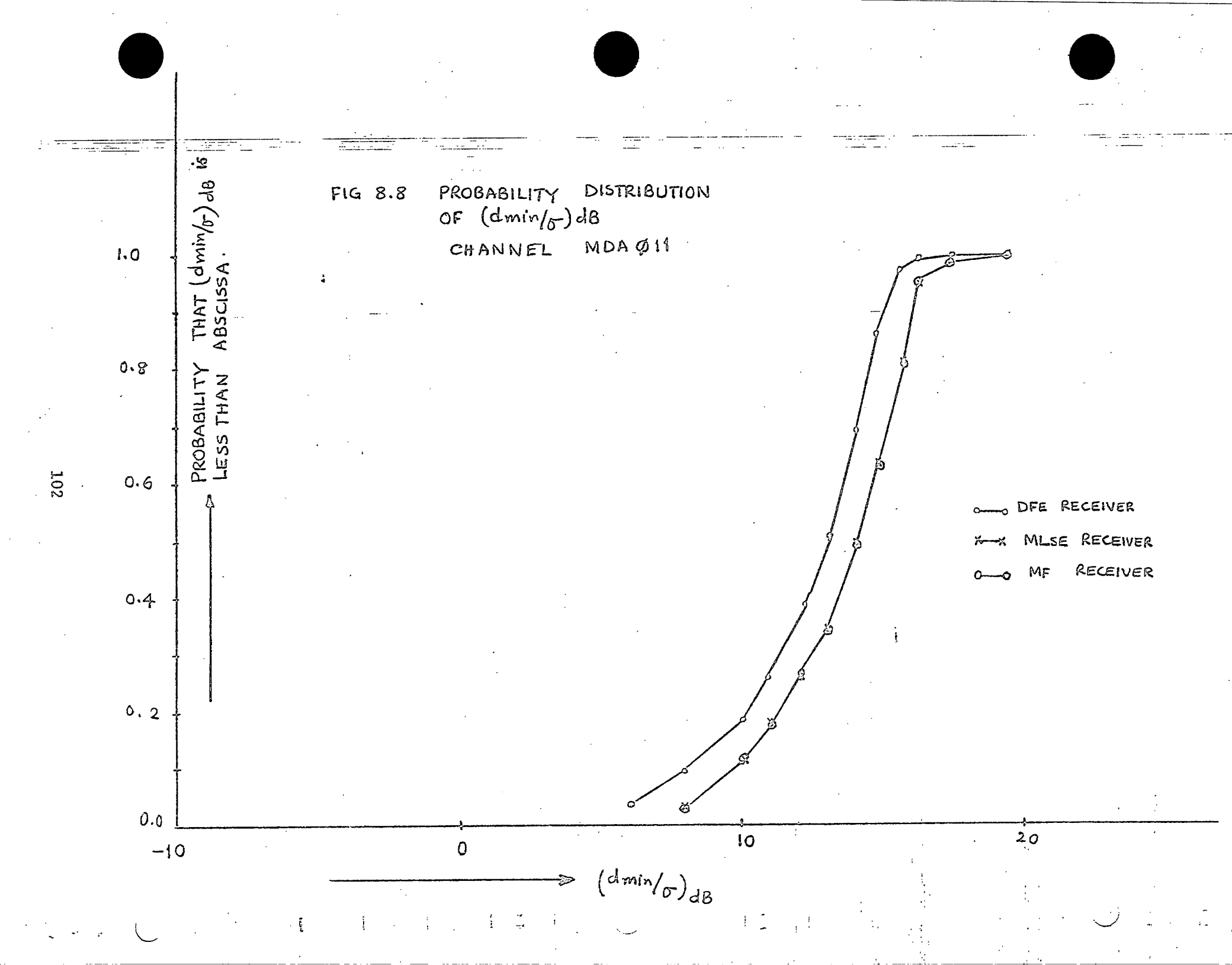
FIG 8.8 PROBABILITY DISTRIBUTION OF $(d_{min}/\sigma)_{dB}$
CHANNEL MDA Ø11
PROBABILITY THAT $(d_{min}/\sigma)_{dB}$ IS LESS THAN ABSCISSA.
1.0
0.8
0.6
0.4
0.2
0.0
-10
0
10
20
$(d_{min}/\sigma)_{dB}$
DFE RECEIVER
MLSE RECEIVER
MF RECEIVER

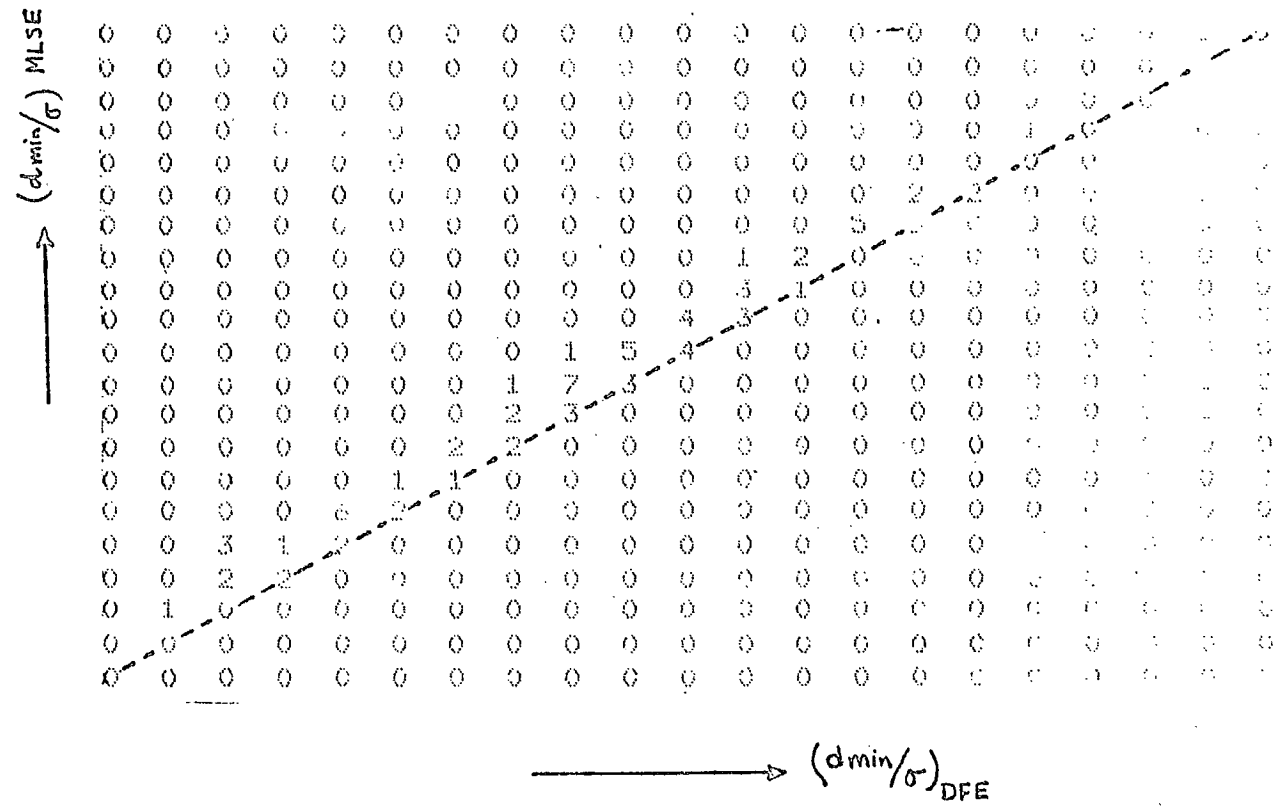

FIG 8.9 PERFORMANCE COMPARISON OF DFE AND MLSE RECEIVERS

CHANNEL MDA $\phi 1 \phi$

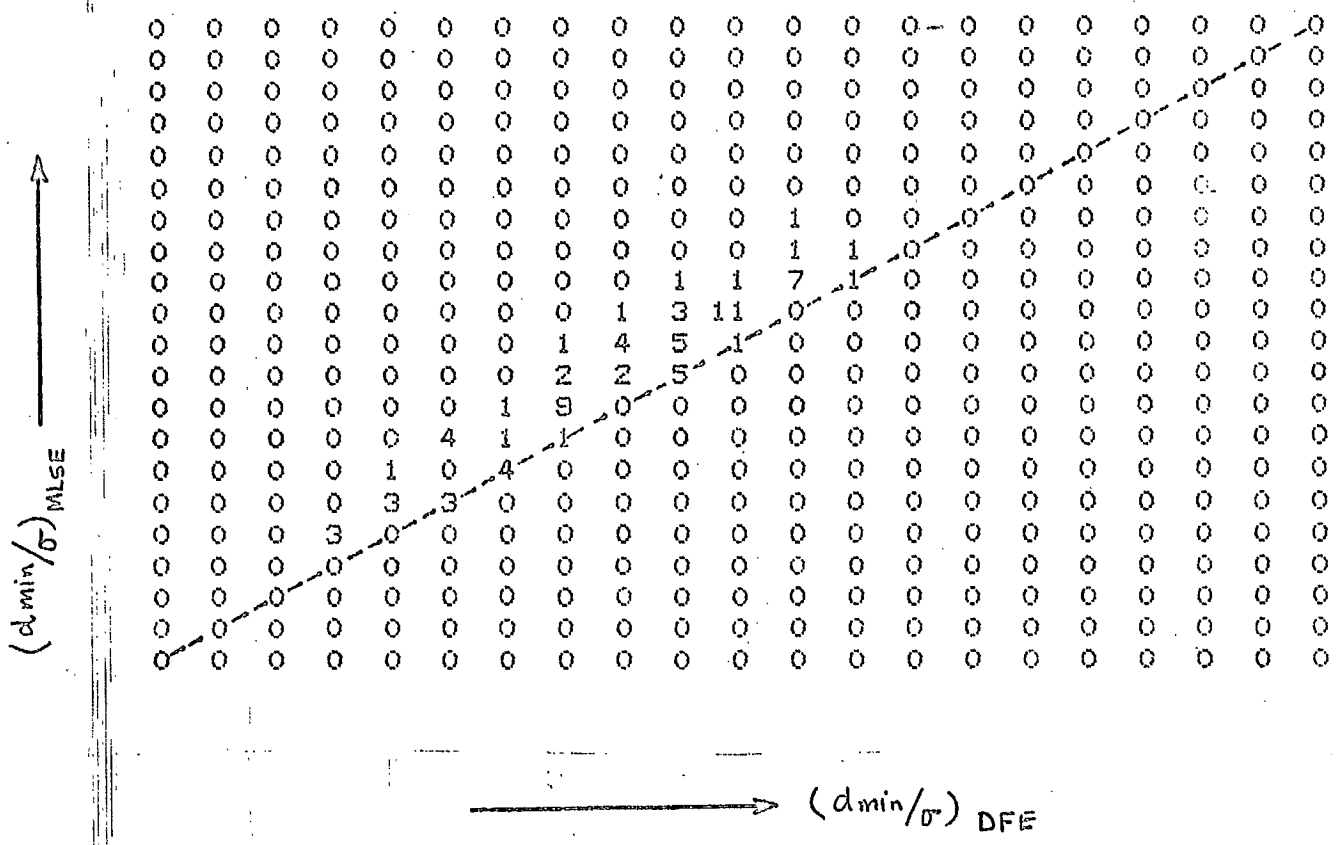

FIG. 8.10 PERFORMANCE COMPARISON OF DFE AND MLSE RECEIVERS CHANNEL MDA ϕ11

9. SIMULATION OF THE DFE RECEIVER

Figure 9.1 shows the block diagram of a decision feedback equalization (DFE) receiver that was simulated to process the complex baseband demodulated signal received from HF channels. This signal was derived as shown in Figure 3.1 and was presented to the DFE as complex samples, T/2 seconds apart, where T is the duration of one symbol (.83213 msec.). Preliminary simulation experiments resulted in the choice of a 1200 hz 6dB bandwidth with 20% raised-cosine rolloff for the demodulator's low pass filters in the DFE receiver. The preliminary simulations also established the choice of the number of equalizer tap coefficients: 20 T/2-spaced forward tap coefficients $\{W_i\}$ and 7 feedback tap coefficients $\{F_i\}$; i.e. $N_1=10$, $N_2=7$, $p=3$, $p_1=2$.

The complex multiplication by $\exp(\pm j\pi n/4)$ before and after the decision-making quantizer shown in Figure 9.1 compensates for the 45^o phase increment that the transmitter added to each data symbol. The problem of error propagation due to 90^o ambiguity in the decided data symbols was avoided by differential encoding of the data. Accordingly, the receiver's output decisions were obtained by differential decoding as shown in Figure 9.1. The output QPSK data symbols had the four possible values $(\pm 1 \pm j)/\sqrt{2}$. As a result of the AGC used in the HF receiver and scaling in the simulation program, the complex-valued input samples entering the DFE's forward filter had a RMS value close to unity under conditions of little or no channel time variation.

9.1 DFE Adaptation

Both LMS and FRLS adaptation algorithms were implemented. The LMS adaptation parameter γ was set to 0.035, a value determined by experimentation. The FRLS adaptation algorithm was that described in section 5.4, with $\lambda = 0.97$ and $\delta = 1.0$.

Three variations of the periodic restart procedures of section 5.5 for the FRLS algorithm were tried. All relied on an auxiliary LMS adaptation algorithm to provide the equalizer's output Q_n during each restart interval. The three restart procedures were as follows:

Restart Procedure 1

The DFE tap coefficients $\underline{C}(n)$ were not re-initialized at the initiation of each restart (at n=K). In this case it can be shown [CK 83] that following a restart at time kT the DFE FRLS algorithm minimizes for $n \geq K$

$$S(n) = \delta\lambda^{n-k} \left| \underline{C}(n) - \underline{C}(K) \right|^2 + \sum_{k=k}^{n} \left| \underline{C}(n)^* \underline{Z}(k) - a_k \right|^2 \lambda^{n-k} \qquad (9.1)$$

where $\underline{C}(K)$ is the value of the tap coefficients updated just prior to restart. If the parameter δ is reasonably large then $\underline{C}(n)$ should not stray too far from $\underline{C}(K)$ during the restart interval. However a too-large choice of δ may hamper the algorithm's ability to track channel variations during the restart interval. For equalizer inputs with an RMS value of around 1.0, a suitable choice for δ was 1.0. The desired filter output used for adaptation in Restart Procedure 1 was that of equation (5.41), with $d_n = \hat{a}_n$.

9. SIMULATION OF THE DFE RECEIVER

Figure 9.1 shows the block diagram of a decision feedback equalization (DFE) receiver that was simulated to process the complex baseband demodulated signal received from HF channels. This signal was derived as shown in Figure 3.1 and was presented to the DFE as complex samples, T/2 seconds apart, where T is the duration of one symbol (.83213 msec.). Preliminary simulation experiments resulted in the choice of a 1200 hz 6dB bandwidth with 20% raised-cosine rolloff for the demodulator's low pass filters in the DFE receiver. The preliminary simulations also established the choice of the number of equalizer tap coefficients: 20 T/2-spaced forward tap coefficients $\{W_i\}$ and 7 feedback tap coefficients $\{F_i\}$; i.e. $N_1=10$, $N_2=7$, $p=3$, $p_1=2$.

The complex multiplication by $\exp(\pm j\pi n/4)$ before and after the decision-making quantizer shown in Figure 9.1 compensates for the 45^o phase increment that the transmitter added to each data symbol. The problem of error propagation due to 90^o ambiguity in the decided data symbols was avoided by differential encoding of the data. Accordingly, the receiver's output decisions were obtained by differential decoding as shown in Figure 9.1. The output QPSK data symbols had the four possible values $(\pm 1 \pm j)/\sqrt{2}$. As a result of the AGC used in the HF receiver and scaling in the simulation program, the complex-valued input samples entering the DFE's forward filter had a RMS value close to unity under conditions of little or no channel time variation.

9.1 DFE Adaptation

Both LMS and FRLS adaptation algorithms were implemented. The LMS adaptation parameter γ was set to 0.035, a value determined by experimentation. The FRLS adaptation algorithm was that described in section 5.4, with $\lambda = 0.97$ and $\delta = 1.0$.

Three variations of the periodic restart procedures of section 5.5 for the FRLS algorithm were tried. All relied on an auxiliary LMS adaptation algorithm to provide the equalizer's output Q_n during each restart interval. The three restart procedures were as follows:

Restart Procedure 1

The DFE tap coefficients $\underline{C}(n)$ were not re-initialized at the initiation of each restart (at n=K). In this case it can be shown [CK 83] that following a restart at time kT the DFE FRLS algorithm minimizes for $n \geq K$

$$S(n) = \delta\lambda^{n-k} \left| \underline{C}(n) - \underline{C}(K) \right|^2 + \sum_{k=k}^{n} \left| \underline{C}(n)^* \underline{Z}(k) - a_k \right|^2 \lambda^{n-k} \qquad (9.1)$$

where $\underline{C}(K)$ is the value of the tap coefficients updated just prior to restart. If the parameter δ is reasonably large then $\underline{C}(n)$ should not stray too far from $\underline{C}(K)$ during the restart interval. However a too-large choice of δ may hamper the algorithm's ability to track channel variations during the restart interval. For equalizer inputs with an RMS value of around 1.0, a suitable choice for δ was 1.0. The desired filter output used for adaptation in Restart Procedure 1 was that of equation (5.41), with $d_n = \hat{a}_n$.

Restart Procedure 2

In this restart procedure, the equalizer's tap coefficients $\underline{C}(n)$ were set to all-zeroes at the initiation of each restart. Equation (5.41) was used to provide the desired output.

Restart Procedure 3

Like Procedure 2, $\underline{C}(n)$ was set to all-zeroes, but equation (5.42) was used for the desired output.

Figure 9.2 shows an example of the application of restart methods initiated at the $n=300^{th}$ symbol interval for channel MDA010. The signal-to-noise ratio SNR on the vertical axis is the ratio of 1 (the mean squared data symbol) to the observed mean squared value of the error e(n) between the decision-making quantizer's input and its output. The averaging of the mean squared error (MSE) at the n^{th} symbol interval is as follows:

$$MSE(n) = 0.9\ MSE(n) + 0.1\ |e(n)|^2, \tag{9.2}$$

and the SNR at this time is

$$SNR(n) = 1/MSE(n) \tag{9.3}$$

In the case shown in Figure 9.2 the restart interval is 40 symbol intervals. During this period the useful equalizer output (the input to the decision-making quantizer) is taken from an auxiliary DFE which adapts according to the LMS algorithm, and whose tap coefficients were initialized to the tap coefficients of the FRLS DFE at the beginning of the restart period. In Figure 9.2 the SNR obtained from this LMS filter is shown by the solid line between n=300 and n=340.

During the 40-symbol-interval restart interval, the FRLS algorithm adapted from an initial state restarting at n=300. After n=340 the FRLS-adapting DFE took over from the LMS-adapting DFE. Figure 9.2 shows the SNR for the three restart procedures beyond n=340. In this example, Restart Procedure 1 gave slightly better performance than Restart Procedure 2, which in turn was somewhat better than Procedure 3.

The differences among these restart procedures in the same example are emphasized in Figure 9.3, which shows the measured SNR between n=300 and n=340, where the SNR is now defined as the reciprocal of the MSE, defined as in (9.2) for the still-restarting FRLS algorithm, instead of the LMS algorithm. The MSE was initialized to zero at n=300, which accounts for the large values of SNR near n=300. It is clear that Restart Procedure 1, in which the equalizer tap coefficients were not zeroed, caused little disruption to the FRLS adaptation during the restart period, while the other two procedures involving zeroed coefficients, required at least 40 iterations to restore a reasonably low mean squared error. Figures 9.4 and 9.5 correspond to Figures 9.2 and 9.3 for the next restart interval, beginning at n=640. In this case, Figure 9.4 shows less difference among the SNR's of the various procedures.

On the basis of simulation results like these we concluded that a valid and efficient procedure for periodically restarting the FRLS adaptation algorithm applied to a DFE receiver is Restart Procedure 1: do not initialize the FRLS equalizer tap coefficients to zero; supply the decision-making quantizer from

an auxiliary LMS-adapting DFE during the short startup interval; and use equation (5.41) as the desired output of the FRLS-adapting DFE for purposes of adaptation, with the $\underline{C}$ vector appearing in (5.41) being the current $\underline{C}$ vector of the auxiliary LMS algorithm. This is the restart procedure employed in all FRLS simulations described henceforth.

It is interesting to recall that in restarting the channel estimation FRLS algorithm with all coefficients being zeroed, equation (5.42) was generally found to yield a higher SNR than equation (5.41). The reason for this difference in the two types of adaptive filters is not known, although the differences i SNR between equations (5.41) and (5.42) have been observed to be small.

Figure 9.6 shows the DFE receiver's measured SNR for the first 800 symbol intervals on channel MDA010 and for both the FRLS adaptation algorithm and the LMS adaptation algorithm. The FRLS algorithm used the preferred restart procedure just described; this figures includes both restart intervals shown in Figures 9.2 to 9.5. Note that there is no noticeable disruption as a result of the periodically initiated restarts, although the measured SNR does exhibit relatively large fluctuations for this channel. Note too, that for some periods shown in the figure, the LMS-adapting DFE (not the same as the auxiliary LMS algorithm employed during the FRLS restart period) exhibits higher SNR than the FRLS algorithm.

9.2 Performance Comparison of FRLS and LMS Adaptation Algorithms (Ideal Reference Mode)

Simulated DFE equalizers adapted according to the LMS algorithm and also according to the FRLS algorithm with periodic restart Procedure 1 were compared with respect to error rate. The error rates were measured in 2 ways:

(1) Fraction of data symbols in error.

(2) Probability distribution of the number of symbols errors occurring in blocks of 100 transmitted symbols.

The total number of transmitted symbols in each simulation was 30000 (300 blocks). In the simulations reported in this section, the data symbols a_n which enter the feedback filter of the DFE and which are used for adaptation purposes were not receiver decisions, but instead were the known transmitted data symbols. This is the ideal reference mode. The results of these simulations shed light on the inherent capabilities of the DFE equalizer and its adaptation methods. The simulation results reported in section 9.4 are for the realistic case where the data symbols used by the adaptive receiver are its own decisions, and thus include the effects of error propagation or "crashes" caused during deep fades.

Figure 9.7 shows the block error distribution - the probability that more than n errors occur in a block of 100 as a function of n - for the ideal reference mode on channel MDA011. FRLS restart intervals of 30 and 40 symbol intervals are shown, the shorter restart interval yielding a slightly lower percentage of blocks containing one or more errors. Subsequent simulations used a FRLS restart interval of 30. The LMS-adapting DFE

exhibited on the order of twice the block error rate of the FRLS-adapting DFE. Figure 9.8 shows the corresponding ideal reference block error statistics for channel MDA010. For this channel there was less difference between the performance of the FRLS and LMS adaptation algorithms. Both channels exhibited error bursts due to fading. The largest numbers of consecutive blocks containing errors were 6 for the LMS algorithm on MDA011 and 19 for the LMS algorithm on MDA010. The last 16000 symbols on channel MDA010 were transmitted error-free in all cases. Tables in section 9.4 will summarize the error statistics.

It is clear that for these two channels in the ideal reference mode, the FRLS adaptation algorithm enjoyed only a slight performance advantage over the simpler LMS algorithm. This lack of a clear-cut advantage for the fast-adapting FRLS algorithm may be attributable to low signal-to-noise ratios during periods of rapid fading.

9.3 Crashes

The statistical results reported in Chapter 8 show periods of quite low (less than 10dB) signal-to-noise ratio on HF channels. This characteristic was also mirrored in the bursty nature of the errors observed in the ideal reference simulations. For a sufficiently deep fade, the receiver's error rate can become high enough that the sequence of decisions used for filter adaptation become unreliable; then the adapted equalizer tap coefficients may wander far from their optimal values, and catastrophic error propagation occurs. The onset of this

disastrous error propagation or "crash" can only be hastened by the use of filter adaptation algorithms which rapidly adapt to changing channel conditions. Such crashes for decision-directed adaptation were observed during deep fades in our simulations; decision-directed adaptation algorithms, both FRLS and LMS, usually failed to re-converge within a reasonable time following a crash.

Therefore, subsequent simulations which used the receiver's decisions $\{\hat{a}_n\}$ for equalizer adaptation and for decision feedback equalization were modified in the following way called the decision-directed mode: during every restart period once every 330 symbol intervals, the receiver's decisions were replaced by the portion of the known pseudo-random data sequence during that period; i.e. it was assumed that an ideal reference "training sequence" of 30 data symbols was transmitted once every 330 symbol intervals. Thus 9.1% of the transmitted data was an ideal reference training sequence. Periodic resynchronization of the adaptive receiver with an ideal reference appears to be a practical measure for fading HF channels. An alternative approach to crash recovery is transmission of a training sequence on demand via a feedback channel as suggested in [HGDP 80]. In our simulation the equalizer tap coefficient vector was never reset to zero; however there may be some advantage to resetting this vector to all-zeroes when the receiver's estimated signal-to-noise radio has been below a threshold for more than some given time interval. The periodic training sequence was applied to both LMS and FRLS receivers. In the case of the FRLS algorithm the training sequence coincided with each restart period. period.

9.4 Performance Comparison of FRLS and LMS Adaptation Algorithms (Decision-Directed Mode)

Figures 9.9 and 9.10 show the block error distributions for channels MDA011 and MDA010 respectively in the decision-directed mode. It is seen that the absence of an ideal reference except during the periodic training periods greatly increased the total number of symbol errors. The fraction of blocks containing one or more errors did not increase much for the receiver using the decision-directed FRLS algorithm. However the block error rate tripled for the LMS receiver on channel MDA011. This was the only case observed in which the FRLS algorithm displayed marginally superior performance. Table 9.1 for channel MDA011 and Table 9.2 for MDA010 summarize the average error rates observed in each of the 30,000-symbol simulations of DFE receivers. Figure 9.11 shows the blocks (numbered from 1 to 300) containing one or more errors in each simulation. Isolated erroneous blocks are shown as vertical lines, groups of two or more consecutive erroneous blocks are shown as rectangles. The ideal reference results are shown above, and the decision-directed results below the horizontal lines. Again, the very bursty nature of the decision errors is apparent. The times of occurrence of error bursts coincide with dips in the channel's signal-to-noise ratio shown in Figures 9.12 and 9.13 for channels MDA011 and MDA010 respectively. The measurements in Figures 9.12 and 9.13 were made using the LMS channel identification algorithm; the mean

Table 9.1

Summary of Error Rates for Channel MDA011

	Ideal Reference		Decision Directed	
	LMS	FRLS	LMS	FRLS
Block Error Rate	.103	.06	.193	.06
Bit Error Rate	.005	.003	.077	.010

Table 9.2

Summary of Error Rates for Channel MDA010

	Ideal Reference		Decision Directed	
	LMS	FRLS	LMS	FRLS
Block Error Rate	.140	.137	.153	.133
Bit Error Rate	.014	.012	.056	.045

squared error used to determine the SNR was averaged over 500 symbol intervals, so as to present an overall picture over 30000 symbol intervals, minimizing instantaneous fluctuations. Superimposed on these figures are the error bursts shown in Figure 9.11.

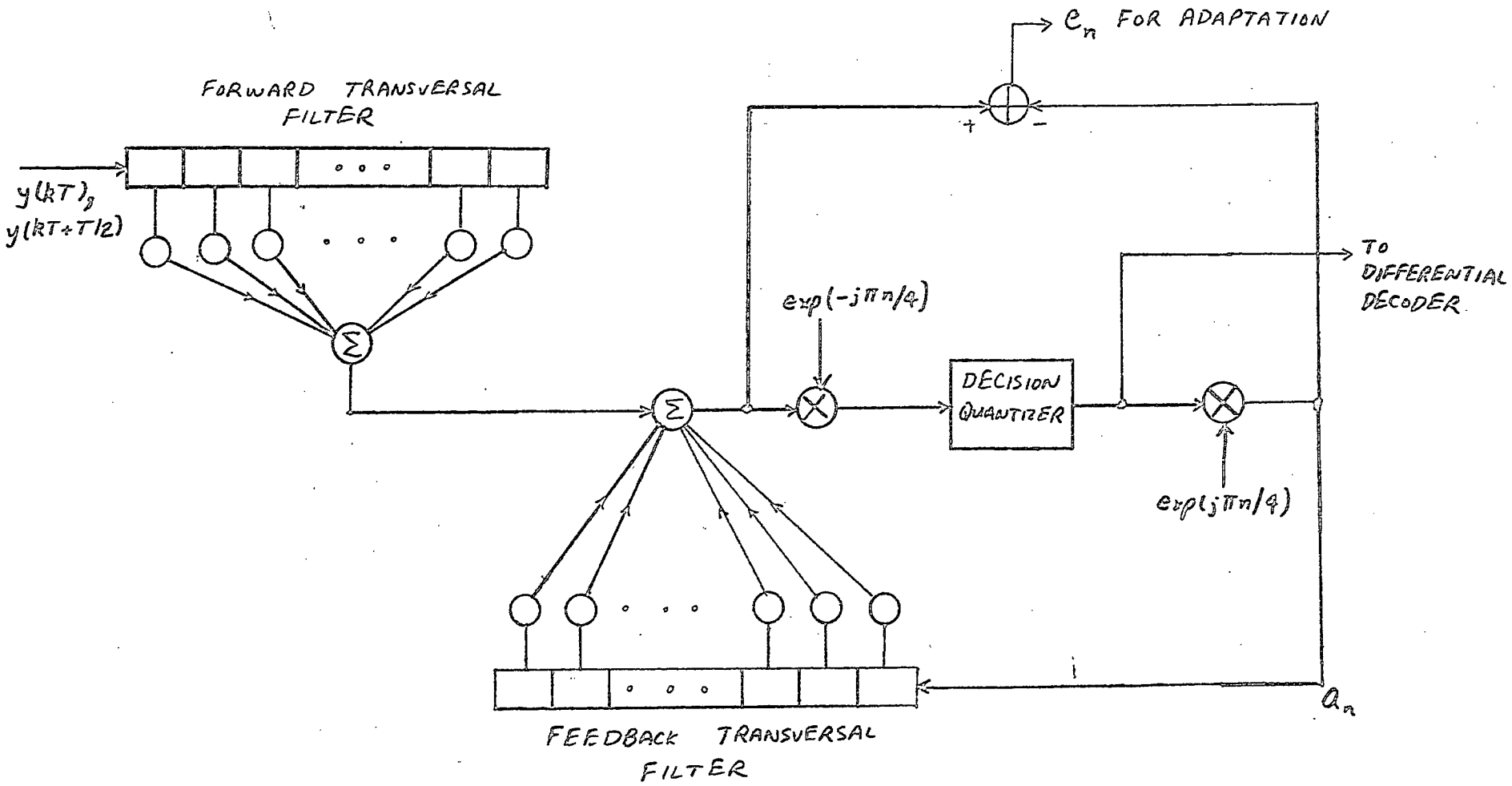

FIG. 9.1 DFE BLOCK DIAGRAM

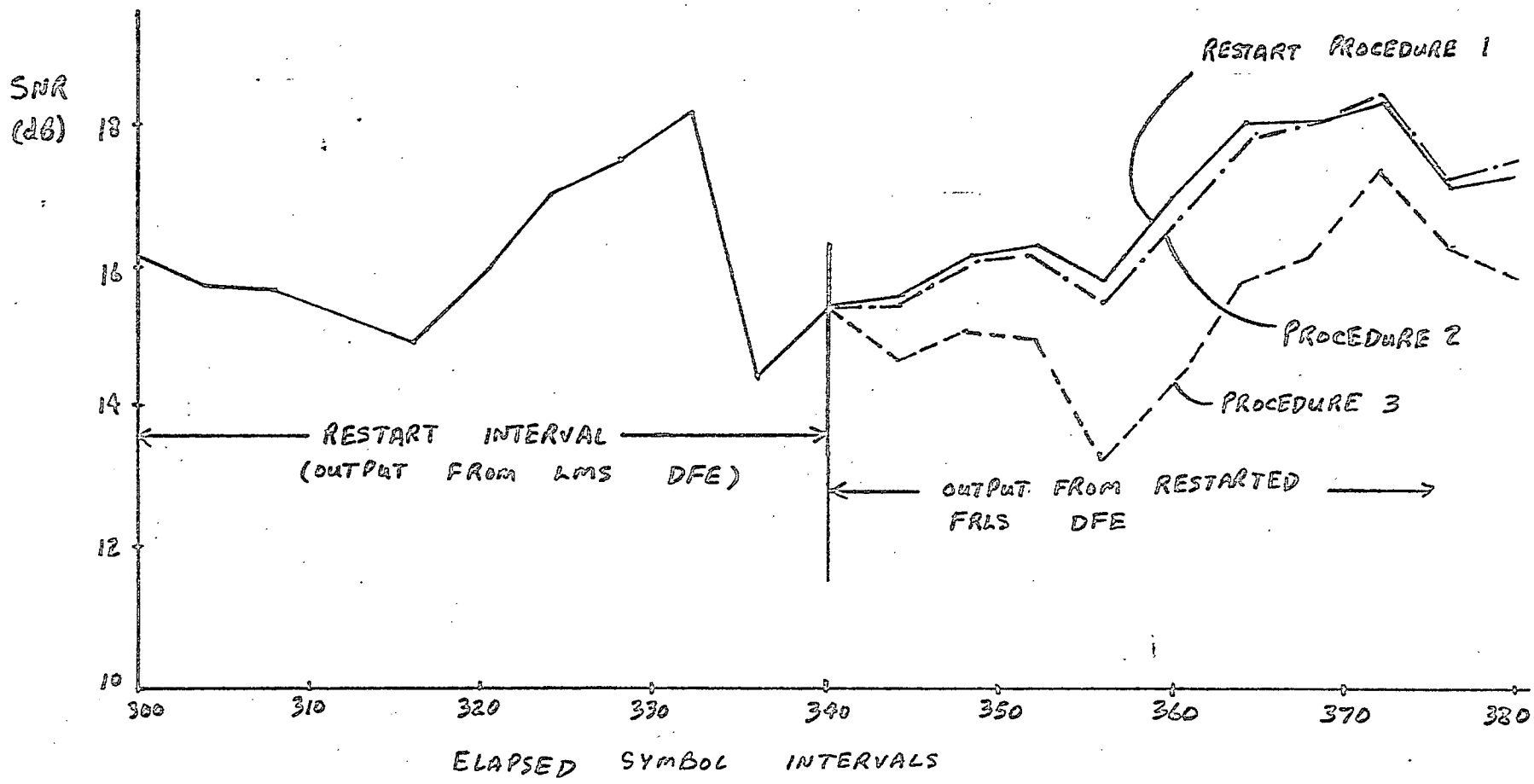

FIG. 9.2 EXAMPLE OF RESTART PROCEDURES FOR FRLS DFE
(CHANNEL MDA 010)

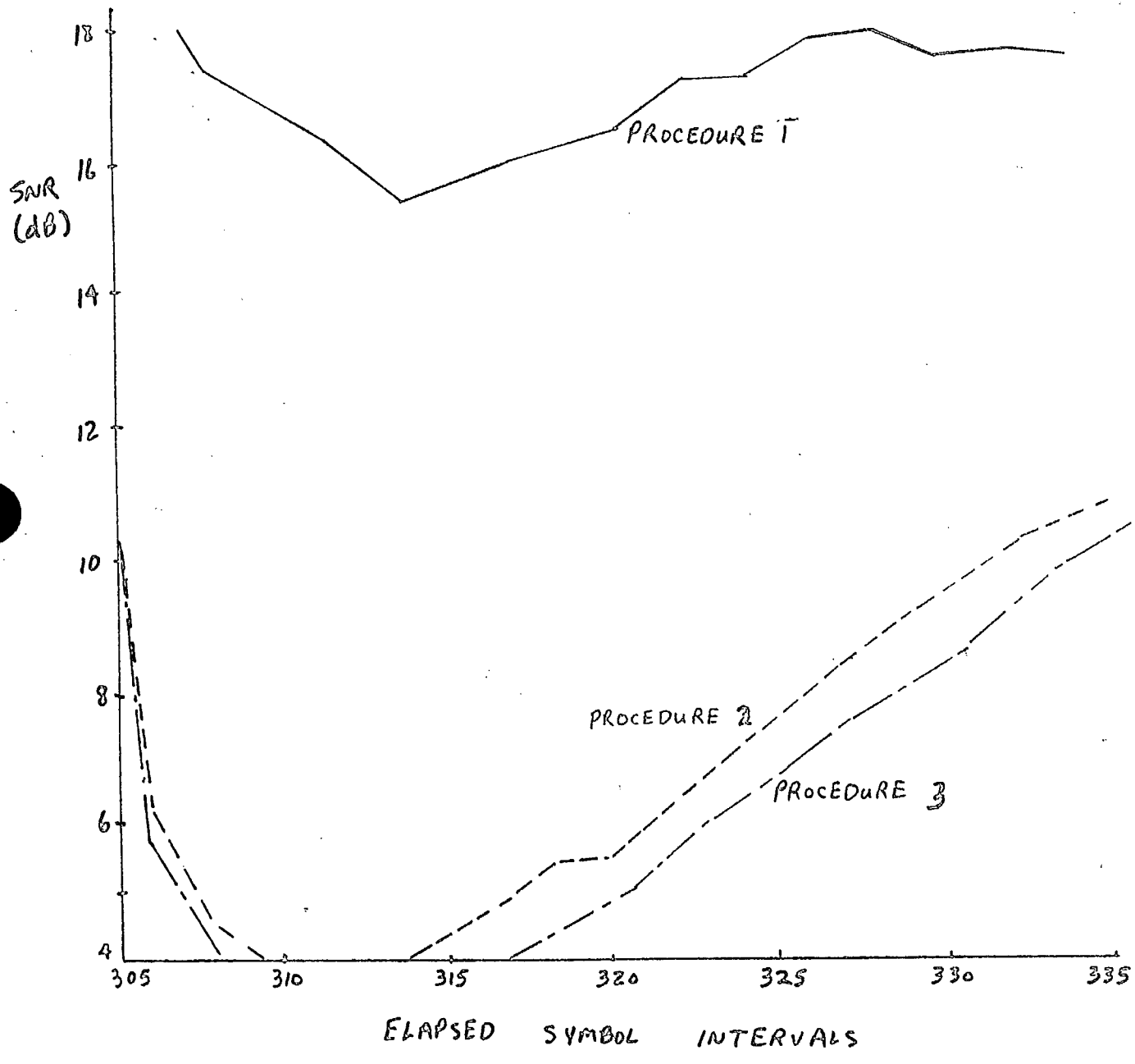

FIG. 9-3 SNR OF FRLS ALGORITHM FOR CHANNEL MDA 010 (RESTART AT 300)

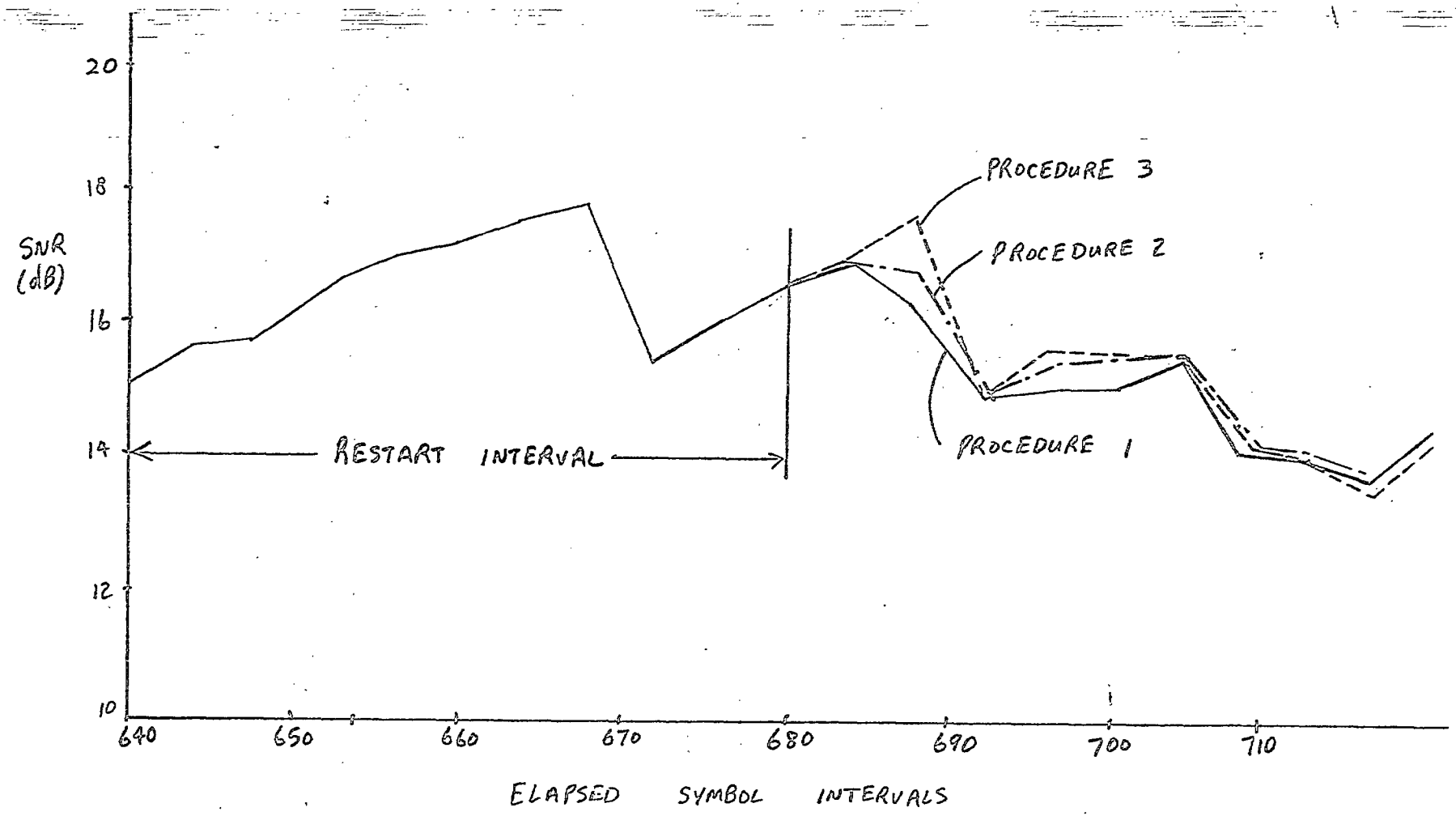

FIG. 9.4 EXAMPLE OF RESTART PROCEDURES FOR FRLS DFE (CHANNEL MDA 010)

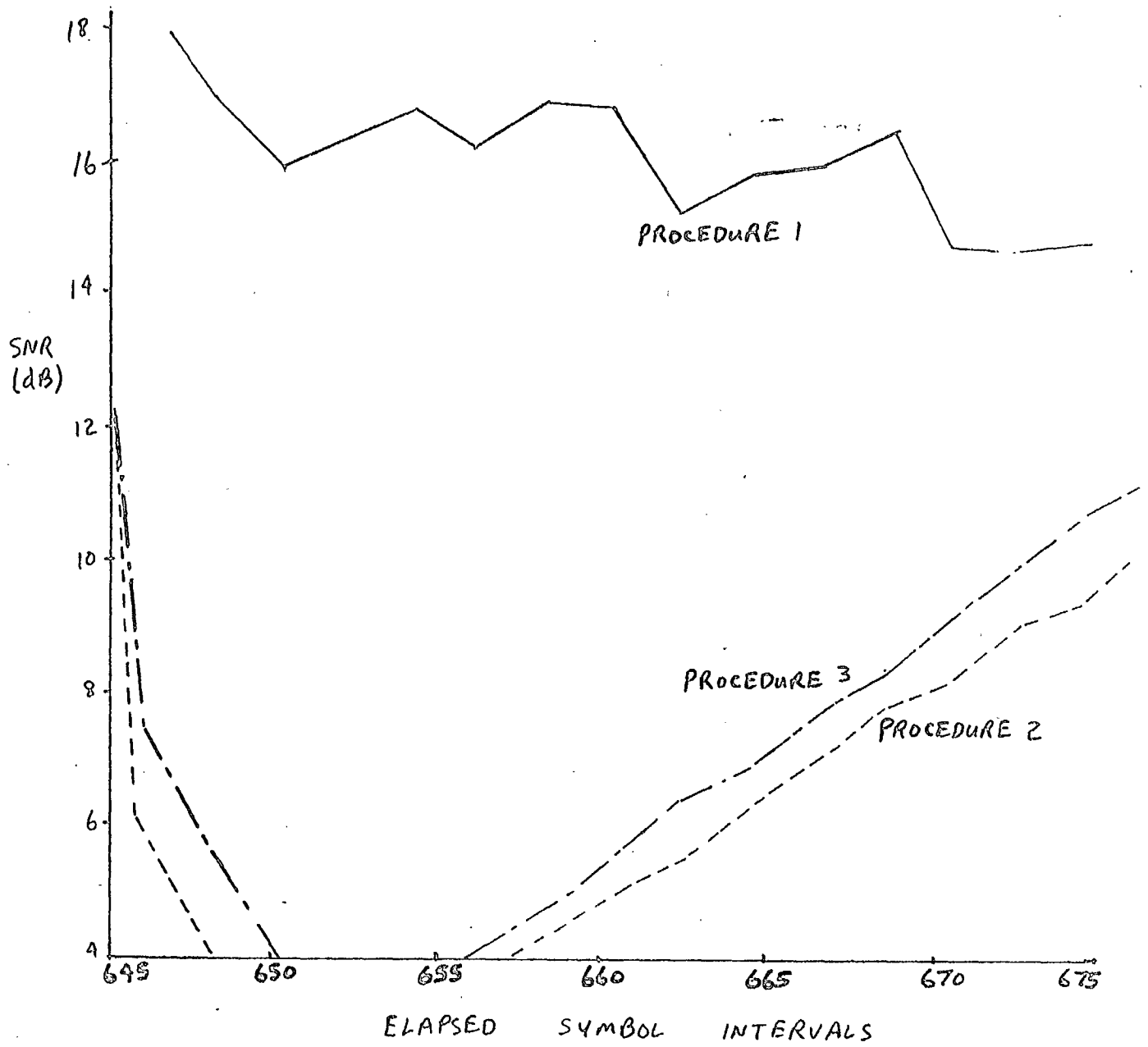

FIG. 9.5 SNR OF FRLS ALGORITHM FOR CHANNEL MDA 010 (RESTART AT 640

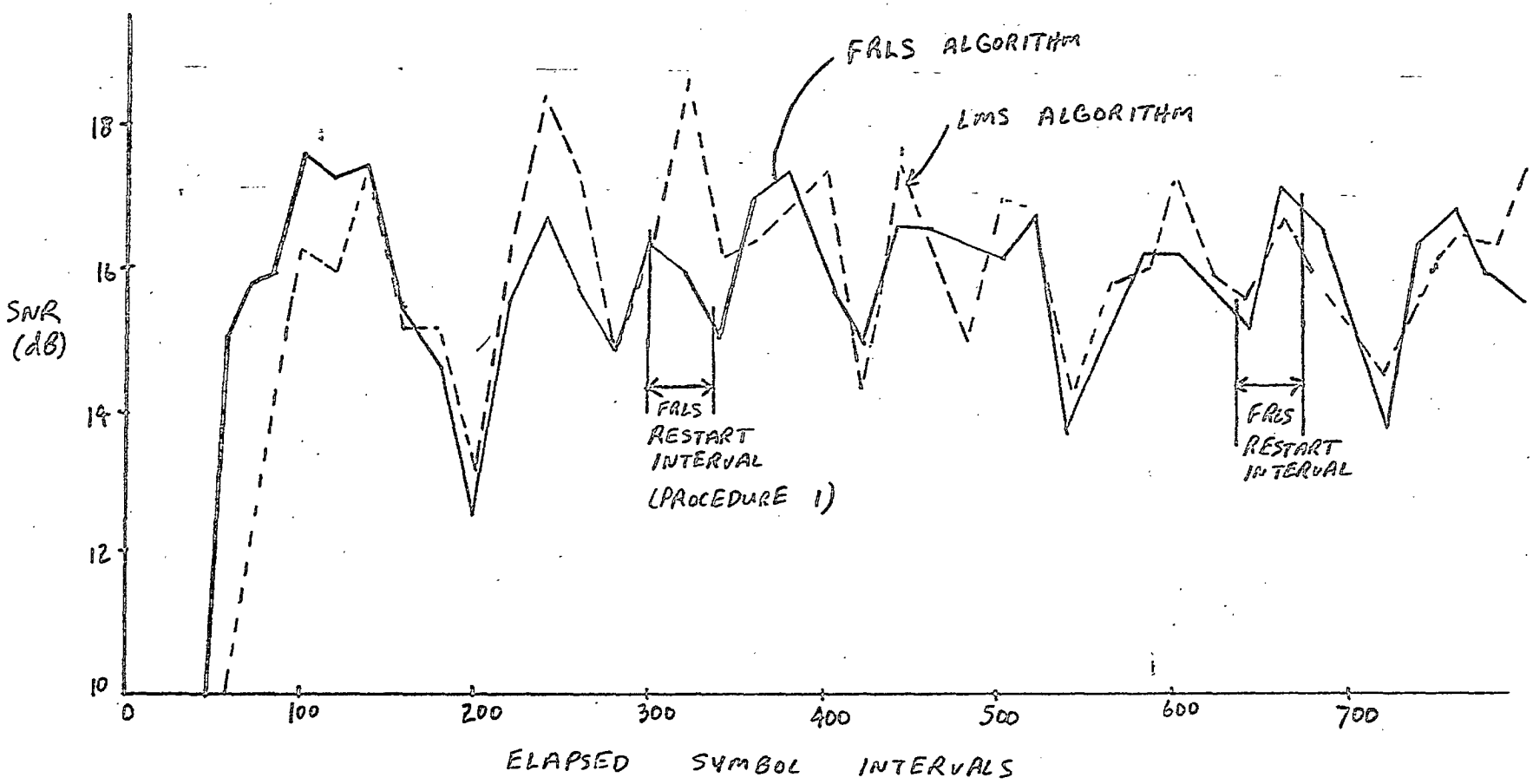

FIG. 9.6 COMPARISON OF FRLS AND LMS ADAPTATION FOR DFE ON CHANNEL MDA 010

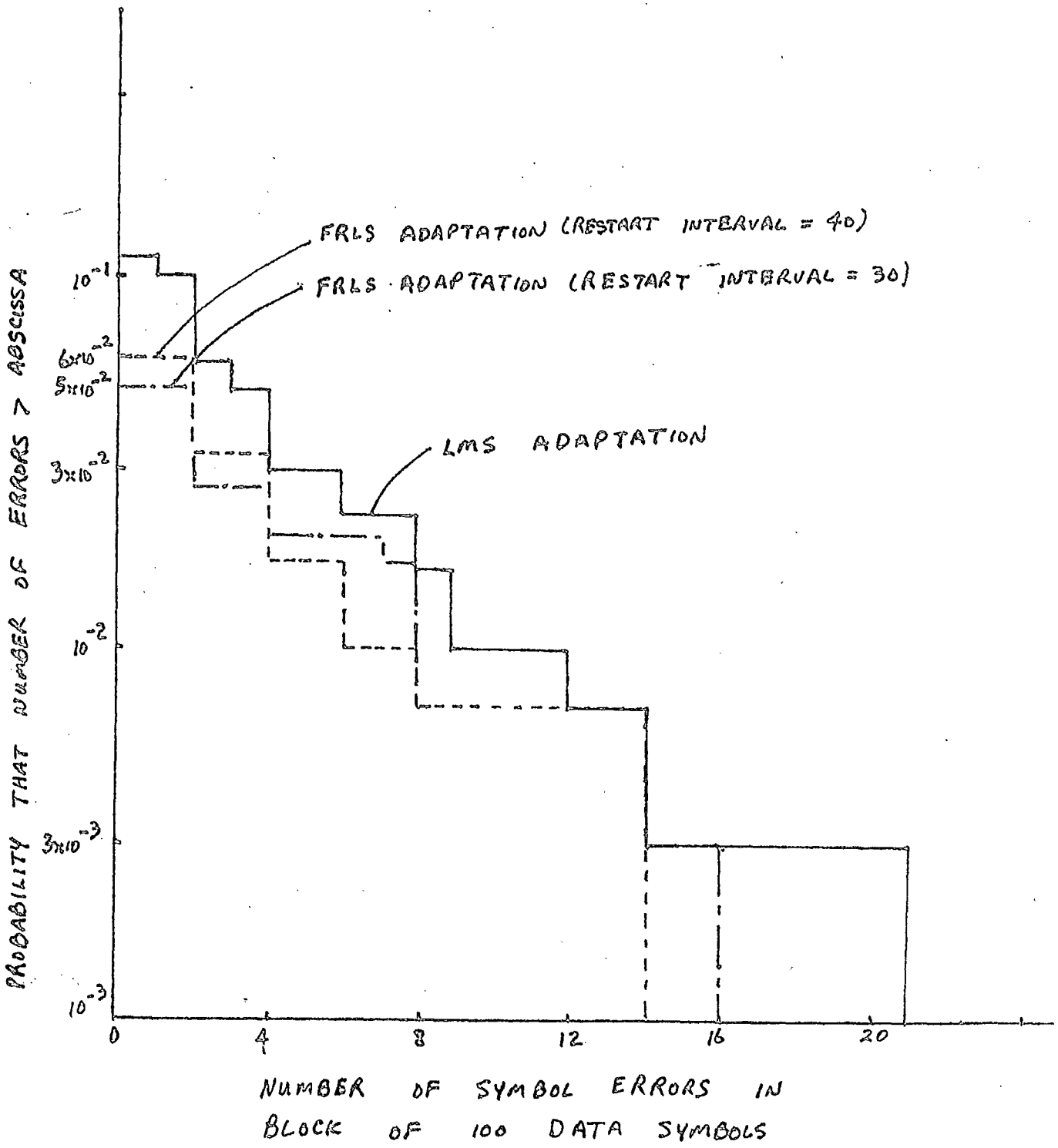

FIG. 9.7 ERROR STATISTICS FOR FRLS AND LMS DFE ON CHANNEL MDA 011 (IDEAL REFERENCE MODE)

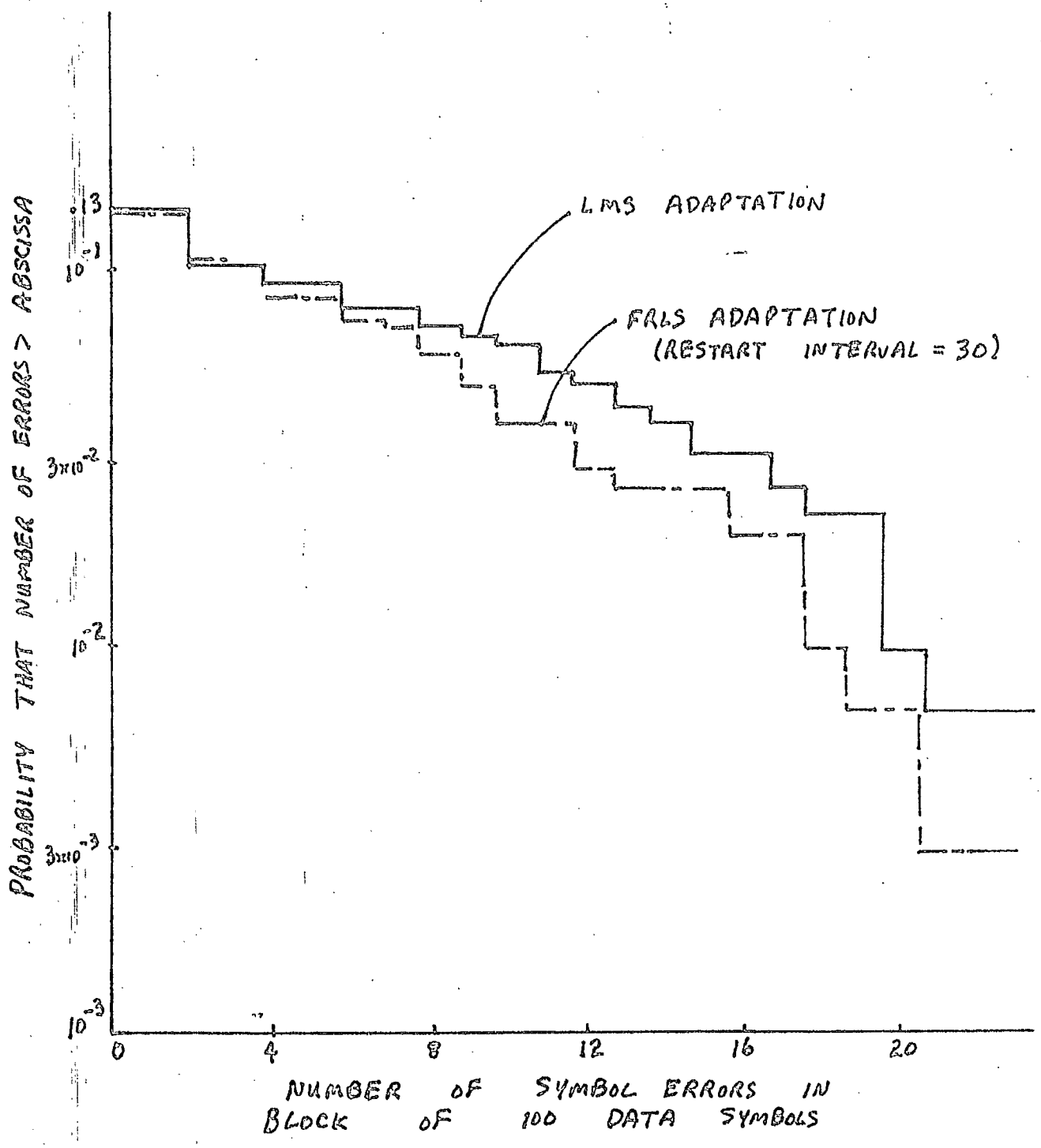

FIG. 9.8 ERROR STATISTICS FOR FRLS AND LMS DFE ON CHANNEL MDA 010 (IDEAL REFERENCE)

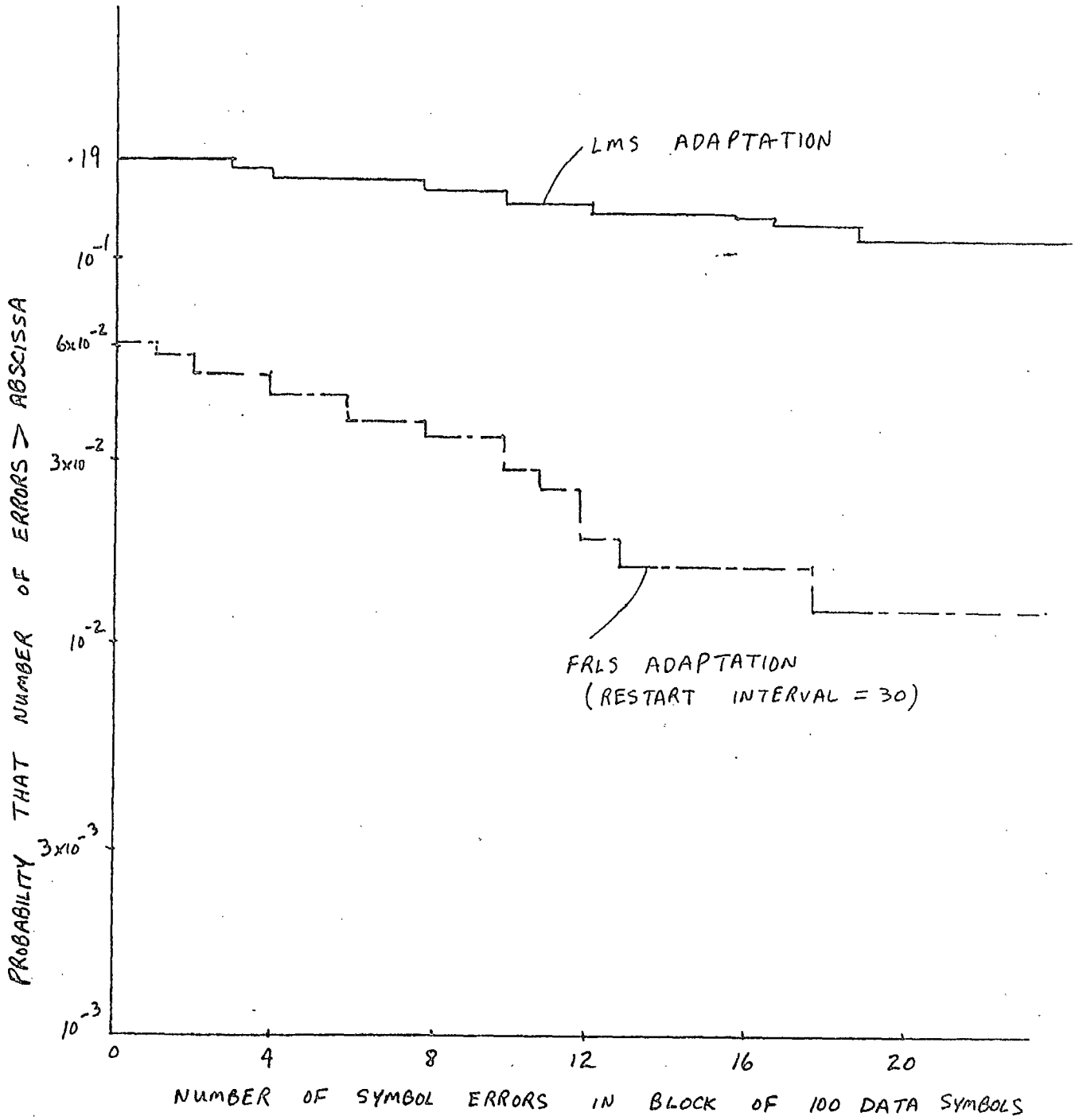

FIG. 9.9 ERROR STATISTICS FOR FRLS AND LMS DFE ON CHANNEL MDA 011 (DECISION-DIRECTED

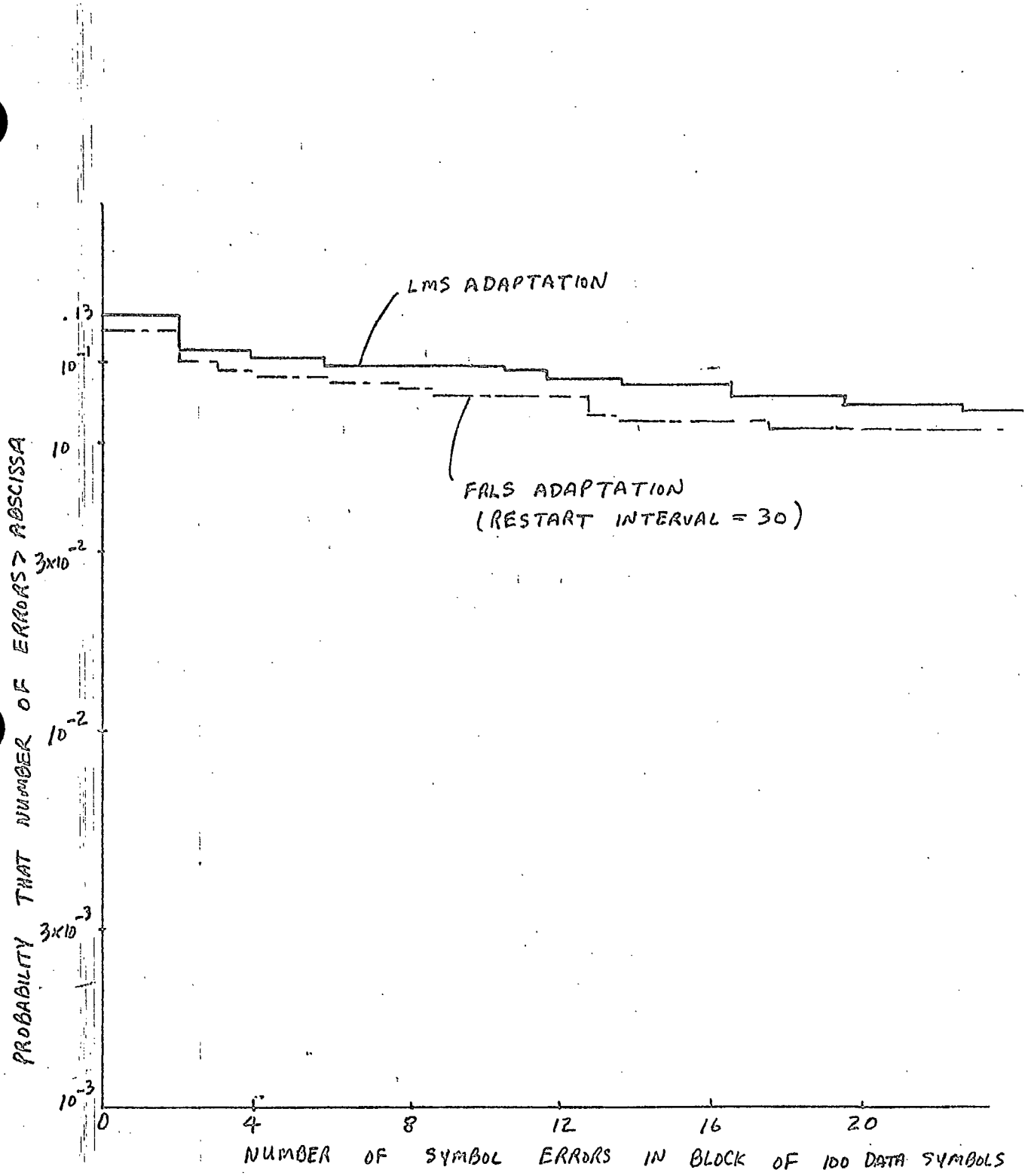

FIG. 9-10 ERROR STATISTICS FOR FRLS AND LMS DFE ON CHANNEL MDA 010 (DECISION-DIRECTED)

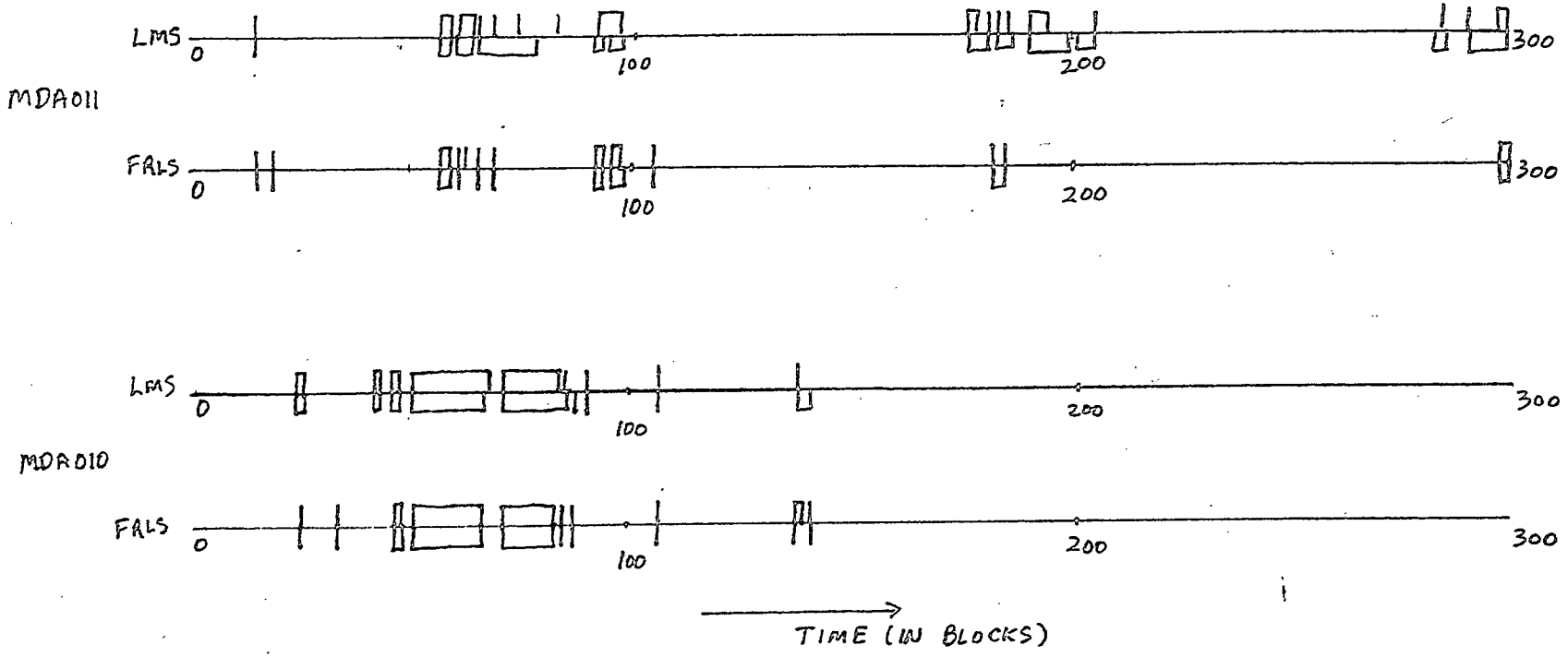

FIG. 9.11 BLOCKS CONTAINING ONE OR MORE ERRORS. IDEAL REFERENCE CASES SHOWN ABOVE, DECISION-DIRECTED CASES SHOWN BELOW.

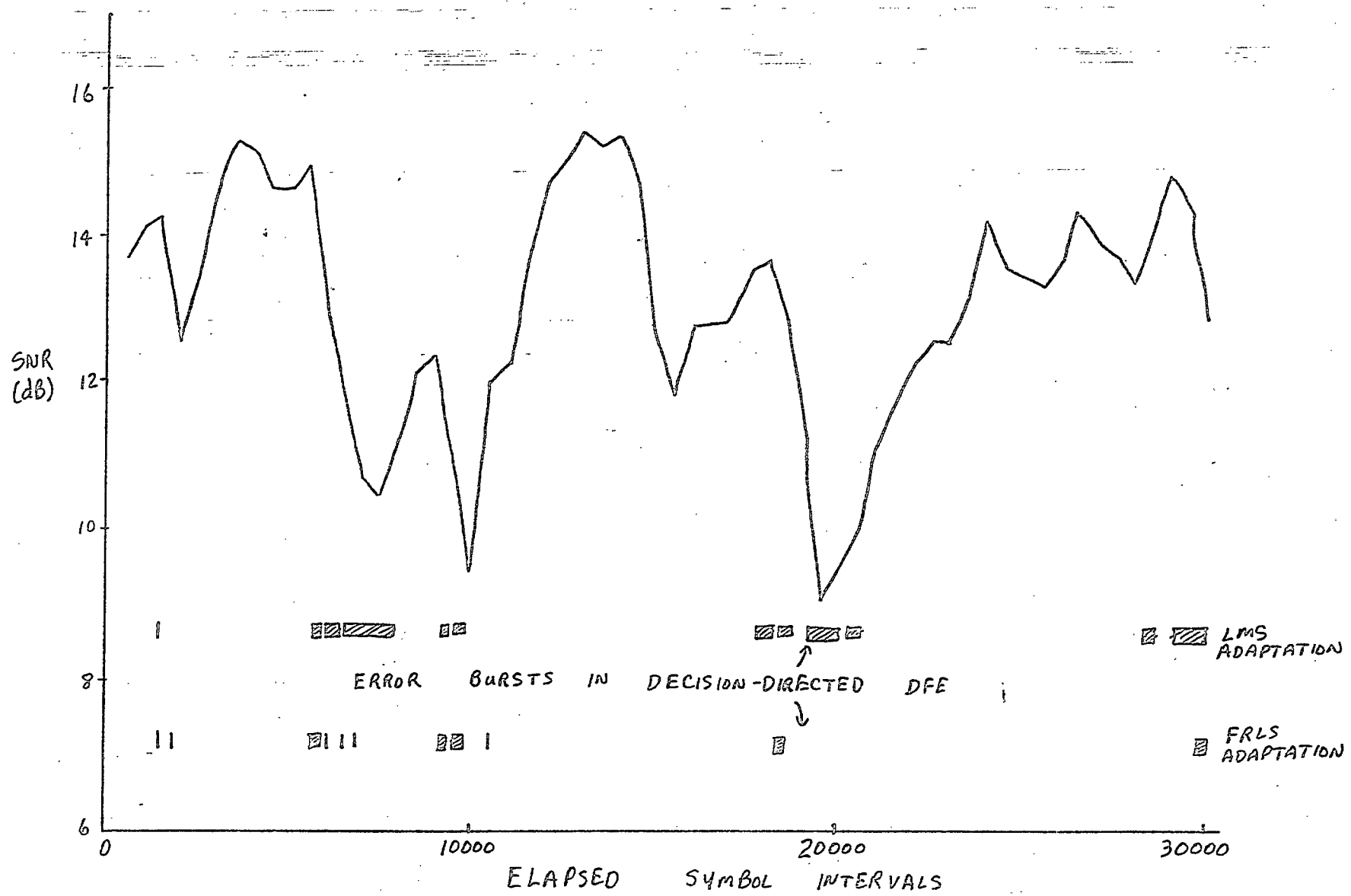

FIG. 9.12 SNR VERSUS TIME FOR CHANNEL MDA011
(SNR AVERAGED WITH 500-SYMBOL-INTERVAL TIME CONSTANT)

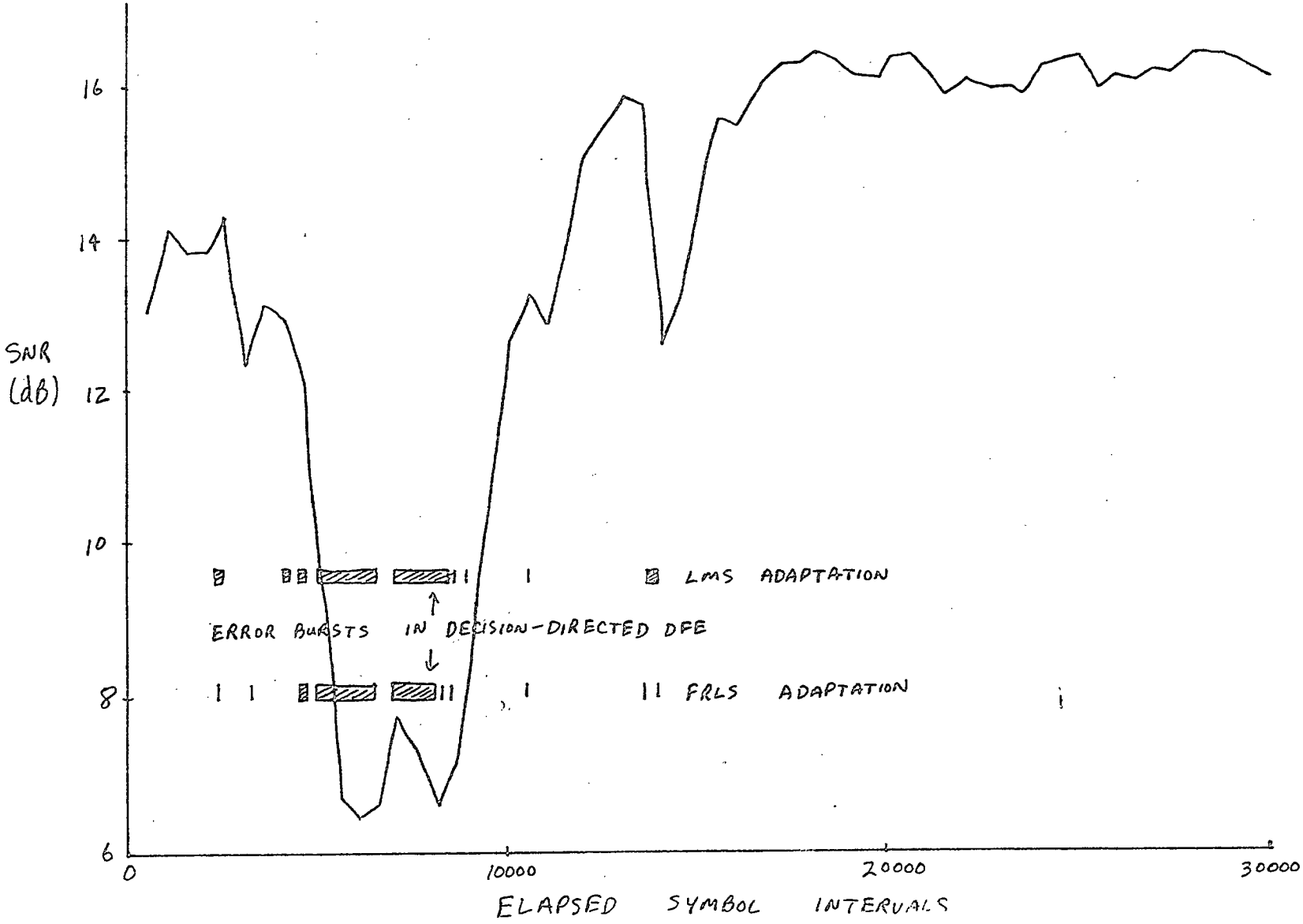

FIG. 9-13 SNR VERSUS TIME FOR CHANNEL MDA 010
(SNR AVERAGED WITH 500-SYMBOL INTERVAL TIME CONSTANT)

10. SUMMARY AND CONCLUSIONS

10.1 Comparison of DFE and MLSE Receivers

Determination of the effective SNR parameter d/σ from measured channel impulse responses suggests that for the two HF channels which were extensively investigated, the theoretical DFE performance falls within about 1 dB of the theoretical MLSE or matched filter performance. (See Figures 8.7 and 8.8). Moreover the measured impulse response duration statistics, summarized in Table 8.3 indicates that channel impulse responses effectively 8 to 10 symbol intervals long can occur. A MLSE (Viterbi algorithm) receiver designed to accommodate such impulse responses would require on the order of 4^{10} storage locations and operations per symbol interval. Thus there seems to be little reason to adapt the MLSE approach on the basis of these results. A further problem with MLSE is the effect of the decision delay on the adaptation speed. On the other hand, if the MLSE algorithm could be approximated by a simpler algorithm, we have seen that the filter adaptation algorithm associated with an MLSE receiver can be considerably simpler than that associated with a DFE receiver. It is worth noting here that Monsen has drawn similar conclusions on the relative worth of DFE and MLSE reception for fading tropospheric scatter channels with diversity [Mon 71], [Mon 73], [Mon 74], [Mon 77].

10.2 Comparison of FRLS and LMS Adaptation Algorithms

Relatively rapid impulse response variations were observed, as illustrated in Table 8.4. For channel identification with the

order of 10 adaptive tap coefficients LMS adaptation appears adequate, especially in a low SNR environment. (See Figures 5.6 and 5.7). The problem of instability due to accumulating roundoff error in FRLS algorithms was met and dealt with by means of a periodic restart procedure. By restarting (zeroing) only the interval algorithm variables and modifying the desired adaptive filter outputs during restart to account for the step function in the filter inputs during restart, disruptions due to restart were minimized. As well as the periodically-applied restart procedures for the FRLS adaptation algorithms it was found necessary to modify the normal decision-directed mode of operation (use of receiver decisions in the DFE feedback signal and for filter adaptation) by periodically inserting a training sequence of 30 known data symbols. For the FRLS algorithm this coincided with the restart periods. Although 9.1% of the transmitted data capacity was thereby lost, periodic retraining allowed the adaptive receiver to recover from the effects of severe fades. The complete DFE and FRLS adaptation and restart algorithm is specified in Appendix B.

Simulations of decision-directed DFE receivers using both LMS and FRLS adaptation algorithm were carried out for channels MDA011 and MDA010. The results were summarized in Figures 9.6 to 9.13. The block error rate for the FRLS algorithm was reduced to about one third of its value for the LMS algorithm in the case of channel MDA011. However in the case of channel MDA010, there was little difference in the block error rate performance of the two adaptation algorithms. We feel that the failure of the fast-

adapting but more computation-intensive FRLS adaptation algorithm to show a spectacular performance advantage over the LMS adaptation algorithm is due to the relatively low average signal-to-noise ratios seen on these channels. Higher signal-to-noise ratios would probably have considerably increased the performance differences between the two algorithms. This conclusion is borne out by other performance comparisons between FRLS and LMS adaptation algorithms reported in [HGDP 80], and [LP 83] in which Rayleigh-fading HF channels with a wide range of signal-to-noise ratios were simulated.

10.3 Recommendations for Future Work

It is recommended that similar studies be conducted using recordings from a much wider selection of HF channels - for different path lengths, times of day and seasons, frequencies relative to the M.U.F. etc. Among the other results of such a study should be a better statistical characterization of the average signal-to-noise ratio encountered under various conditions. We have seen that the signal-to-noise ratio not only strongly influences performance in an obvious way but also influences the choice of the filter adaptation algorithm.

If the low SNR's encountered in our investigation are felt to be typical, then a prototype digital HF communications system employing a decision feedback equalizer adapted according to the LMS algorithm should be built and tested on a variety of HF channels. Such an implementation should be within the capabilities of existing programmable signal processing devices. Implementation of an FRLS adaptation algorithm at present would

likely require non-programmable hardware due to its complexity, but this algorithm should be within the capabilities of digital signal processing devices in the near future.

There is also a need for further studies of alternate transmitter and receiver signal processing. Transmission of data in independent blocks or packets, preceded by known training sequences is an effective method for crash recovery. Packet length and training-sequence length should be investigated for various adaptation algorithms to maximize throughput and reliability. Finally, there may be room for innovation in the MLSE type of receiver, if low-complexity practical approximations to the MLSE detection algorithm can be found which work well on HF channels.

10.4 Major Conclusions of the Study

(1) For the HF channels investigated, DFE reception offers a more favourable performance/complexity tradeoff than MLSE reception.

(2) For the channels investigated the relatively small performance advantage enjoyed by a DFE receiver using the FRLS adaptation algorithm may not justify its much greater complexity relative to the DFE receiver using LMS adaptation. However if higher average signal-to-noise ratios are expected in practice, the FRLS-adapting DFE receiver may be much more attractive.

(3) An efficient restart procedure for the FRLS adaptation algorithm has been developed. This circumvents the

numerical stability problems to which the FRLS algorithm is subject, without significantly compromising its ability to track rapidly time-varying channels.

[CTLL 82] S. Crozier, K. Tiedemann, R. Lyons and J. Lodge, "An Adaptive Maximum Likelihood Sequence Estimation Technique for Wideband HF Communications", presented at 1982 Military Communications Conference, Boston, October 1982.

[Dar 75] Darnell, M., Channel Estimation Techniques for HF Communications, AGARD-NATO Advanced Study Conf. Proceedings No.173 (Radio Systems and Ionosphere), March 1975.

[DC 78] H.B. Doan and A. Cantoni, "Fast Adaptation of Equalizer and Desired Response for Digital Data Receivers", Electronic Circuits and Systems, Vol.2, No.5, September 1978, pp.159-166.

[DMM 74] D.L. Duttweiler, J. Mazo and D.G. Messerschmitt, "An Upper Bound on the Error Probability in Decision-Feedback Equalization", IEEE Trans. Inform. Theory, Vol.IT-20, No.4, July 1974, pp.490-497.

[ED 82] Eijselendoorn, J. and Den Dulk, R.C., "Improved Phase-Locked Loop Performance with Adaptive Phase Comparators", IEEE Trans. on Aerospace and Electronic Systems, pp.323-332, May 1982.

[EWH 81] El-Tanany, M., Wight, J.S. and Hafez, H.M., "A Fast Carrier Recovery Circuit for CPFSK Signals", NAECOM81, pp.134-139, Dayton, Ohio, May 1981.

[Fal 76a] D.D. Falconer, "Jointly Adaptive Equalization and Carrier Recovery in Two-Dimensional Digital Communication Systems", BSTJ, Vol.55, No.3, March 1976, pp.317-334.

[Fal 76b] D.D. Falconer, "Application of Passband Decision Feedback Equalization in Two-Dimensional Data Communications Systems", IEEE Trans. Commun., October 1976, pp.1159-1166.

[FF 73] D.D. Falconer, G.J. Foschini, "Theory of Minimum Mean-Square Error QAM Systems Employing Decision Feedback Equalization", BSTJ, Vol.52, No.10, December 1973, pp.1821-1849.

[FL 78] D.D. Falconer, and L. Ljung, "Application of Fast Kalman Estimation to Adaptive Equalization", IEEE Trans. Commun., Vol.COM-26, No.10, October 1978, pp.1439-1446.

[FM 73] D.D. Falconer and F.R. Magee, Jr., "Adaptive Channel Memory Truncation for Maximum-Likelihood Sequence Estimation", BSTJ, Vol.52, November 1973, pp.1541-1562.

References

[Agar 79] AGARD, Special Topics on HF Radio Propagation, Agard Conference Proceedings No.263, June 1979.

[BGR 80] A. Benveniste, M. Goursat and G. Ruget, "Robust Identification of a Nonminimum Phase System: Blind Adjustment of a Linear Equalizer in Data Communications", IEEE Trans. on Automatic Control, June 1980, pp.385-399.

[BF 75] Barry, G. and Fenwick, R.B., Techniques for Real Time HF Measurements and Optimum Data Transmissions, AGARD-NATO Advanced Study Conf. Proceedings No.173 (Radio Systems and Ionosphere), March 1975.

[Bet 67] Betts, J.A., High Frequency Communications, English Universities Press, London 1967.

[BP 79] C.A. Belfiore and J.H. Park, Jr., "Decision Feedback Equalization", Proc. IEEE, Vol.67, No.8, August 1979, pp.1143-1156.

[CHD 78] A.P. Clark, J.D. Harvey and J.P. Driscoll, "Near-Maximum-Likelihood Detection Processes for Distorted Data Signals", Radio and Electronic Engineer, Vol.48, No.6, June 1978, pp.301-309.

[Cla 81] A.P. Clark, "Detection of Digital Signals Transmitted Over A Known Time-Varying Channel", IEE Proc., Vol.128, Pt.F, No.3, June 1981, pp.167-174.

[CK 83] J.M. Cioffi and T. Kailath, "Fast, Fixed-Order Least-Squares Algorithms for Adaptive Filtering", to be published in IEEE Trans. Acoustics, Speech and Signal Processing.

[CKH 79] A.P. Clark, C.P. Kwong, J.D. Harvey, "Detection Processes for Severely Distorted Digital Signals", Electronic Circuits and Systems, Vol.3, No.1, January 1979, pp.27-37.

[CM 81] A.P. Clark, F. McVerry, "Channel Estimation for an HF Radio Link", IEE Proc., Vol.128, Pt.F, February 1981, pp.33-42.

[CM 82a] R.S.W. Cheung and P.J. McLane, "Carrier Reference Sensitivity of a Viterbi Detector for PAM Data Transmission", IEEE Trans. Commun., Vol.COM-30, No.2, February 1982, pp.410-414.

[CM 82b] A.P. Clark and R.S. Marshall, "Developments of the Conventional Nonlinear Equalizer", IEE Proc., Vol.129, Pt.F., No.2, April 1982, pp.85-94.

[CTLL 82] S. Crozier, K. Tiedemann, R. Lyons and J. Lodge, "An Adaptive Maximum Likelihood Sequence Estimation Technique for Wideband HF Communications", presented at 1982 Military Communications Conference, Boston, October 1982.

[Dar 75] Darnell, M., Channel Estimation Techniques for HF Communications, AGARD-NATO Advanced Study Conf. Proceedings No.173 (Radio Systems and Ionosphere), March 1975.

[DC 78] H.B. Doan and A. Cantoni, "Fast Adaptation of Equalizer and Desired Response for Digital Data Receivers", Electronic Circuits and Systems, Vol.2, No.5, September 1978, pp.159-166.

[DMM 74] D.L. Duttweiler, J. Mazo and D.G. Messerschmitt, "An Upper Bound on the Error Probability in Decision-Feedback Equalization", IEEE Trans. Inform. Theory, Vol.IT-20, No.4, July 1974, pp.490-497.

[ED 82] Eijselendoorn, J. and Den Dulk, R.C., "Improved Phase-Locked Loop Performance with Adaptive Phase Comparators", IEEE Trans. on Aerospace and Electronic Systems, pp.323-332, May 1982.

[EWH 81] El-Tanany, M., Wight, J.S. and Hafez, H.M., "A Fast Carrier Recovery Circuit for CPFSK Signals", NAECOM81, pp.134-139, Dayton, Ohio, May 1981.

[Fal 76a] D.D. Falconer, "Jointly Adaptive Equalization and Carrier Recovery in Two-Dimensional Digital Communication Systems", BSTJ, Vol.55, No.3, March 1976, pp.317-334.

[Fal 76b] D.D. Falconer, "Application of Passband Decision Feedback Equalization in Two-Dimensional Data Communications Systems", IEEE Trans. Commun., October 1976, pp.1159-1166.

[FF 73] D.D. Falconer, G.J. Foschini, "Theory of Minimum Mean-Square Error QAM Systems Employing Decision Feedback Equalization", BSTJ, Vol.52, No.10, December 1973, pp.1821-1849.

[FL 78] D.D. Falconer, and L. Ljung, "Application of Fast Kalman Estimation to Adaptive Equalization", IEEE Trans. Commun., Vol.COM-26, No.10, October 1978, pp.1439-1446.

[FM 73] D.D. Falconer and F.R. Magee, Jr., "Adaptive Channel Memory Truncation for Maximum-Likelihood Sequence Estimation", BSTJ, Vol.52, November 1973, pp.1541-1562.

[FM 76a,b] D.D. Falconer and F.R. Magee, Jr., "Evaluation of Decision Feedback Equalization and Viterbi Algorithm Detection for Voiceband Data Transmission, Parts I and II", IEEE Trans. Commun., Vol.COM-24, Nos. 10 and 11, October and November 1976, pp.1130-1139 and 1238-1245.

[For 72] G.D. Forney, Jr., "Maximum-Likelihood Sequence Estimation of Digital Sequences in the Presence of Intersymbol Interference", IEEE Trans. Inform. Theory, Vol.IT-18, May 1972, pp.363-378.

[Fri 82] B. Friedlander, "Lattice Filters for Adaptive Processing", Proc. IEEE, Vol.70, No.8, August 1982, pp.829-867.

[Gar 79] F.M. Gardner, "Phaselock Techniques", Second Edition, Wiley-Interscience, John Wiley & Sons, 1979, Chapter 11.

[GBS 71] D.A. George, R.R. Bowen and J.R. Storey, "An Adaptive Decision Feedback Equalizer", IEEE Trans. Commun., Vol.COM-19, No.3, June 1971, pp.281-293.

[GM 77] R.D. Gitlin and F.R. Magee, Jr., "Self-Orthogonalizing Adaptive Equalization Algorithms", IEEE Trans. Commun., Vol.COM-25, No.7, July 1977, pp.666-672.

[GMW 82] R.D. Gitlin, H.C. Meadors and S.B. Weinstein, "The Tap-Leakage Algorithms: An Algorithm for the Stable Operation of a Digitally Implemented Fractionally Spaced Adaptive Equalizer", BSTJ, Vol.61, No.8, October 1982, pp.1817-1839.

[God 74] D. Godard, "Channel Equalization Using a Kalman Filter for Fast Data Transmission", IBM J. Res. & Dev., May 1974, pp.267-273.

[God 80] D.N. Godard, "Self-Recovering Equalization and Carrier Tracking in Two Dimensional Communication Systems", IEEE Trans. Communications, November 1980, pp.1867-1875.

[GW 81] R.D. Gitlin and S.B. Weinstein, "Fractionally-Spaced Equalization: An Improved Digital Transversal Equalizer", BSTJ, Vol.60, No.2, February 1981, pp.275-296.

[Gol 66] Goldberg, B., 300 KHz - 30 MHz MF/HF, IEEE Trans. on Communication Technology, Vol.COM-14, pp.767-784, December 1960.

[HA 70] W.S. Hurd and T.C. Anderson, "Digital Transition Tracking Synchronizer for Low SNR Coded Systems", IEEE Transactions on Communications Technology, Vol.COM-18, No.4, April 1970, pp.141-146.

[HGDP 80] F.M. Hsu, A.A. Giordano, H.E. DePedro and J.G. Proakis, "Adaptive Equalization Techniques for High Speed Transmission on Fading Dispersive HF Channels", NTC 80, Houston, December 1980.

[Hsu 82] F.M. Hsu, "Square Root Kalman Filtering for High-Speed Data Received Over Fading Dispersive HF Channels", IEEE Trans. Inform. Theory, Vol.IT-28, No.5, September 1982, pp.753-763.

[HM 82] M.L. Honig and D.G. Messerschmitt, "Comparison of LS and LMS Lattice Predictor Algorithms Using Two Performance Criteria", submitted to IEEE Trans. ASSP.

[Hon 82] M.L. Honig, "Convergence Models for Lattice Joint Process Estimators and Least Squares Algorithms", to be published.

[Ins 69] Inston, H., Dispersion of HF Pulses by Ionospheric Reflection, Proc. IEE, Vol.116, pp.1789-1793, November 1969.

[LH 77] W.U. Lee and F.J. Hill, "A Maximum-Likelihood Sequence Estimator with Decision-Feedback Equalization", IEEE Trans. Comm., September 1977, Vol.COM-25, pp.971-979.

[LMF 78] L. Ljung, M. Morf and D.D. Falconer, "Fast Calculation of Gain Matrices for Recursive Estimation Schemes", Int. J. Control, January 1978.

[LP 82] F. Ling and J.G. Proakis, "Generalized Least Squares Lattice Algorithm and its Application to Decision Feedback Equalization", Proc. Int. Conf. on Acous., Speech and Sig. Proc., Paris, April 1982, pp.1764-1769.

[LP 83] F. Ling and J.G. Proakis, "Adaptive Lattice Decision Feedback Equalizers and Their Application on Fading Dispersive Channels", Int. Conf. on Commun., June 1983, Boston.

[Mak 78] J. Makhoul, "A Class of All-Zero Lattice Digital Filters: Properties and Applications", IEEE Trans. ASSP, Vol.ASSP-26, No.4, August 1978, pp.304-314.

[Mas 82] N.M. Maslin, "High Data Rate Transmission Over HF Links", Radio & Electronic Engineer, Vol.52, No.2, February 1982, pp.75-87.

[McL 80] P. McLane, "A Residual Intersymbol Interference Bound for Truncated-State Viterbi Detectors", IEEE Trans. Inform. Theory, Vol.IT-26, No.5, September 1980.

[Mes 73] D.G. Messerschmitt, "A Geometric Theory of Intersymbol Interference, I and II", BSTJ, Vol.52, October 1973.

[Mes 74] D.G. Messerschmitt, "Design of a Finite Impulse Response for the Viterbi Algorithm and Decision Feedback Equalizer", Conf. Rec. Int. Conf. on Commun., June 1974, pp.37D-1-37D-5.

[Mes 79] Messerschmitt, D.G., "Frequency Detectors for PLL Aquisition in Timing and Carrier Recovery", IEEE Trans. on Communications, Vol.COM-27, No.9, September 1979, pp.1288-1295.

[MG 75] J.D. Markel and A.H. Gray, Jr., "Roundoff Noise Characteristics of Orthogonal Polynomial Structures", IEEE Trans. ASSP, Vol.ASSP-23, October 1975, pp.473-486.

[ML 79] M. Morf and D.T. Lee, "Recursive Least Squares Ladder Forms for Fast Parameter Tracking", Proc. 1978, IEEE Conf. Decision & Control, San Diego, Calif., January 1979, pp.1326-1367.

[MLK 76] M. Morf, L. Ljung and T. Kailath, "Fast Algorithms for Recursive Identification", Proc. IEEE Conf. on Decision and Control, Clearwater Beach, Fla., December 1976.

[MLNV 77] M. Morf, D.T. Lee, J.R. Nicholls and A. Viera, "A Classification of Algorithms for ARMA Models and Ladder Realizations", Conf. Rec. of 1977 IEEE Int. Conf. ASSP, May 1977, pp.13-19.

[Mon 71] P. Monsen, "Feedback Equalization for Fading Dispersive Channels", IEEE Trans. Inform. Theory, Vol.IT-17, No.1, January 1971, pp.56-64.

[Mon 73] P. Monsen, "Digital Transmission Performance on Fading Dispersive Diversity Channels", IEEE Trans. Comm., January 1973, p.33.

[Mon 74] P. Monsen, "Adaptive Equalization of a Slow Fading Channel", IEEE Trans. COmm., August 1974, p.1064.

[Mon 77] P. Monsen, "Theoretical and Measured Performance of a DFE Modem on a Fading Multipath Channel", IEEE Trans. Commun., VOLCOM-25, No.10, October 1977, pp.1144-1153.

[Mor 77] M. Morf, "Ladder Forms in Estimation and System Identification", 11th Annual Asilomar Conf. on Circuits, Systems and Computers, Monterey, Calif., November 1977.

[MP 73] R.F. Magee and J.G. Proakis, "Adaptive Maximum-Likelihood Sequence Estimation for Digital Signaling in the Presence of ISI", IEEE Trans. Inform. Theory, Vol.IT-19, January 1973, p.120.

[Mue 81] M.S. Mueller, "Least Squares Algorithms for Adaptive Equalizers", BSTJ, Vol.60, No.8, October 1981, pp.1905-1925.

[MV 78] J. Makhoul and R. Viswanathan, "Adaptive Lattice Methods for Linear Prediction", Proc. Int. Conf. on Acous., Speech & Sig. Proc., 1978, pp.83-86.

[Obe 71] Oberst, T.F., "Generalized Phase Comparators for Improved Phase-Locked Loop Aquisition", IEEE Trans. on Communication Technology, pp.1142-1148, December 1971.

[Par 70] Park, J.H., "An FM Detector for Low SIN", IEEE Trans. on Communication Tech., Vol.COM-18, No.2, April 1970, pp.110-118.

[Pic 74] Picquerard, A., Radio Wave Propagation, (Philip Technical Library), J. Wiley, New York 1974.

[Pri 72] R. Price, "Nonlinearly Feedback-Equalized PAM vs. Capacity of Noisy Filter Channels", Conf. Rec. Int. Conf. on Commun., Philadelphia, June 1972.

[Pro 75] J.G. Proakis, "Advances in Equalization for Intersymbol Interference, in Advances in Communication Systems, Vol.4, pp.123-198, Academic Press, 1975.

[Pro 83] J.G. Proakis, "Digital Communications", McGraw-Hill, New York, 1983.

[SA 78] E.H. Satorius and S.T. Alexander, "Channel Equalization Using Adaptive Lattice Algorithms", IEEE Trans. Commun., Vol.COM-27, No.6, June 1978, pp.899-905.

[Sal 73] J. Salz, "Optimum Mean-Square Decision Feedback Equalization", BSTJ, Vol.52, No.8, October 1973, pp.1341-1374.

[She 80] M.J. Shensa, "A Least Squares Lattice Decision Feedback Equalizer", Proc. Int. Conf. on Commun., Seattle, June 1980.

[Shi 82] E.S. Shichor, "Fast Recursive Estimation Using the Lattice Structure", BSTJ, June 1982.

[Sim 69] M.K. Simon, "An Analysis of the Steady State Noise Performance of a Digital Data Transition Tracking Loop", International Communications Conference, ICC-69, Conference Record, pp.20.9-20.15.

[Sim 70] M.K. Simon, "Non-Linear Analysis of an Absolute Value Type of an Early-Late Gate Bit Synchronizer", IEEE Transactions on Communications Technology, Vol.COM-18, No.10, October 1970, pp.589-596.

[SP 81] E.H. Satorius and J.D. Pack, "Application of Least Squares Lattice Algorithms to Adaptive Equalization", IEEE Trans. Commun., Vol.COM-29, No.2, February 1981, pp.136-142.

[Spi 77] J.J. Spilker, "Digital Communications By Satellite", Prentice-Hall Information Theory Series, Prentice-Hall, 1977, Chapter 14.

[Tom 77] Toman, K., Estimating Ionospheric Height from Doppler Measurements, IEEE Trans. on Antennas and Propagation, pp.273-276, March 1977.

[Ung 72] G. Ungerboeck, "Theory on the Speed of Convergence in Adaptive Equalizers for Digital Communication", IBM J Res. & Dev., November 1972, pp.546-555.

[Ung 74] G. Ungerboeck, "Adaptive Maximum-Likelihood Receiver for Carrier-Modulated Data Transmission Systems", IEEE Trans. Commun., COM 22, No.5, May 1974, pp.624-636.

[VH 74] F.L. Vermuelen and M.E. Hellman, "Reduced State Viterbi Decoders for Channels with Intersymbol Interference", Conf. Rec. of Int. Conf. on Commun., ICC74, Minneapolis, 1974.

[VH 81] G.M. Vachula and F.S. Hill, Jr., "On Optimal Detection of Band-Limited PAM Signals with Excess Bandwidth", IEEE Trans. Commun., Vol.COM-29, No.6, June 1981, pp.886-810.

[VM 76] R. Viswanathan and J. Makhoul, "Sequential Lattice Methods for Stable Linear Prediction", EASCON Conv. Record 1976, pp.155A-155H.

[WH 60] B. Widrow and M.E. Hoff, "Adaptive Switching Circuits", 1960 WESCON Conv. Rec., Pt.4, pp.96-140.

[WJB 70] Waterson, C.C., Juroshek, J.R., and Bensema, W.D., Experimental Confirmation of an HF Model, IEEE Trans. Comm. Tech., Vol.18, pp.792-803, December 1970.

[WL 69] Wintz and Luecke, "Performance of Optimum and Suboptimum Synchronizers", IEEE Transactions on Communications Technology, Vol.COM-17, No.6, June 1969, pp.380-389.

[WMLJ 76] B. Widrow, J.M. McCool, M.G. Larimore, C.R. Johnson, Jr., "Stationary and Nonstationary Learning Characteristics of the LMS Adaptive Filter", Proc. IEEE, Vol.64, No.8, August 1976, pp.1151-1162.

[YL 72] Yeh, K.C. and Liu, C.H., Theory of Ionospheric Waves, Academic Press, New York 1972.

Appendix A

PROCESSING THE HF DATA TAPES

The recorded data format created originally by the DEC computer is different from the standard format used by CP6. In particular, two sixteen-bit DEC integers will appear per 36-bit CP-6 integer read. The data file in the CP-6 consists of a series of fixed length records. The records will be 128 CP-6 words in length, corresponding to a block of 512 DEC bytes.

A Fortran unformatted READ statement of the form "READ (22) [K]" can be used in order to read the data from the data file, where

22: is a logical unit number (it is arbitrary)

K : is the output list

In our case, since every record contains 128 words, a 128 array list has to be used as an output list. Before invoking the program containing this READ statement, one would give the IBEX command: !SET 22 [file name].

As we mentioned above, the data output is somewhat scrambled. In the sequel we shall try to explain with a particular example the procedure which should be followed step by step in order to unscramble the data.

Consider the following 36-bit CP-6 integer word in octal form:

110 001 . 256 011

That 36-bit word contains two sixteen bit DEC integers. The period separates those two numbers. Therefore every half CP-6 word contains two DEC 8 bit bytes which are scrambled. The octal byte representation of the above word will be:

110 001 . 256 011

In order to find the actual integer number, we should follow the steps:

1. Reverse the order of the bytes of every CP-6 half word, i.e.,

   001 110 . 011 256

2. The binary equivalent is

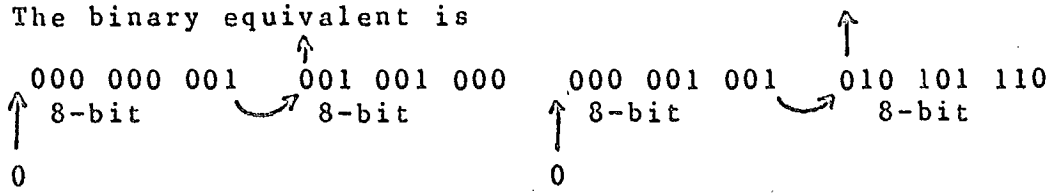

3. According to the above pattern we form the new binary equivalent by deleting the 10th and 28th bits and inserting zeroes in the first and 19th positions as shown.

   000 000 000 101 001 000 000 000 100 110 101 110

4. The above binary number in octal form is

   000 510 004 656

Therefore the octal unscrambled equivalent form is

00510 . 004656

which corresponds to the decimal integers

$5x8^2 + 5x8^1 + 0x8^0 = 328$

$4x8^3 + 6x8^2 + 5x8^1 + 6x8^0 = 2478$

In our Fortran program the GETTWO subroutine performs the appropriate unscrambling operation.

Correspondence of integers to signal values, e.g.,

-5 V 0000_8

0 V 4000_8

5 V 7777_8

The following FORTRAN program performs the appropriate unscrambling operation and stores the unscrambled data in array for further processing.

```
C  THE FOLLOWING PROGRAM READS AND UNSCRAMBLES
C  DATA FROM THE CRCMDAA2D DATA FILES.
C
C  INT(128):   128 INTEGER ARRAY READ FROM THE
C              DATA FILE.READS THE WHOLE RECORD.
C  IHI(128):   TEMPORARY ARRAY WITH UNSCRMBLED
C              DATA.CONTAINS FIRST HALF OF EACH
C              CP-6 WORD.
C  ILO(128):   TEMPORARY ARRAY WITH UNSCRAMBLED
C              DATA.CONTAINS SECOND HALF OF EACH
C              CP-6 WORD.
C  RC(256):    CONTAINS THE UNSCRAMBLED DATA IN
C              A SEQUENTIAL ORDER.
C
      INTEGER INT(128),ILO(128),IHI(128),RC(256)
      DO 100 I=1,10172
      READ(22) (INT(I1),I1=1,128)
      IF(I.LE.99) GO TO 100
      PRINT*,"DATA BLOCK"
      WRITE(23,10) (INT(I2),I2=1,128)
   10 FORMAT((4013))
      DO 50 J=1,128
      CALL GETTWO(INT(J),ILO(J),IHI(J))
      RC(2*J)=ILO(J)
      RC(2*J-1)=IHI(J)
   50 CONTINUE
      WRITE(23,20) (RC(I3),I3=1,256)
   20 FORMAT(8I6)
  100 CONTINUE
      STOP
      END
C
C
```

```
      SUBROUTINE GETTWO(INT,ILO,IHI)
C
C  SUBROUTINE UNSCRAMBLES INTEGERS CREATED BY
C  DEC RSX-11 TAPE.
C
C  INPUT:  INT(36 BIT INTEGER READ FROM TAPE)
C  OUTPUT:  IHI(FIRST SEQUENTIAL 16-BIT INTEGER)
C           ILO(SECOND SEQUNTIAL 16-BIT INTEGER)
C  NOTE:     16-BIT INTEGERS ARE TREATED AS UNSIGNED
C  CONSTANTS .THUS,IF NEGATIVE INTEGERS ARE EXPECTED,
C  THE ROUTNE MUST BE MODIFIED TO ALLOW FOR SIGN
C  PROPAGATION.
C
      ILO=IAND(INT,255)
      ITEM=IAND(INT,130560)
      ILO=ISL(ILO,8)+ISL(ITEM,-9)
      ITEM2=ISL(INT,-18)
      IHI=IAND(ITEM2,255)
      ITEM=IAND(ITEM2,130560)
      IHI=ISL(IHI,8)+ISL(ITEM,-9)
      RETURN
      END
```

The following JOB file has been used in order to mount and copy on disk the magnetic tapes with file name 'CRCMDAA2D'. Between the CP6 library names and the tape names there is the following correspondence:

AA0066	CRCMDA
AA0067	MDA 002 (Oct.13)
AA0068	MDA 002 (Dec.3)
AA0069	MDA 003
.	
.	
.	
AA0077	MDA 011

```
!JOB
!RESOURCE LT(8008PI)=1
!MESSAGE PLS MOUNT TAPE AA0076 AS MDA010 NORING,...
!PCL
MOUNT LT#MDA010
REW LT#MDA010
L(A) LT#MDA010
REW LT#MDA010
COPY LT#MDA010/'CRCMDA.A2D' TO CRCMDAA2D
REW LT#MDA010
REL LT#MDA010
END
!
```

Appendix B

FAST RECURSIVE LEAST SQUARES (FRLS) ALGORITHM APPLIED TO A DECISION FEEDBACK EQUALIZER (DFE)

Parameters: $2N_1$ forward complex tap coefficients $\{W_i^*\}$ and N_2 feedback tap coefficients $\{F_i^*\}$. $p_1=2$ complex channel outputs enter equalizer in each symbol interval. Total number of coefficients $N=2N_1+N_2$.

Equalizer output at n^{th} symbol interval:

$$Q_n = \underline{C}(n-1)^* \underline{Z}(n) \tag{1}$$

where $\underline{C}$ is tap coefficient vector;

$$\underline{C}(n-1)^* \equiv (W_o^*, W_1^*, \ldots W_{2N_1-1}^* \mid F_1^*, F_2^*, \ldots F_{N_2}^*) \tag{2}$$

Forward Tap Coefficients | Feedback Tap Coefficients

and $\underline{Z}(n)$ is the N-dimensional vector of equalizer inputs;

$$\underline{Z}(n)^* \equiv (y(nT)^*, y(nT-T/2)^*, \ldots y(nT-N_1T+T/2)^* \mid \hat{a}_{n-1}^*, \ldots \hat{a}_{n-N_2}) \tag{3}$$

complex channel output samples at T/2-sec. intervals | previous data decisions

Desired output at n^{th} symbol interval: $\hat{a}_n$

Error for adaptation:

$$e(n) = \hat{a}_n - \underline{C}(n-1)^* \underline{Z}(n) \tag{4}$$

Initialization at n=0 of FRLS algorithm

$$y(nT) = y(nT-T/2) = \hat{a}_n = 0 \text{ for } n \leq 0 \tag{5}$$

N-dimensional complex vectors: $\underline{k}(n)$, $\underline{C}(n)$, $\underline{y}$, $\underline{g}(n)$

with $\underline{C}(n) = \underline{k}(n) = \underline{0}$ for n=0 (6)

N-by-3 complex matrices:

$$F(n) = B(n) = [0] \text{ for } n=0 \tag{7}$$

3-by-3 complex matrix:

$$E_{33}(n) = \delta \begin{pmatrix} 1 & 0 & 0 \\ 0 & 1 & 0 \\ 0 & 0 & 1 \end{pmatrix} \quad \text{where } \delta \text{ is a positive constant}$$

for n=0 (8)

The following will be 3-dimensional complex vectors:

$\underline{f}_3(n)$, $\underline{f}_3(n)'$, $\underline{x}_3$, $\underline{\rho}_3(n)$, $\underline{\xi}_3(n)$, $\underline{\mu}_3(n)$, $\underline{b}_3(n)$

Real-valued scalar:

$\Gamma(n) = 1$ at n=0

FRLS Algorithm for $n \geq 1$:

$\underline{\xi}_3(n)$ = vector of 3 newest inputs to DFE

$$\equiv \begin{pmatrix} y(nT+T) \\ y(nT+T/2) \\ \hat{a}_n \end{pmatrix} \tag{9}$$

$\underline{\rho}_3(n)$ = vector of 3 oldest inputs to DFE

$$\equiv \begin{pmatrix} y(nT-N_1T+T) \\ y(nT-N_1T+T/2) \\ \hat{a}_{n-N} \end{pmatrix} \tag{10}$$

$$\underline{f}_3(n) = \underline{\xi}_3(n) + F(n-1)^* \underline{Z}(n) \tag{11}$$

$$F(n) = F(n-1) - \underline{k}(n-1) \underline{f}_3(n)^* \tag{12}$$

$$\underline{f}_3(n)' = \Gamma(n-1) \underline{f}_3(n) \tag{13}$$

$$E_{33}(n) = \lambda E_{33}(n-1) + \underline{f}_3(n) \underline{f}_3(n)'^* \tag{14}$$

$$\underline{x}_3 = E_{33}(n)^{-1} \underline{f}_3(n)' \tag{15}$$

$$\underline{y} = \underline{k}(n-1) + F(n) \underline{x}_3 \tag{16}$$

Form $\begin{bmatrix} \underline{g}(n) \\ \hline \underline{\mu}_3(n) \end{bmatrix}$ from $\begin{bmatrix} \underline{x}_3 \\ \hline \underline{y} \end{bmatrix}$ (17)

as shown in Figure 5.2

Form $\begin{bmatrix} \underline{Z}(n+1) \\ \hline \underline{\rho}_3(n) \end{bmatrix}$ from $\begin{bmatrix} \underline{\xi}_3(n) \\ \hline \underline{Z}(n) \end{bmatrix}$ (18)

in exactly the same way.

$$\underline{b}_3(n) = \underline{\rho}_3(n) + B(n-1)^* \underline{Z}(n+1) \quad (19)$$

$$B(n) = [B(n-1) - \underline{g}(n)\ \underline{b}_3(n)^*][I_{33} - \underline{\mu}_3(n)\underline{b}_3(n)^*]^{-1}$$

where I_{33} = 3-by-3 identity matrix (20)

$$\underline{k}(n) = \underline{g}(n) - B(n)\ \underline{\mu}_3(n) \quad (21)$$

$$\Gamma(n) = [\Gamma(n-1) - \underline{f}_3(n)^* \underline{x}_3][1 - \underline{\mu}_3(n)^* \underline{b}_3(n)]^{-1} \quad (22)$$

Constraints:

If $\mathrm{Im}(1 - \underline{\mu}_3(n)^* \underline{b}_3(n)) = 0$ set it to 0.

If $1 - \underline{\mu}_3(n)^* b_3(n)$ is negative set it to .00001.

If $1 - \underline{\mu}_3(n)^* b_3(n)$ exceeds 1 set it to 1.0.

If $\mathrm{Im}(\Gamma(n)) \neq 0$ set it to 0.

If $\Gamma(n) < 0$ set $\Gamma(n) = .00001$.

If $\Gamma(n) > 1$ set $\Gamma(n) = 1.0$.

Tap Coefficient Update:

$$\underline{C}(n) = \underline{C}(n-1) + \underline{k}(n-1)\ e(n)^* \quad (23)$$

where e(n) was determined in (4).

Restart mechanism initiated at n=K:

Initiate restart exactly as in (5)-(8) withthe following exceptions:

(1) Do not reset $\underline{C}(K)$ to $\underline{0}$ at initiation of restart unless measured MSE has been high.

(2) <u>During restart interval</u> use auxiliary LMS algorithm:

$$e(n)_{LMS} = \hat{a}_n - \underline{C}(n-1)_{LMS}^{*}\ \underline{Z}(n)$$

$$\underline{C}(n)_{LMS} = \underline{C}(n-1)_{LMS} + \gamma\, e(n)_{LMS}^{*}\ \underline{Z}(n),$$

with $\underline{C}(K-1)_{LMS} = \underline{C}(K-1)$

and where $\{\hat{a}_n\}$ are decisions obtained from output of LMS DFE.

(3) <u>During restart interval</u> for FRLS algorithm replace $e(n)$ in (4) with

$$e(n) = \hat{a}_n - \underline{C}(n-1)_{LMS}^{*}\ \underline{Z}(n)^{(-)} - \underline{C}(n-1)^{*}\ \tilde{\underline{Z}}(n)$$

where $\underline{Z}(n)^{(-)}$ is $\underline{Z}(n)$ with all components which entered at $n \geq K$ replaced by 0 and $\tilde{\underline{Z}}(n)$ is $\underline{Z}(n)$ with all components which entered prior to $n=K$ replaced by 0. Then in the FRLS algorithm during restart, replace $\underline{Z}(n)$ by $\tilde{\underline{Z}}(n)$.